THESIS FOR THE DEGREE OF DOCTOR OF PHILOSOPHY

Amyloid Proteins in Neurodegenerative Disease – Role of Extrinsic Modifiers

NIMA SASANIAN

Department of Life Sciences

CHALMERS UNIVERSITY OF TECHNOLOGY

Gothenburg, Sweden 2023

Amyloid Proteins in Neurodegenerative Disease – Role of Extrinsic Modifiers
NIMA SASANIAN
ISBN 978-91-7905-772-5

Doktorsavhandlingar vid Chalmers tekniska högskola
Ny serie nr 5238
ISSN 0346-718X

Department of Life Sciences
Chalmers University of Technology
SE-412 96 Gothenburg
Sweden
Telephone + 46 (0)31-772 1000

Cover:
The cover image shows the processing, interactions, and localizations of the Alzheimer's disease peptide Aβ in a mammalian cell. The modulatory effects of different extrinsic modifiers on the Aβ studied in this thesis are also illustrated.

Printed by Chalmers Reproservice
Gothenburg, Sweden 2023

Amyloid Proteins in Neurodegenerative Disease – Role of Extrinsic Modifiers

NIMA SASANIAN
Department of Life Sciences
Chalmers University of Technologies

ABSTRACT

Self-assembly of disease-associated proteins into fibrillar homopolymers, so-called "amyloid fibrils" is a pathological hallmark of several debilitating human disorders, including Alzheimer's disease (AD) and Parkinson's disease (PD). AD and PD are associated with the formation of amyloid fibrils from the proteins amyloid-β (Aβ) and α-syn (α-syn), in the extracellular and intracellular space, respectively. In Aβ pathogenesis, there are different molecules such as metal ions and lipids that can interact with Aβ, and affect amyloid fibril formation but also other important pathological features such as cellular uptake, which contributes to the intracellular build-up of aggregates that precede the deposition of extracellular plaques.

This thesis describes my research on the effects of different extrinsic modulators, mainly metals and lipids, in Aβ and α-syn aggregation, as well as in the cellular uptake of Aβ. I showed that Cu^{2+} inhibits Aβ(1-42) amyloid formation by impairment of the fibril elongation mechanism whereas Cu^{+} catalysed primary nucleation, indicating an important role of copper redox chemistry in AD. I further showed that Cu^{2+}, and also Zn^{2+}, whilst acting aggregation inhibitory, enhance Aβ(1-42) uptake and thereby contribute to other pathological effects, including prion-like cell-to-cell propagation.

In a second part of my work, I explored the effect of lipid vesicles of biological and synthetic origin on the Aβ(1-42) aggregation process. I found that cell-derived extracellular vesicles impede the elongation process and induce the formation of amyloid fibrils with distinct morphology. Synthetic lipid vesicles, on the other hand, were found to have diverse effects on the Aβ(1-42) aggregation rate and mechanism and I showed that both lipid chemistry and the physical properties of the bilayers they participate in, contribute to the modulatory role of membrane in Aβ(1-42) aggregation.

To analyse physical attributes of amyloid fibrils, I developed a nanofluidic-based method for visualization of single amyloid fibrils in solution and used it to compare persistence lengths of different fibril types as well as within samples, addressing the concept of polymorphism. Lastly, my work has contributed to the understanding of how graphene-based nanoparticles can modulate amyloid formation by interfering with both primary nucleation and secondary processes in aggregation.

Keywords: Alzheimer's disease, protein aggregation, amyloid fibril, amyloid-β, Aβ(1-42), α-synuclein, extracellular vesicles, lipid vesicle, kinetics, nanofluidics, fluorescence microscopy, atomic force microscopy

List of publication

This thesis is based on the work contained in the following research papers, referred to by Roman numerals in the text:

I. **Inhibition of Aβ(1-42) aggregation by cell-derived extracellular vesicles**
Vesa Halipi, Nima Sasanian, Julia Feng, Jing Hu, Quentin Lubart, David Bernson, Daniel van Leeuwen, Doryaneh Ahmadpour, Emma Sparr and Elin K. Esbjörner*
Manuscript

II. **Ganglioside GM1 slows down Aβ(1-42) fibril formation by a primary nucleation inhibitory mechanism that is modulated by lipid membrane sphingomyelin and cholesterol**
Nima Sasanian, Vesa Halipi, Mikaela Sjögren, Johannes Bengtsson, David Bernson and Elin K. Esbjörner*
Manuscript

III. **Redox-dependent copper ion modulation of amyloid-β (1-42) aggregation in vitro**
Nima Sasanian, David Bernson, Istvan Horvath, Pernilla Wittung-Stafshede and Elin K. Esbjörner*
Biomolecules 2020, 10, 924; doi:10.3390/biom10060924

IV. **Copper and zinc enhance the intracellular accumulation, cell-cell transfer, and cytotoxicity of Alzheimer's diseases peptide Aβ(1-42)**
Nima Sasanian, Andrea Ramnath, Shadi Rahimi, Daniel van Leeuwen, Emelie Wesén, David Bernson, Ivan Mijakovic and Elin K. Esbjörner*
Manuscript

V. **Probing physical properties of amyloid fibrils using nanofluidic channels**
Nima Sasanian, Rajhans Sharma, Quentin Lubart, Sriram KK, Marziyeh Ghaeidamini, Kevin D. Dorfman, Fredrik Westerlund* and Elin K. Esbjörner*
Manuscript

VI. **Graphene oxide sheets and quantum dots inhibit α-synuclein amyloid formation by different mechanisms**
Marziyeh Ghaeidamini, David Bernson*, Nima Sasanian, Ranjeet Kumar and Elin K. Esbjörner*
Nanoscale, 2020, 12, 19450–19460; doi: 10.1039/d0nr05003b

Additional paper not included in this thesis:

VII. **Ginsenoside Rg3 reduces the toxicity of graphene oxide used for pH-responsive delivery of Doxorubicin to liver and breast cancer cells**
Shadi Rahimi, Daniel van Leeuwen, Fariba Roshanzamir, Santosh Pandit, Lei Shi, Nima Sasanian, Jens Nielsen, Elin K. Esbjörner and Ivan Mijakovic*
Pharmaceutics 2023, 15, 391. https://doi.org/10.3390/pharmaceutics15020391

Contribution report

My contribution to the papers appended in this thesis is as follows:

I. I contributed to experiment design and the analysis of the kinetic data together with V.H. I performed and setup preliminary experiments. I contributed to the interpretation of results. I did not write the paper.

II. I conceived the idea together with E.K.E, designed and performed most of the experiments together with some help from V.H, M.S, J.B. I analysed and interpreted the data and wrote the paper together with E.K.E.

III. I conceived the idea together with E.K.E, designed and performed all experiments except TEM microscopy. I analysed and interpreted the data and wrote the paper together with D.B and E.K.E.

IV. I conceived the idea together with E.K.E, designed and performed all experiments except the cell division assay. I analysed and interpreted the data and wrote the paper together with E.K.E.

V. I conceived the idea together with E.K.E and F.W. I designed and performed most experiments and did preliminary experiments together with R.S. I analysed and interpreted the data and wrote the paper together with F.W and E.K.E.

VI. I contributed to the experiment design and AFM microscopy. I analysed the AFM images and contributed to the interpretation of results. I did not write the paper.

PREFACE

This dissertation is submitted for the partial fulfilment of the degree of Doctor of Philosophy. The content of this thesis is based on work that was carried out between August 2018 and February 2023 at the Department of Life Sciences (named Department of Biology and Biological Engineering until January 2023) at Chalmers University of Technology under the supervision of Associate Professor Elin K. Esbjörner. The research was funded by the Chalmers Area of Advance Nano Excellence PhD program, the Swedish Research Council and the Knut and Alice Wallenberg foundation.

Nima Sasanian

February 2023

To my loving parents

Table of contents

Introduction

It has been 120 years since Dr. Aloysius Alzheimer diagnosed a patient with abnormal behavior with a 'special illness' associated with a substance distributed all over the cortex of the brain[1,2]. Nowadays, this 'special illness' is known as Alzheimer's disease (AD) and around 50 million people are affected. It is estimated that this number will rise to 150 million by 2050[3] unless new treatments that can cure the illness are developed. The research which has been carried out in the last 120 years, has taught us that the brain substance which was observed by Dr. Alzheimer consist of fibrillar aggregated proteins which are called amyloid fibrils[2]. In addition, we now know that amyloid fibrils are not only associated with AD but rather numerous diseases including Parkinson's disease (PD). We also know the exact amino acids sequence of the disease-causing amyloidogenic proteins, such as amyloid-β (Aβ) and α-synuclein (α-syn), which are associated with AD and PD, respectively.

With time, we have gained detailed knowledge of the amyloid formation mechanism and the kinetics of the aggregation process *in vitro*. This has allowed researchers to determine how different modulators affect the aggregation process by interfering with different microscopic steps in the protein self-assembly. In, addition, science has taught us that different molecules such as lipids and metal ions, which are at focus in this thesis, interact with Aβ in the brain and co-aggregate with Aβ into amyloid plaques. Despite this extensive knowledge we have developed on amyloid aggregation, and the role of various modifiers in this process, we still need further insight into the molecular mechanisms and the exact role of different modulators in amyloidogenesis to enable the successful design of new therapeutic strategies and effective medicines.

This thesis contributes to better understanding of the role of modifiers in amyloid formation by first addressing cell-derived extracellular vesicles (EVs) and their role in the *in vitro* aggregation of Aβ(1-42) (**paper I)**. I also studied the individual and combinatorial effect of different lipids, which are relevant in Aβ pathogenesis, in a larger systematic aggregation study of Aβ(1-42) **(paper II).**

In **paper III** and **IV**, I focused on metal ions, and I have contributed to deepen the current knowledge around the interaction of metal ions with Aβ and the associated modulatory roles that this interaction can have in Aβ pathogenesis. In paper III, I studied the effect of copper ions on the aggregation of Aβ(1-42) into amyloid fibrils. After providing information on the effect of two redox states of copper ions (Cu) in the aggregation of Aβ(1-42), I demonstrated that divalent copper (Cu^{2+}), and also zinc (Zn^{2+}) ions, contribute to increase the uptake and cell-to-cell propagation of Aβ(1-42) by human neuroblastoma cells (**paper IV).**

In **paper V**, I developed a nano-fluidic based approach to visualize and study single amyloid fibrils, which turned out to be useful to characterize their biophysical properties and used the method to determine the persistence length of amyloid fibrils formed from Aβ(1-42) and α-syn. This way of analysing individual amyloid fibrils gave new insights into the concept of fibril polymorphism.

Lastly, in **paper VI**, I contributed to a study of two graphene-based nanoparticles exploring their aggregation inhibitory potential and possible role as a novel therapeutic agent to tackle the amyloid

formation of α-syn which is involved in Parkinson's disease. We showed that these nanoparticles can impede α-syn aggregation leading to formation of shorter amyloid fibrils and provided insights into their respective inhibitory mechanisms.

In the beginning of this thesis, I present a brief overview of the field (Chapter 1 and 2), including an introduction to the concept of protein folding and misfolding and its relation to disease, I describe the role and relevance of Aβ and α-syn in the pathology of AD and PD and introduce different extrinsic modifiers that have been implicated in the pathogenesis of AD. In Chapter 3, I briefly describe the main methods that I have used in **paper I-VI**. In Chapter 4-7, I present my original work and summarize the main results of **paper I-VI**. This is followed by conclusions and an outlook in Chapter 8.

Background

1. Proteins and amyloid fibrils

1.1 Proteins chemistry

Proteins are biomolecules that consist of chains of amino acids connected through covalent peptide bonds; therefore, proteins are also called polypeptides. Amino acids are organic compounds composed of an amine ($-NH_2$), a carboxylic acid (-COOH) and a central carbon which attaches to the functional group (Fig. 1). There are 20 amino acids encoded in the human genome and the combination of them into polypeptides allow for the formation of all functional proteins in the human body.

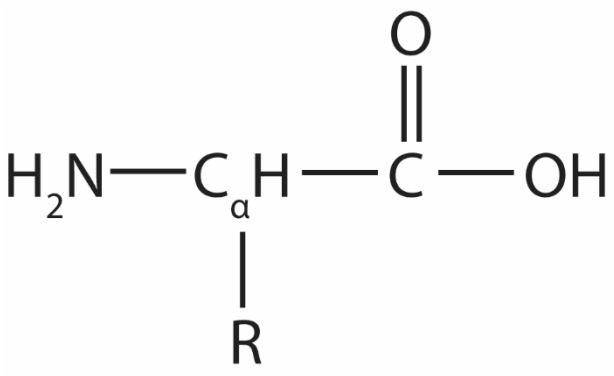

Figure 1. General chemical structure of amino acids with R denoting the functional group (or side chain).

The 20 amino acids are α-amino acid i.e., the functional group (R), carboxylic and amine group are linked to α-carbon atom. The amino acids are zwitterions at physiological pH as the amine group and carboxylic group are respectively, protonated and deprotonated. The functional groups can confer additional charges. In α-amino acids, the functional group (R) is referred to as the side chain. The chemical properties of functional groups determine the functionality of the amino acids and they are therefore usually divided into different categories as shown in Table 1.

Table 1. Names and chemical properties of the 20 genetically encoded amino acids.

	Amino acid	3-letter abbreviation	1-letter abbreviation
Aliphatic	Glycine	Gly	G
	Alanine	Ala	A
	Valine	Val	V
	Isoleucine	Iso	I
	Leucine	Leu	L
Hydroxyl-or sulfur-containing	Serine	Ser	S
	Threonine	Thr	T
	Cysteine	Cys	C
	Methionine	Met	M
Aromatic	Phenylalanine	Phe	F
	Tyrosine	Tyr	Y
	Tryptophan	Trp	W
Basic	Arginine	Arg	R
	Histidine	His	H
	Lysine	Lys	K
Acidic and amides	Aspartic acid	Asp	D
	Glutamic acid	Glu	E
	Asparagine	Asn	N
	Glutamine	Gln	Q
Cyclic	Proline	Pro	P

1.2 Protein structure

Proteins are generally described at four different levels of structure: primary, secondary, tertiary and quaternary structure. The sequence by which amino acids are linked together to form the polypeptide (protein) is referred to as the primary structure. The covalent peptide bonds that conjugated the amino acids have double bond characteristics and are therefore planar (Fig. 2). Consequently, the amino acids can only rotate around the α-carbon. These two rotations are described by two torsion angels ϕ and ψ, and the sterically possible geometric arrangements of peptides bonds are describable by a so-called Ramachandran plot of ψ versus φ[4].

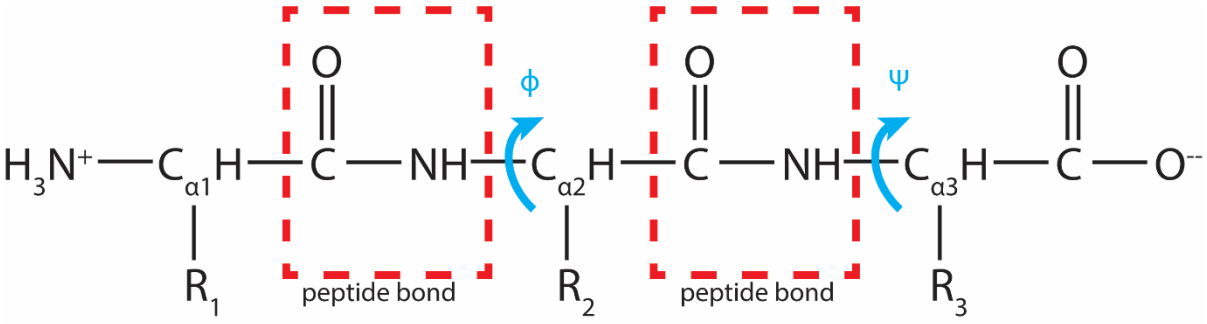

Figure 2. Schematic of three amino acids linked together via peptide bonds.

In addition to the described steric constraints, peptide side chains interact with each other and allows the polypeptide chain to fold into three-dimensional arrangements which, in most cases, are essential for proteins to be able to fulfill their functions. Both secondary and tertiary structures contribute to the specific three-dimensional structure of proteins. Secondary structure describes the local three-dimensional arrangement of polypeptides. The two most common secondary structures are α-helix and β-sheet (Fig. 3). In the α-helix structure, a single chain of polypeptide twists around itself to form a helix with a pitch of 3.6 residues per turn. The α-helix structure is stabilised by hydrogen bonds between the carbonyl oxygen in one peptide bond and the amine group of the peptide bond four residues further up the helix.

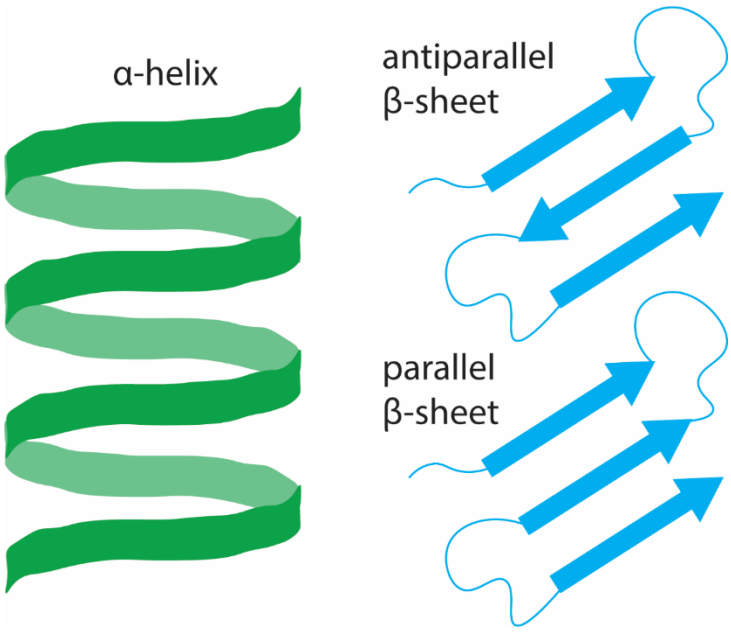

Figure 3. Schematic structure of secondary structure of proteins; α-helix and β-sheet.

The β-sheet structure is also stabilised by hydrogen bonds between the carbonyl oxygen and amine group, but these hydrogen bonds form between two neighboring polypeptide chains running either parallel or antiparallel to each other. The peptides that have been studied in this thesis i.e., amyloid-β (Aβ) and α-synuclein (α-syn) tend to form amyloid fibrils which are characterised by the formation of highly ordered and specific β-sheet structure which is described in more detail in the subsequent part of the thesis. Tertiary structures of proteins describe their three-dimensional fold. Among various tertiary

structures, the globular fold is most common, Tertiary structures are typically stabilized by the hydrophobic effect, in addition to hydrogen bonding and other forces. This means that hydrophobic amino acids are preferentially buried in the structural core of the protein whereas hydrophilic amino acids face outwards and in contact with the surrounding aqueous solvent. The quaternary structure of proteins describes the arrangements of different units in protein complexes.

1.3 Protein folding

Most proteins must adopt a specific three-dimensional structure (often referred to as the native structure) to be able to perform their functions. The process of adopting the native state is called protein folding. All the needed information for the protein folding process is encoded in the primary structure of proteins[5]. Furthermore, the native state of a protein has the minimum free energy, thus there is generally only one conformation or one native state for each protein[6]. There are many contributory factors in reaching the minimum free energy and converting proteins to their native folded state, including hydrogen bonding involving the peptide bond as well as side-chains, van der Waals forces, electrostatic and hydrophobic forces. The hydrophobic forces are playing a role in determining the native conformation as the hydrophobic amino acids tend to bury in the interior side of the protein not exposed to water and oppositely to the exterior side of the protein in a lipid rich environment[7]. Considering the unique configuration of the native state, there arises a paradoxical question regarding the kinetics of protein folding which was originally proposed by Cyrus Levinthal in 1968[8]. The question is how a protein can find its correct folded state in a short time scale (ranging from microsecond to seconds)[9,10] while there are numerous of different combinations by which a protein could theoretically fold and therefore sample. Later in 1990s, the three-state model was established explaining that an unfolded polypeptide can randomly fold to so-called "folding intermediates" states which are meta-stable letting proteins search for the transient state from which it can fold quickly to the native folded state[11,12]. This model is described as a "funnel-like" model depicted in Fig. 4.

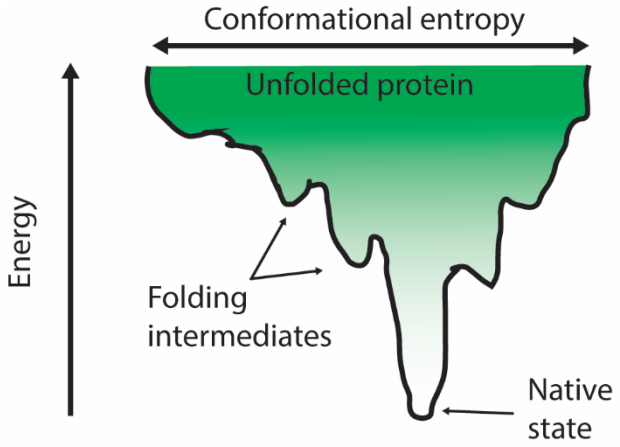

Figure 4. Schematic of simplified illustration of the energy landscape of protein folding. The y-axis shows the energy for proteins.

1.4 Protein misfolding and amyloid fibrils

The folding processes of proteins into their native states are usually assisted by other proteins called molecular chaperons[13]. If the protein folding fails or proteins are unable to maintain the correctly folded structure, proteins will unfold or adopt other structures. This process is called misfolding and leads to the formation of inactive or dysfunctional proteins[14]. The misfolding process sometimes results in the formation of highly structured fibrillar aggregates which are called amyloid fibrils[15]. Amyloid fibrils are associated with several human diseases (Table 2)[15] including Alzheimer's and Parkinson's disease.

Table 2. Examples of amyloidosis-related diseases and the associated amyloid-forming proteins.

Disease	Associated protein
Neurological disorders	
Alzheimer's disease	Amyloid-β, Tau
Parkinson's disease	α-synuclein
Huntington's disease	Huntingtin with poly-Q expansions
Frontotemporal dementia with Lewy bodies	Tau
Amyotrophic lateral sclerosis	Superoxide dismutase 1, TAR DNA-binding protein-43
Non-neurological systemic disorders	
AL amyloidosis	Immunoglobulin light chain
AA amyloidosis	Serum amyloid A
Hemodialysis-related amyloidosis	B2-microglobulin
Familial amyloidotic polyneuropathy	Transthyretin
Lysozyme amyloidosis	Lysozyme

The process of misfolding and aggregation of proteins into amyloid aggregates, which are linear and fibrillar protein homopolymers consisting of β-sheet structure running perpendicular to the fibril long axis[16], can be described by extending the protein folding energy landscape depicted in Fig. 4. The amyloid aggregates are typically more thermodynamically stable than the native states of the protein[17-19]; therefore, the amyloid state associates with a new minimum global free energy (Fig. 5). Folded proteins must first partially or completely unfold to reach the amyloid state, as this requires conformational rearrangements of amino acid chains[20]. Interestingly, many of the aggregation-prone proteins associated with the different diseases are intrinsically disordered, which facilitates their aggregation into amyloid fibrils[21].

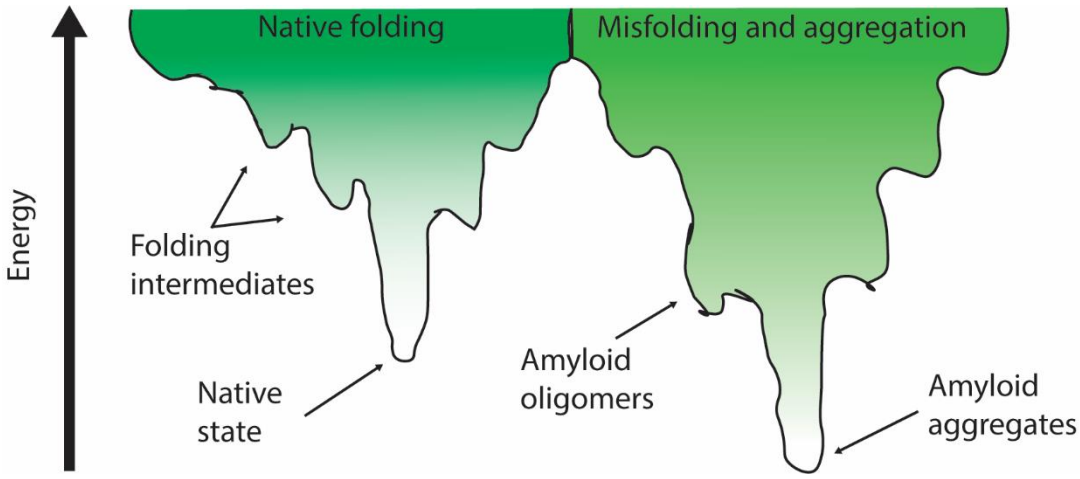

Figure 5. Schematic of simplified illustration of the energy landscape of protein folding, including misfolding and aggregation. The y-axis shows the energy for proteins. Amyloid energy minimum is included.

Amyloid fibrils are typically unbranched protein filaments that are 4-10 nm thick but can be very long, up to tens of micrometers[16,22]. Amyloid fibrils share several important characteristics despite the variety in the primary structure of the proteins they are formed from. The cores of amyloid fibrils consist of repetitively stacked β-sheets oriented perpendicular to the fibril axis. Amyloid fibrils are characterised by a typical diffraction pattern known as cross-β and observable upon examination by X-ray diffraction. The X-ray diffraction pattern contains two characteristic main reflections at ~ 4.7 Å and ~ 10-11 Å (Fig. 6). The first reflection is associated with the intrastrand distance between adjacent monomers, and the second reflection corresponds to the distance between two β-sheet layers[23-25]. Amyloid fibrils typically consist of two or several protofilaments that twist around each other[26,27]. Development of advanced techniques in structural biology such as solid state nuclear magnetic resonance (ssNMR) and more lately cryogenic electron microscopy (cryoEM) has revolutionized our understanding of the amyloid fibril fold and provided a wealth of high-resolution structures. Recent studies have shown that the structure of amyloid fibrils core is more complex and diverse than the original idea of the cross-β hairpin suggests[28-36]. In addition, these studies have shown that several structural variants of amyloid fibrils can form from the same protein and even co-exist in the same sample. This phenomenon is known as polymorphism and can be the result of different numbers of protofilaments in the fibril, different packing arrangements of the protofilaments or different folds of the monomer units in each layer of the fibril protofilaments[29,30,32]. Different polymorphic structures have been proposed for Aβ(1-42) via help of cryoEM and ssNMR structure. The cross section of protofilaments in these polymorphs consist of two monomers which can form different stable folds with very distinct intermonomer interfaces and different N-terminal domain structures[28,29,31,33,36]. In addition, Aβ(1-42) amyloid fibrils with different number of protofilaments have been reported. There are thus several factors contributing to Aβ(1-42) amyloid fibril polymorphism[28].

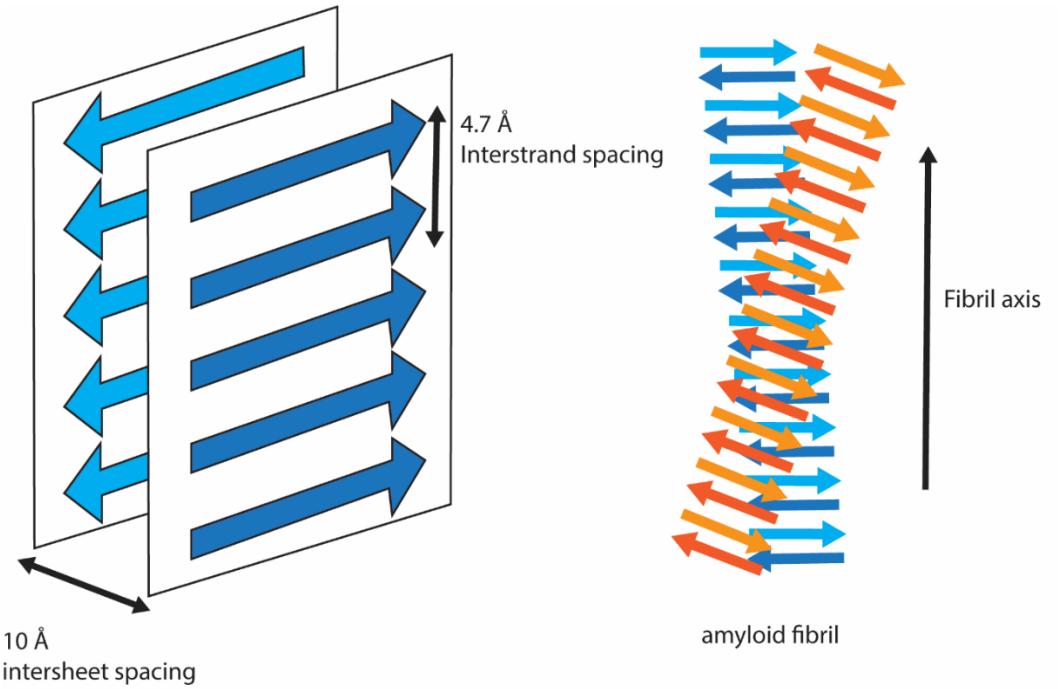

Figure 6. Amyloid fibril structure illustration. The left image illustrates the arrangement of β-structure within the amyloid fibril and the characteristic spacings that are associated with the cross-β fold. The right image illustrates an example of how protofilaments are adjoined in a twisted fashion to form the amyloid fibril structure.

To be able to propose therapeutic strategies that could tackle the underlying cause of amyloid associated diseases, it is important to understand how and why amyloid aggregates form. Many intrinsic factors such as post-translational modifications[37-40] and point mutations[41,42] influence amyloid formation. There are also many extrinsic factors ranging from simple environmental conditions such as pH[41] or temperature[43,44] to complex molecules[45-47], that modify amyloid formation and that are important because they are known to interact with disease-causing amyloid proteins *in vivo*. Nowadays, it is possible to monitor the aggregation process of a give protein and determine with high accuracy and reproducibility its aggregation rate. With help of mathematical models that describe the kinetics of amyloid formation, it is furthermore possible to obtain detailed information about the rates of different microscopic step in the self-assembly process[48]. Amyloid formation starts with so-called "primary nucleation", a process through which monomers assemble into growth-competent small nuclei[49]. This process is the slowest process in amyloid formation and thus associated with the lowest rate constant. Then, the formed nuclei can grow by the addition of monomers to their ends, which is referred to as the elongation process. Elongation has a higher rate constant[49]. One additional mechanism that can contribute to amyloid formation is fragmentation. If fibrils fragment, due to for example shear forces or other stimuli, this results in more fibril ends through which fibrils can elongate further[50,51]. The fragmentation process, therefore, increases the rate of elongation effectively. Another highly important mechanism in amyloid formation is the secondary nucleation process. This mechanism reflects the formation of new nuclei on the surface of existing fibrils and implies that surfaces of fibrils act as catalysts, accelerating the nucleation rate[52-54]. Thus, secondary nucleation has a much higher rate constant than primary nucleation rate (Fig. 7). As a result of secondary mechanisms i.e., fragmentation and secondary nucleation which are working as a positive feedback loop due to their dependence on both the monomer and fibril concentration, amyloid formation kinetics typically follow a sigmoidal trajectory (Fig. 8).

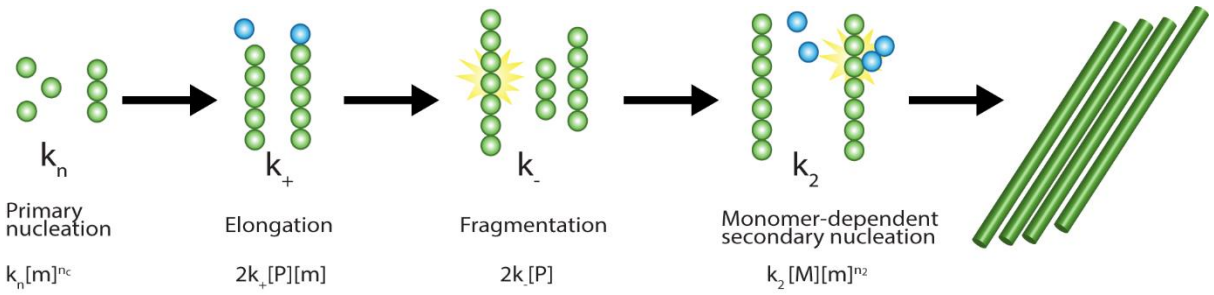

Figure 7. Schematic illustration of the different mechanistic steps that are involved in amyloid formation.

The sigmoidal kinetic curve consists of three phases. The first phase is called lag phase and is signified by that the growth of fibrils is not observable. The lag phase is dominated by the formation of primary nuclei and has also been associated with the formation of meta-stable oligomeric species[55,56] which can elongate or dissolve. Hence, the lag phase is associated with considerable dynamics and is not to be considered as a stationary waiting step. The second phase of the sigmoidal kinetic curve is called the growth phase. Here the aggregation reaction proceeds rapidly, and fibrils form at high rate, majorly due to the effectiveness of the secondary nucleation process. Finally, the reaction reaches a stationary phase of the reaction where fibrils and monomers exist in equilibrium[57]. This phase is associated with the depletion of most of the monomeric peptides into amyloid aggregates for some proteins such as amyloid-β (Aβ)[58].

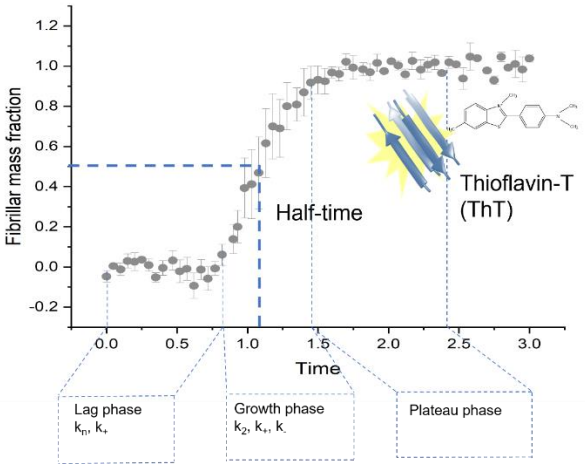

Figure 8. Amyloid formation kinetic of 2 μM Aβ(1-42). The three distinctive phases that occur along the time trajectory of the amyloid formation reaction, and the major rate constants associated with these are shown.

The kinetics of amyloid formation can be described by a single master equation (Equation 1). This makes it possible to high quality fit kinetic data and determine the rate constants of the different contributory microscopic processes depicted in Fig. 7[48,58-61]. The master equation has the following form:

$$\frac{M(t)}{M_\infty} = 1 - \left(\frac{B_+ + C_+}{B_+ + C_+ e^{\kappa t}} \times \frac{B_- + C_+ e^{\kappa t}}{B_- + C_+}\right)^{\frac{k^2_\infty}{\kappa k_\infty}} \times e^{-k_\infty t} \quad (1)$$

where

$$\lambda = \sqrt{2k_+ k_n m(0)^{n_c}}$$

$$\kappa = \sqrt{2k_+ k_2 m(0)^{n_2+1}}$$

$$B_\pm = (k_\infty \pm k'_\infty)/(2\kappa)$$

$$C_\pm = \pm\lambda^2/(2\kappa^2)$$

$$k_\infty = \sqrt{\frac{2\kappa^2}{n_2(n_2+1)} + \frac{2\lambda^2}{n_c}}$$

$$k'_\infty = \sqrt{{k_\infty}^2 - 4C_+ C_- \kappa^2}$$

As a result, it is possible to determine, not only the intrinsic aggregation behavior of amyloid proteins but also how the presence of different modulators (intrinsic or extrinsic) changes the reaction rate and to identify the different microscopic mechanisms that the modulators act on. The fitting of the

experimental aggregation reaction kinetic to this rate law model has been facilitated by the development of a web based software called Amylofit[62].

1.5 Lipids and lipid model membranes

Lipids are biomolecules that play an important role in signaling as well as energy storage[63], but that are also the main structural component of cellular membranes. Lipids can be divided into different chemical classes including for example phospholipids, fatty acids, sterols and fat-soluble vitamins. Phospholipids are amphiphilic molecules and the main building blocks of cellular membranes. They are composed of a hydrophilic headgroup linked via a glycerol backbone to hydrophobic fatty acid tails. Several different phospholipid head-groups are common in biological systems, including phosphatidylcholine (PC), phosphatidylethanolamine (PE), phosphatidylserine (PS), phosphatidylinositol (PI), phosphatidylglycerol (PG) and phosphatidic acid (PA). PC and PE are zwitterionic whereas PS, PI, PG and PA are negatively charged. In addition to the head-group, the length and saturation level of the lipid acyl-chains define the chemistry of phospholipids. Amphiphilic molecules such as phospholipids self-assemble into different morphologies in aqueous solution in a way that hydrophobic parts of phospholipids (acyl-chain) direct inwards facing each other, and hydrophilic parts (phosphate head group) direct outwards facing the solvent. This characteristic of phospholipids results in formation of lipid bilayer membranes. The formation of lipid bilayers into vesicles, sometimes referred to as liposomes, provide researchers with suitable model membranes for studying the interactions of different lipids and biomolecules. Liposomes can consist of one (unilamellar) or several bilayers (multilamellar). In **paper II**, I used large unilamellar vesicles composed of 1,2-dioleoyl-sn-glycero-3-phosphocholine (DOPC) and 1,2-dimyristoyl-sn-glycero-3-phosphocholine (DMPC) as model membrane to study the interactions and modulatory effects of different lipids (sphingomyelin (SM), ganglioside (GM1) and cholesterol (Chol)) on the aggregation of Aβ(1-42) (Fig. 9).

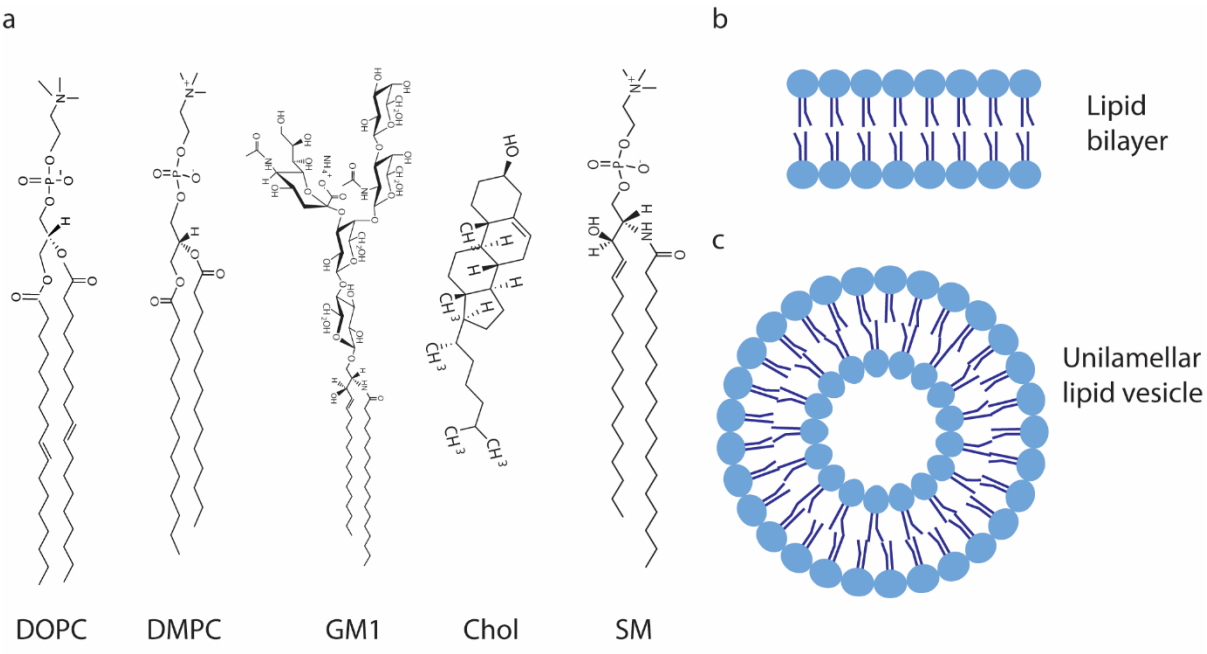

*Figure 9. Lipids and membrane formation. a, chemical structures of the different lipids that were used in **paper (II)**. b, schematic illustration of a lipid bilayer. c, schematic illustration of a biolayer folding into a unilamellar vesicle.*

2. Alzheimer's and Parkinson's disease

2.1 Pathology of Alzheimer's disease

The major focus of this thesis is to understand the effect of different extrinsic modifiers on the aggregation of the Aβ peptide. The thesis also focuses on biological aspects of such modifiers relating to Aβ peptide uptake. The aim of the thesis is to shed light on molecules and interactions that are important in the pathology of Alzheimer's disease (AD) and to address them from a biophysical and cell biological perspective. The aim of this chapter is to provide a general background on AD pathology and its relation to Aβ and to present different molecules that can interact with Aβ and have an influence on its aggregation and contribution to AD pathology.

AD is a fatal neurodegenerative disease that is characterised by a progressive loss of neurons and a concomitant reduction in cognitive function[64]. Alzheimer's disease is one of the most significant causes of death in the industrialized world[65] and the main cause of dementia globally[66]. The prevalence of AD is correlated with age, and the prevalence increases from 1% in ages lower than 64 years old to 10% and 30% after 65 and 85 years old respectively[65,67]. Around 50 million people are suffering from AD worldwide and this number is expected to double every 20 years[68,69] unless new discoveries are made to enable a cure or effective disease-modifying treatments. AD presents in both familial and sporadic forms. Familial AD can progress more rapidly in lower ages, but it only accounts for 5% of AD cases[70]. The familial forms of AD are often related to mutations in the Aβ precursor proteins APP or mutation in proteins playing a role in Aβ production, as explained later[71-73]. The sporadic forms of AD, which are called late-onset AD, develops at later ages compared to familial AD and are associated with certain risk factors such as genetic risk[74] and lifestyle[75] which can lower the age of onset of AD development significantly[76].

Amyloid-β aggregation and accumulation into so-called "senile plaques" in the extracellular spaces of the brain is the classic hallmark of AD[2]. AD is also associated with aggregation and accumulation of the tau protein into intracellular neurofibrillary tangles[77]. Amyloid-β was discovered in the mid-1980s for the first time[78] and later it was found that it is a proteolytic cleavage product of a membrane-bound protein which is called the amyloid precursor protein (APP)[79]. APP has 695 amino acids and localizes to the plasma membrane, the membranes of intravesicular cell compartments, the endoplasmic reticulum (ER) and the Golgi system[80]. The biological function of APP is not yet fully understood but it has been suggested that APP can function as a cell surface receptor[79], be involved in cell adhesion[81] or in intracellular signaling[82]. The Aβ release is the result of the sequential cleavage of APP by β- and γ-secretases leading to the release of Aβ peptides that are 38-42 amino acids in length[83,84]. β-secretase cleavage of APP produces a membrane-bound β-CTF domain with 99 amino acids that can further get cleaved by γ-secretase to release the Aβ peptides[65,80]. APP can also be processed via a non-amyloidogenic cleavage pathway initiated by α-secretase cleavage in the middle of the Aβ peptide sequence[80] (Fig. 10). The cleavage position of the β-CTF by γ-secretase determines the length and hence isoform of Aβ peptides. The majority of the peptides produced in the brain have 40 amino acids[85].

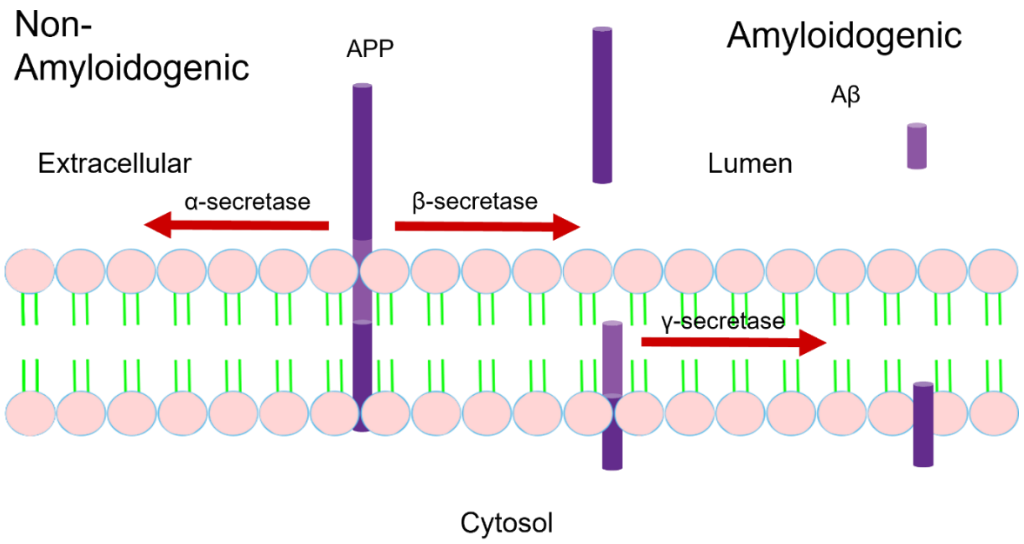

Figure 10. Schematic illustration of Aβ release through processing of APP via β- and γ-secretase. APP can also undergo non-amyloidogenic cleavage initiated by α-secretase.

The focus of this thesis is, however on the Aβ variant with 42 residues (Aβ(1-42)) as this, second most abundant isoform, is more prone to aggregation and found in higher proportion in the core of amyloid plaques[61,86]. Amyloid-β and APP play a pivotal role in AD pathogenesis, as evidenced by several mutations within the Aβ or within APP at sites that affect Aβ production. Hardy and Higgins proposed the so-called amyloid cascade hypothesis in 1992[87], suggesting that the accumulation of Aβ peptides into amyloid plaques is the initial event in AD. However, due to weak correlations between amyloid plaque loads and the severity of dementia[88], it is nowadays believed that the pathological role of Aβ peptides in AD starts earlier than with the accumulation of them into the amyloid plaques[89].

2.2 Amyloid-β and lipids

As discussed previously, Aβ peptides are released from a membrane-bound protein in various lipid rich environments, primarily endosomes[79]. Aβ peptides can thereafter be secreted from cells into the extracellular space[90,91] but also re-internalized via endocytosis [92,93]. This accentuates the importance of understanding the interactions of Aβ peptides with membrane lipids. Aβ aggregation can occur in both intra- and extracellular locations of the brain[80], but intraneuronal build-up of Aβ in endolysosomal compartments is one of the earliest pathological alterations in AD, suggesting that this is a preceding effect in the Aβ aggregation cascade[94,95]. Intracellular Aβ has, moreover, been found in association with lipid membrane rich environments including neuronal synapses[96], mitochondria[97], trans-Golgi network[98], endoplasmic reticulum (ER)[99] and endolysosomes[94,100,101]. The latter is in line with endosomal enlargement being an early pathological hallmark of AD[102,103]. Moreover, Aβ has been reported to play a role in lipid homeostasis[104-106] and Aβ-lipid interactions may directly induce cell toxicity through pore formation[107,108] and/or membrane fluidity alterations[109]. Various biophysical studies have shown that Aβ, in different forms, can interact with specific lipids or membrane compositions leading to modulation of Aβ amyloid formation[110]. Specific lipids such as glycosphingolipids, cholesterol and sphingomyelin which are at focus in this thesis and that are conspicuously found as co-aggregated species with Aβ in the core of amyloid plaques[111-113]. In addition, genetic risk factors for late-onset AD such as ε4 allele of the apolipoprotein E (APOE) encoding gene regulate the metabolism of cholesterol emphasizing the importance of the role of lipids, lipid regulation and membranes in Aβ pathology[76,114,115]. In this thesis, I explored the effect of lipid vesicles in the form

of high complexity and cell-derived biological extracellular vesicles (EVs), which are secreted from cells to fulfil various communication purposes, on the *in vitro* aggregation of Aβ. In addition, I investigated the effect of different lipids using synthetic lipid vesicles with systematic variations in lipid content to better understand how different lipids, individually or in combination, contribute to Aβ fibril formation.

2.3 Amyloid-β and metal ions

Metal ions are other moieties whose homeostasis are dysregulated in the brain of patients suffering from AD[116-118]. As for lipids, metal ions are found to co-aggregate with Aβ in the cores of amyloid plaques[119-121]. In addition, the interaction of redox-active metal ions such as copper (Cu) and iron (Fe) with Aβ can drive reactive oxygen species (ROS) production[122-126] and influence the oxidative stress responses of cells in a way that induces neurotoxicity in AD[127]. Dysregulation of Cu ion homeostasis in AD patients manifests as increased Cu level in plasma[116,128], but reduced levels in the amygdala and hippocampal brain regions[129]. The extracellular concentration of Cu in the brain is 0.2 -1.7 μM whereas concentrations of 400 μM have been found in amyloid plaques and of 15 μM in the synaptic cleft[118]. This thesis also focuses on Zn ions. They can be present at staggering 200-300 μM concentration in the synaptic cleft[116,118], but apart from this there is inconsistency in the reports of zinc levels in AD-afflicted brains. It has been proposed that the zinc level is reduced in the neocortex[130], the superior frontal and parietal, the hippocampus and the medial temporal gyrus and the thalamus[131,132]. By contrast, increased levels of zinc have been reported to occur in AD-afflicted amygdala[129,130,133,134], cerebellum[130], olfactory areas[133], hippocampus[129,130] and superior temporal gyrus[135].

It has been shown that metal ions interact with the N-terminus of the Aβ peptide. Cu^{2+} binds via 3N1O coordination resulting in the formation of N-terminal loop that engages the carboxyl group of Asp1, two imidazole nitrogens (His 6, His 13, or His 14) or Asp1 and all three histidines[136-139]. Cu^{2+}-Aβ dissociation constants are reported to be in the picomolar to low nanomolar range[140]. The interaction of Cu^{2+} with Aβ is dependent on the buffer conditions, for example, the binding affinity[141], stoichiometry[142] and coordination geometry[138,139,143] is pH sensitive. Cu^{2+} can bind to monomeric, oligomeric and fibrillar species of Aβ with comparable affinities. The Aβ peptide can also bind to Cu^{+} via a bidentate linear 2N coordination without loop formation that engages two N-imidazoles from His 13 and His 14[144]. The reported dissociation constant for Cu^{+}-Aβ interaction is in the femtomolar range showing that Cu^{+} has higher affinity for Aβ compared to Cu^{2+} [144,145]. Zn ions bind to the N-terminus of Aβ[146] via engaging three histidine residues (His 6, His 13 and His 14) and either Asp1 or Tyr 10 as the fourth ligand[147,148]. The reported dissociation constant for the Zn^{2+}- Aβ interaction is in the micromolar range and thus weaker than that of copper ions[140]. Furthermore, as for copper, a weaker binding of a second Zn^{2+} ion between amino acids 23-28 has been reported[149,150].

Previous *in vitro* studies have shown that both Cu and Zn ions modulate the aggregation of Aβ peptides into amyloid fibrils. However, the outcomes of different reports are not conclusive and both acceleratory and inhibitory effects have been reported[147,151-159]. Furthermore, very few studies address how Aβ-metal ions interactions affect the trafficking and localization of Aβ in the brain. One study suggests that Zn^{2+} could play a pivotal role in the uptake of Aβ peptides into dentate granule cells[160]. In this thesis, I address this further with a focus on the role of Cu/Zn ions on the cellular uptake and endolysosomal accumulation of Aβ.

2.4 Intracellular Aβ and endocytosis

Intraneuronal Aβ in both healthy and AD-afflicted persons was reported for the first time in 1989[161]. In the 1990s novel antibodies were developed that had epitopes on the C-terminal end of Aβ and hence could distinguish Aβ from APP. This allowed better detection of intracellular Aβ[162,163], and lead to the observation that it is especially Aβ with 42 amino acids that is accumulated intraneuronally. It has been suggested that Aβ accumulation starts intracellularly and that seeds, released from inside of cells, initiate the formation of amyloid fibrils and their association into extracellular plaques in AD[94].

Aβ can be effectively internalized into cells via endocytosis. Endocytosis is a process through which lipid vesicles, which are called endosomes, are formed from invaginations of the plasma membrane and it is a means for cells to internalize extracellular molecules[164]. Cells are also using endocytosis processes to regulate their plasma membrane composition, the availability of cell surface receptors and their membrane tension[165,166]. Endocytosis can be divided into clathrin-mediated endocytosis (CME) and clathrin-independent endocytosis (CIE). Clathrin-independent endocytosis can be sub-divided into dynamin-dependent and dynamin-independent endocytosis. Uptake of Aβ into cells is suggested to occur through both endocytosis dependent and independent paths. Besides the direct membrane penetration of Aβ peptides[167], several neurotransmitter receptors including glutamate receptor N-methyl-D-aspartic acid (NMDA)[168], acetylcholine receptor α7 nicotinic cholinergic receptor (α7nChR)[169] as well as apolipoproteins receptors including low-density lipoprotein receptor-related protein 1 (LRP1)[170] mediate the uptake of Aβ through clathrin mediated endocytosis (CME)[170]. In addition to CME, clathrin and dynamin independent endocytosis of Aβ have been reported[92,93].

2.5 Parkinson's disease

Parkinson's disease (PD) is the second most common neurodegenerative disorder after AD[171]. It is characterized by motor system malfunctioning[172-174] and can be associated with cognitive decline in some cases[171]. Similar to AD, PD is present in both sporadic and familial forms, with the familial forms causing around 10-15% of total cases[175].

The formation of cytoplasmic inclusions that are called "Lewy bodies (LBs)" is a pathological hallmark of Parkinson's disease[172]. The main component of Lewy bodies was found to be an intrinsically disordered amyloidogenic protein called α-synuclein (α-syn)[34] which is suggested to play a physiological role in neurotransmission and synaptic function[176]. The α-syn protein is composed of 140 amino acids and the primary sequence can be divided into three domains including an amphipathic N-terminal, the non-amyloid-β component (NAC) and the acidic C-terminal. The amphipathic N terminal is prone to fold into an α-helical structure that increases the affinity of α-syn for lipid bilayers[177]. The NAC region comprises amino acids 61-95, is highly hydrophobic, and essential for amyloid aggregate formation[108,177]. The majority of the familial forms of PD are associated with mutations in the SNCA gene that encodes for α-syn, pointing out the high relevance of α-syn amyloid formation in PD pathology[178].

3. Methodology

This Chapter describes the theory and application of some of the main methods that have been used in this thesis work.

3.1 Absorption and fluorescence spectroscopy

Fluorescence spectroscopy is an optical technique in which the emission of light from a sample is collected following light absorption and excitation of the molecules in the sample to a higher energy state. The energy of absorbed and emitted photons is described by Planck's postulate

$$E = hv = \frac{hc}{\lambda} \quad (2)$$

where h is the Planck's constant (h=6.626e-34 Js), v is the frequency of the photon and E is the photon energy. If the energy of light that interacts with a molecule, is identical to the energy difference between its ground state and an excited state (S_n, n > 0), the molecule can absorb the energy of the photon and reach the excited state. The absorbance of light can be measured by observing the intensity of light before (I_0) and after (I) interaction with the sample and this is used to, for example, determine the concentration of the absorbing molecules in a sample using the Beer-lambert law (Equation 3).

$$A(\lambda) = log\frac{I_0(\lambda)}{I(\lambda)} = \varepsilon cl \quad (3)$$

where c is the concentration of the absorbing molecule in the sample, ε is the molar extinction coefficient of the molecule at the measured wavelength of light, and l is the path length for light to pass through the sample.

The excited states of a molecule are energetically unfavorable; therefore, excited molecules dissipate the excitation energy and relax back to the ground state, either via emission or non-radiative processes. These processes are commonly depicted in a so-called Jablonski diagram (Figure 11).

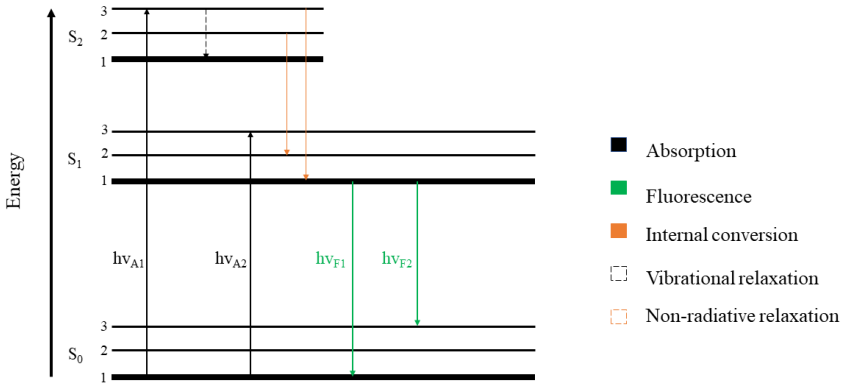

Figure 11. Jablonski diagram depicting the different relaxation pathways of excited molecule to the ground state. Note that the diagram does not show the phosphorescence pathway.

When a molecule returns to the ground state by emitting a photon it does so from the lowest level of the first excited state (S_1) and by releasing energy equal to the energy gap between (S_1) and one of the vibrational levels of the ground state (S_0). The emitted photon therefore typically has a lower energy than the absorbed photon. This is explained by Kasha's rule which states that the emission of a photon can only happen from the lowest excited state (S_1) because the vibrational relaxation processes to the lowest vibrational level of S_1 are much faster than the release of excitation energy through the emission of a photon. The difference between the energy of excitation and emission results in a wavelength shift between absorption and emission (fluorescence) which is referred to as the Stoke's shift. Molecules that emit light are denoted fluorophores. In addition to exhibiting specific excitation and emission properties which give rise to absorption and emission spectra, a fluorophore is also characterized by its fluorescence quantum yield. This is defined as the ratio between the number of emitted photons and the number of absorbed photons (Equation 4). Moreover, the product of extinction coefficient and fluorescence quantum yield is called brightness which is an important criterium for choosing a fluorophore molecule to be used in for example a microscopy experiment. The fluorophores with higher brightness give higher signal to noise ratio which makes studies more accurate.

$$\phi_F = \frac{Emitted\ photons}{Absorbed\ photons} \qquad Brightness = \varepsilon.\phi \tag{4}$$

Fluorescence emission of a sample in solution is typically recorded in a fluorimeter, but many instruments within life sciences use fluorescence read-outs, including optical microscopes, flow cytometers and plate readers as extensively used in this thesis.

In this thesis, absorption spectroscopy and Beer-lambert law was used for calculation of protein solutions concentration. The proteins I have used, i.e Aβ(1-42) and α-syn, have extinction coefficient equals to 1280 $M^{-1}cm^{-1}$ and 5960 $M^{-1}cm^{-1}$ respectively at 280 nm. Fluorescence emission spectroscopy is the main technique behind most of the experiments that have been done in this thesis, and it has been used extensively for aggregation kinetics monitoring, cellular uptake analysis and cellular viability assays in **paper I – IV** and **VI**, and for the visualization of single amyloid fibrils in **paper V**.

3.2 Circular dichroism spectroscopy

Circular dichroism (CD) is an absorption spectroscopy technique in which the difference between a sample's absorption of left-handed and right-handed circularly polarized light is measured. Chiral molecules, such as polypeptides, absorb the two forms of circularly polarized light differently and this gives rise to a CD signal. CD spectra (the collection of CD across a wavelength range) contain useful information about the secondary structure of polypeptides, especially if recorded in the far-UV spectral range. Due to the unique chirality of different secondary structures, the α-helix, β-sheet and random coil conformations of polypeptides display distinctly different CD spectra, making it possible to decipher secondary structure (Fig. 12).

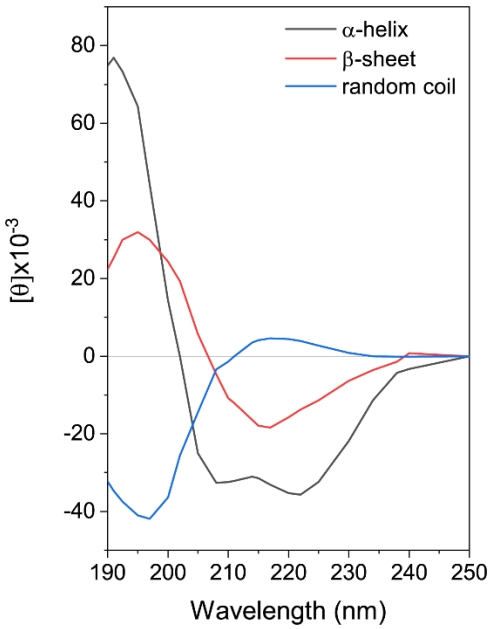

Figure 12. CD spectra of poly-L-lysine as α-helix (black), β-sheet (red) and random coil (blue). CD spectra adopted from Campbell & Dwek[179].

3.3 Fluorescence microscopy

The Stoke's shift, which makes it possible to excite a fluorophore with a specific wavelength of light and then collect the emitted light at a longer wavelength, is a backbone theory for fluorescence microscopy. In a fluorescence microscope, the specimen is illuminated by one or several specific wavelengths (from UV to the near-infrared), and the emitted light is subsequently separated by filters and or dichroic to collect only the longer wavelength-shifted emitted photons.

In wide-field fluorescence microscopy, the entire specimen or wide-field of view is illuminated via a beam of light which excites the fluorophores that the specimen contains, and the emission (fluorescence) is detected by an electronic camera to create an image. Wide-field microscopy provides the possibility to use cameras with fast shutters which increases the speed of imaging (number of frames per seconds). The major drawback of wide-field microscopy is, however, low contrast and low spatial resolution of the resulting image caused by the projection of out-of-focus light onto the image plane. Two main types of wide-field microscopic setups are transmission and epi-fluorescence microscopy. The epi-fluorescence microscope will be further explained below as it has been used in this thesis (**paper V**).

The optical pathway of the most common modes of transmitted light microscopy is depicted in Fig. 13. In this optical setup, light passes through an excitation filter and subsequently through a condenser to illuminate the specimen. The condenser consists of lenses and an aperture diaphragm, and it concentrates the light coming from the light source of the microscope into a cone of light. Fluorescence emitted from the sample passes through an objective lens which is located on the opposite side of the specimen, and it subsequently passes through a band-pass filter that provides wavelength selection.

In epi-fluorescence microscopes (Fig. 13), which are widely used in biological sciences, both the excitation and emission light passes through the objective. Therefore, the objective works also as a condenser. One of the most important components of an epi-fluorescence microscope is the dichroic mirror or dichroic beam splitter. This filter reflects light with wavelengths shorter than its cut-off

wavelength, while it transmits light with longer wavelengths so that only the fluorescence emission and not the excitation light reaches the detector.

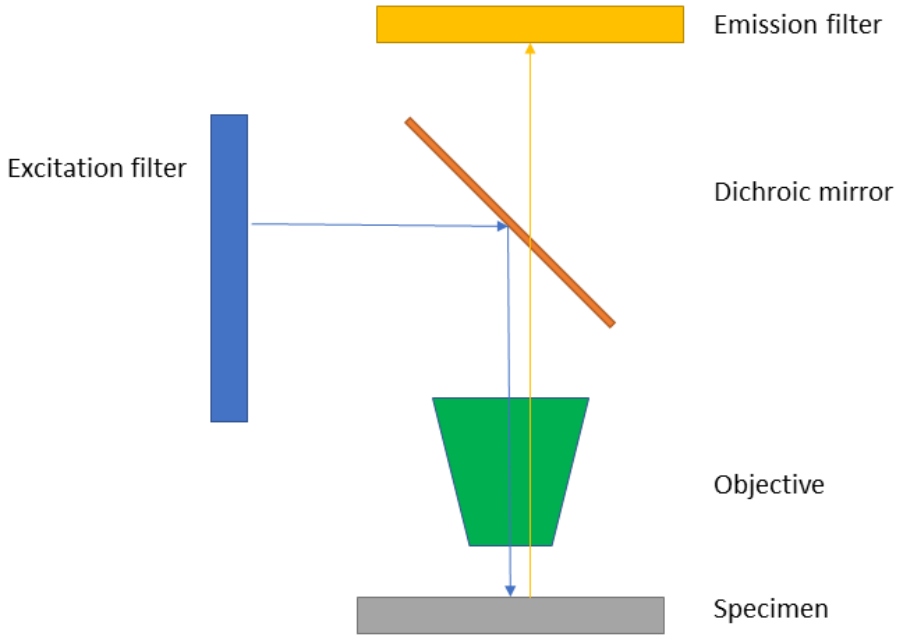

Figure 13. Schematic setup of the optics in an epi-fluorescence microscope.

In fluorescence microscopy various light sources can be used to illuminate the specimen. These days light or laser emitting diodes (LEDs) which emit light within a narrow wavelength range are widely used. A combination of LEDs with different wavelengths can be used to cover the visible region of the spectrum.

One of the most important components of a fluorescence microscope is the objective. It plays a main role in determination of quality, resolution, and magnification of the acquired image. In addition, the objective plays an important role in epi-fluorescence microscopy, as it both focuses the illuminating light, used for excitation of the specimen, as well as collects the fluorescence light to form the image of the specimen. The resolution limit of each objective is determined by three characteristics; the wavelength of the illuminating light, the refractive index of the immersion medium between the objective's front lens and the specimen, and the angular aperture of the light cone captured by the objective. The maximum resolution of each objective can be defined by the Rayleigh criterion

$$d = 0.61 \frac{\lambda}{NA} \qquad (5)$$

where d is the minimum resolvable distance or resolution, λ is the wavelength of the illuminating light and NA is the numerical aperture of the objective. The numerical aperture determines the ability of the objective to capture light and it is defined by

$$NA = n \sin \theta \quad (6)$$

where n is the refractive index of the immersion medium and $2 \times \theta$ is the angle of the cone of light which the objective is capable to collect.

In fluorescence microscopy, filters are used for collecting only light emitted from the intended fluorophore(s) and filtering out other unwanted light coming from the specimen. Moreover, filters are also used for passing through excitation light within the wanted spectrum even in systems in which monochromatic light sources such as LEDs are used. Basic filters are categorized in long pass, short pass, or band pass filters.

In conventional wide-field fluorescence microscopy, the resolution of the image is compromised by the collection of unwanted emitted light which originates from outside the point of focus. To overcome this obstacle confocal microscopy was developed by Marvin Minsky in the mid-1950s and further development in recent years has opened new possibilities for high resolution imaging, especially in biological sciences by providing deep visualization into live cells and tissue as well as constructing three dimensional images. In a confocal microscope, usage of a pinhole in front of the detector makes it possible to filter out out-of-plane emitted light. This technology boosts the optical resolution. The light pathway in confocal laser scanning microscopy is presented in Fig. 14. Light emitted by the laser passes through a pinhole aperture and is directed through the objective towards the focal plane of the specimen via reflection from a dichroic mirror. The laser beam excites the sample point-by-point by scanning a defined focal plane across the specimen. Emitted photons from both the focal plane and above/below pass through the objective and dichroic mirror, while only photons originating from the focal plane pass the second pinhole and are hence collected by a detector (as opposed to a camera in widefield microscopy).

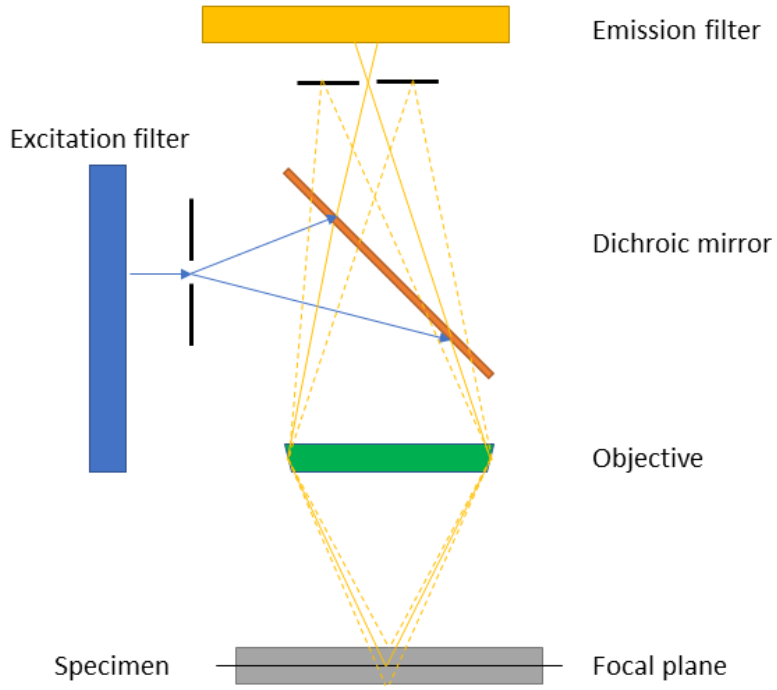

Figure 14. Schematic setup of the optics in a confocal laser scanning microscope.

In scanning confocal microscopes, lasers are the most common excitation sources. There are several types of lasers which elaborating on is far beyond the scope of this thesis.

In this thesis, an epi-fluorescence microscope was used to study Aβ(1-42) and α-syn amyloid fibrils formed from co-aggregation of fluorescently tagged proteins with wild type proteins. The fluorescent amyloid fibrils were studied inside the nanochannels and microchannels to characterise their physical properties in **paper V**. Confocal microscopy was used to study the uptake and distribution of fluorescently tagged Aβ(1-42) peptides by human neuroblastoma cells in **paper IV**.

3.4 Atomic force microscopy

In light microscopy, the resolution of an imaged object is limited by the diffraction limit of light. Several techniques, including advanced optical and electron microscopies have been invented to overcome this limitation. Atomic force microscopy (AFM) is one such technique. In AFM, a sharp probe scans across the sample and measures the surface contact forces between the sample and the probe, hence a topographical image of the specimen is produced (Fig. 15).

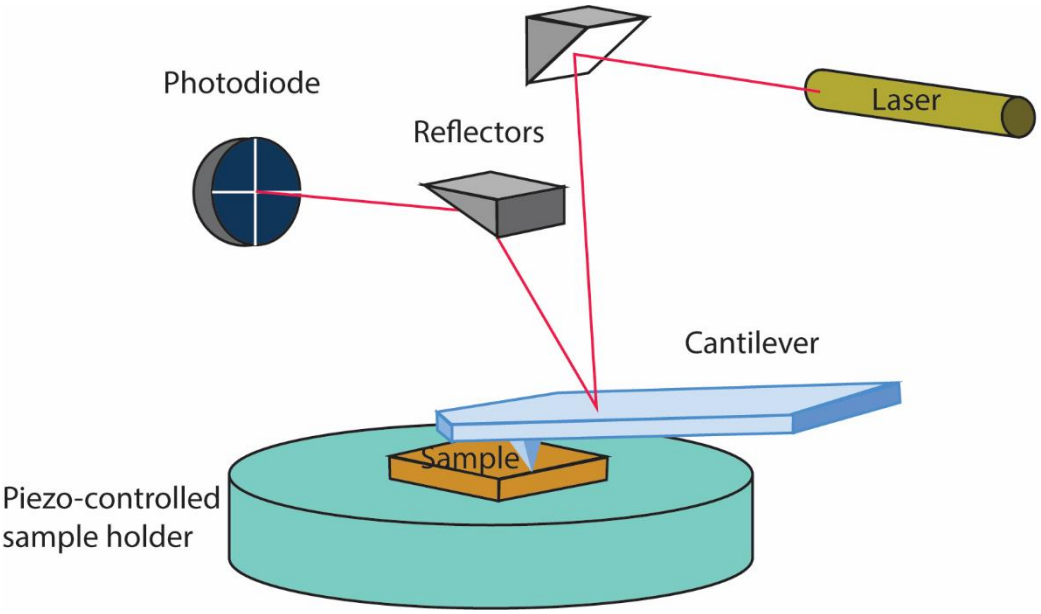

Figure 15. Schematic showing the setup of an atomic force microscope.

To be able to produce images with high resolution, the specimen needs to be stabilised on a surface that is atomically flat. The most commonly used surfaces for AFM imaging of biomolecules are mica and glass surfaces. In this thesis, mica surfaces were used to image amyloid fibrils. The mica surface with an immobilized sample is placed under the AFM scanning head containing the probe and a laser system for detecting the force of interaction of the probe with the sample. The detection laser is directed to the reflective cantilever to which the probe is attached. In this thesis AFM was run in so-called semi-contact mode in which the scanning probe is intermittently in contact with the sample. In the semi-contact mode, the instrument benefits from a piezo-electric crystal to oscillate the cantilever and it keeps the oscillation frequency constant as the probe interacting with the sample. AFM was used in most of my work in this thesis (**paper I-III** and **V-VI**) to study the morphology of amyloid fibrils. With the help of AFM, in addition to general morphological appearance of amyloid fibrils, we were able to retrieve accurate measurement of height and length of amyloid fibrils. In **paper V**, in addition to height and

length of fibrils, the persistence length of amyloid fibrils was estimated from AFM images using the Easyworm software[180].

3.5 Flow cytometry

Flow cytometry is a technique that provides rapid analysis of cells in solution on a cell-by-cell basis. It is used to distinguish and count different cell types in heterogeneous samples and/or to detect specific biomolecular features of the cells using fluorescent markers. Flow cytometry instruments use different techniques to separate cells for one-by-one analysis, including sheath flow and microcapillaries. The instrument that was used in this thesis was equipped with a microcapillary system to separate cells by passing them through a very narrow dimension that presents the one-by-one in front of the flow cytometer's laser system and detector (Fig. 16).

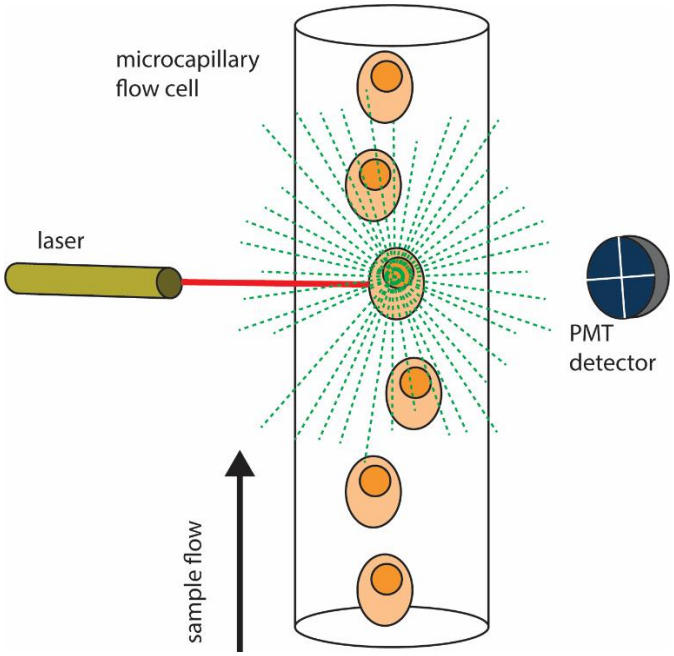

Figure 16. Schematic showing the setup of microcapillary flow cytometer.

The flow cytometer measures both scattered light and emitted fluorescent light from the cells as they pass through the detection point. The scattered light is typically collected as both forward and side scatter. The intensity of the forward scatter provides information about the size of the analysed cell whereas the side scatter provides information about its granularity. The forward (FSC) and side (SSC) scatter is typically analysed in a dot plot, where a population of homogenous cells (for example viable cells of a specific cell type) will appear as a cluster, whereas cell debris, dying cells or other cell types typically appear as distinct. Typically, flow cytometers are equipped with several lasers to enable multiparametric fluorescence analysis. The emitted fluorescent photons are typically collected through photomultiplier tubes (PMTs) coupled with suitable band pass filters. Flow cytometry was used in this thesis to quantify the uptake of Aβ(1-42) and dextran 10 kDa in **paper IV**.

3.6 Large unilamellar vesicles preparation

Lipid vesicles were prepared by hydrating lipid mixture in sodium phosphate buffer (20 mM, pH 8) leading to spontaneous formation of lipid vesicles. This typically results in the formation of multilamellar vesicles, but freeze-thaw cycling by immersion of the sample in liquid nitrogen followed

by fast thawing in a heat block with temperature above the lipids' phase transition temperatures helps towards the formation of more unilamellar lipid vesicles. Unilamellar lipid vesicles are commonly used as model systems in biophysical assays. They are often divided into three groups based on their size. Small unilamellar vesicles (SUVs) have typically diameters between 10 to 80 nm. Large unilamellar vesicles (LUVs), as used in this thesis, are typically have diameter between 50 to 200 nm and the unilamellar vesicles with diameters larger than 200 nm are often called giant unilamellar vesicles (GUVs). LUVs with a specific diameter can be obtained by extruding a sample containing unilamellar vesicles through a polycarbonate filter with suitable pore size. In this thesis, large unilamellar vesicles with 100 nm diameter were prepared by the extrusion method and used in **paper II** as model membranes to study the effect of different lipids on the aggregation of Aβ(1-42).

3.7 Recombinant expression and purification of proteins

Proteins can be produced synthetically if sufficiently small (essentially only possible for peptides due to the errors associated with each amino acid conjugation step) or through recombinant expression in a microorganism. Synthetic production of proteins has several drawbacks including intrinsic impurity. In amyloid formation experiments, it is very critical to start the aggregating reaction from monomer solutions with high purity and homogeneity to study the true kinetics of aggregation. For this reason, purification of a recombinant protein has shown to be superior compared to the use of synthetic proteins/peptides. However, expression and purification of aggregation prone proteins is challenging as they tend to aggregate and/or form insoluble inclusions. To overcome this issue, Abelein et al.[181] made a fusion protein of Aβ(1-42) tagged with an N-terminal domain (NT) of a spider silk protein (spidroin), including a tobacco etch virus (TEV) cleavage site. This has made it possible to produce and purify Aβ(1-42) with high efficiency using BL21(DE3) *E.coli*. In this thesis Aβ(1-42) was expressed from a NT*-Aβ(1-42) encoding plasmid in *E.coli* bacteria. The Aβ(1-42) peptides were purified using immobilized metal affinity chromatography (IMAC) and size exclusion chromatography (SEC). The Aβ(1-42) peptide solutions were lyophilized after purification and dissolved in guanidinium hydrochloride GuHCl and purified once more through SEC immediately prior to each experiment.

3.8 Assays for amyloid aggregation kinetics

After collecting purified monomeric Aβ(1-42) peptides, the aggregation of Aβ(1-42) monomers into amyloid fibrils were monitored using thioflavin T (ThT) fluorescence (Fig. 17). The ThT fluorophore behaves as a so-called molecular rotor. It has a very low quantum yield in solution because it can dissipate its excitation energy through rotational relaxation around a central single bond (Fig. 17). When ThT binds to the regular β-sheet structure of amyloid fibrils, the rotation is restricted, therefore, the ThT molecule will instead dissipate its excitation energy via the emission of light (fluorescence), hence increasing the fluorescence quantum yield. The ThT fluorescence intensity is often proportional to the number of amyloid fibrils formed and ThT does not perturb the aggregation reaction, hence it is a good reporter of aggregation kinetic.

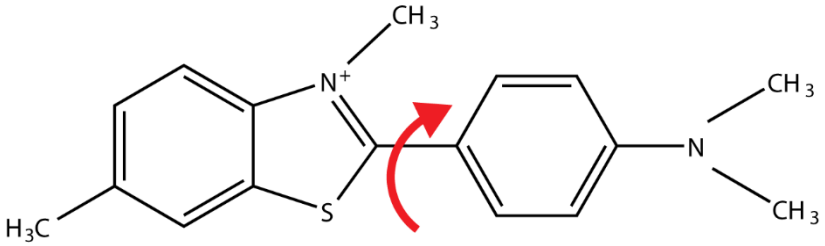

Figure 17. Chemical structure of thioflavin T (ThT). The unconjugated central carbon bond which allows molecular rotation is marked with the red arrow.

The aggregation reaction kinetics can be fitted using mathematical models as described in section 1.4 to obtain the rate constants of different mechanisms involved in the aggregation process. In this thesis, the online Amylofit platform was used to fit the aggregation data with a mathematical model.

Original work

4. Lipid and Aβ fibril formation

This section describes the main results of **paper I** and **II**, which explores the effect of lipids and vesicles on the aggregation mechanism and kinetics of monomeric Aβ(1-42) into amyloid fibrils. In **paper I**, we studied how cell-derived extracellular vesicles (EVs) influence the aggregation of Aβ(1-42) into amyloid fibrils and explored how EVs altered the morphology of the resulting fibrils. In **paper II**, we addressed, systematically, the effect of synthetic lipid vesicles (LUVs) composed of different brain-relevant lipids.

4.1 Cell-derived extracellular vesicle inhibit Aβ(1-42) amyloid formation

Extracellular vesicles (EVs) have gained significant attention in recent years as potential disease biomarkers as well as therapeutic agents[182]. They have also been suggested to have pathological roles in various diseases, including in neurodegenerative disorders such as AD[183] where they could contribute to the cell-cell transfer of protein aggregates that is commonly referred to as prion-like propagation[184]. This putative role of EVs in AD pathology brought us to investigate their effect on the aggregation kinetics of monomeric Aβ(1-42) into amyloid fibrils. We also assessed the effect of EVs on the morphology of the resulting fibrils. The ThT assay (Chapter 3.8) was used to monitor the change in aggregation kinetics in presence of increasing concentrations of EVs purified from the conditioned serum-free medium (CM) of human neuroblastoma cells (SH-SY5Y) and embryonic kidney (HEK293-T) cell cultures. Our results show that EVs from both cell types inhibit the aggregation of Aβ(1-42) (Fig 18a-b) as further depicted by the increase in aggregation reaction half-times (Fig. 18c). Interestingly, EVs from the two different cell lines were found to have the same inhibitory effects. Moreover, the highest concentrations of EVs used were 7.2e9 particles per milliliter, which approximatiely corresponds to a concentration of 4 µM lipid in a 100 nm LUVs system (representing the way we report lipid vesicle concentrations in **paper II**). This shows that EVs have a much stronger inhibitory effect on the aggregation of Aβ(1-42) compared to lipid vesicles made out of a limited number of different lipids and in absence of membrane associated proteins which are abundant in EVs.

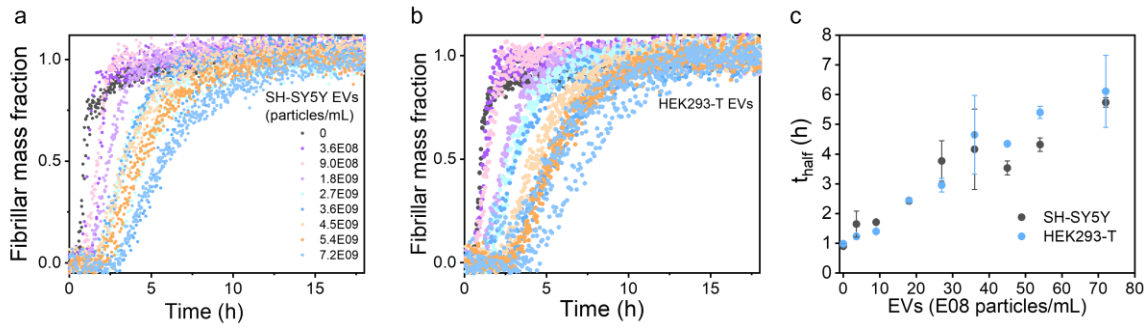

Figure 18. Aβ(1-42) aggregation kinetics in the presence of EVs. a-b, Normalized aggregation kinetics of 2 µM Aβ(1-42) in presence of increasing concentrations of EVs purified from a, SH-SY5Y and b, HEK293-T cells. c, Normalized Aβ(1-42) aggregation reaction half-times as function of EV concentration, derived from the data in a and b.

To better understand the mechanism by which the EVs slow down Aβ(1-42) aggregation, we repeated the kinetics experiments, but this time in presence of pre-formed Aβ(1-42) amyloid fibril seeds. Seeding bypasses primary nucleation. Furthermore, the addition of high concentrations of seeds changes the

dominating mechanism of aggregation from secondary nucleation to elongation[52]. We observed an inhibitory effect of EVs under both seeded conditions (Fig. 19) which thus suggest that EVs inhibit the aggregation reaction by interfering with elongation process, that is the attachment of monomers to the growing fibril ends.

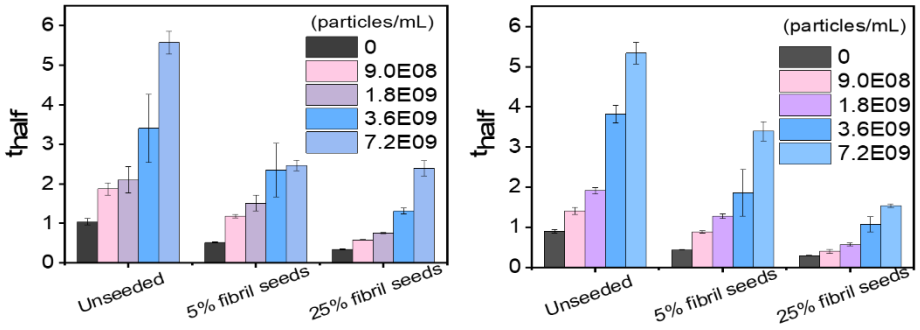

Figure 19. Seeds effect on the Aβ(1-42) aggregation halftime in presence of EVs. a, Half-time of seeded aggregation of Aβ(1-42) in presence of EVs purified from SH-SY5Y cells. b, Half-time of seeded aggregation of Aβ(1-42) in presence of EVs purified from HEK293-T cells.

To complement the seeding experiments, we fitted mathematical models of amyloid formation to the aggregation kinetic data as explained in section (1.4). We observed that the best fit (mathematically assessed by the lowest error value) was obtained when the elongation rate constant (k_+) was fitted as a free parameter, supporting the conclusion that EVs inhibit fibril elongation. The fitting suggests that the elongation rate decreases approximately 30-fold and 40-fold in presence of the highest concentrations of EVs.

In addition to inhibiting Aβ(1-42) aggregation, we found that the EVs induce the formation of significantly shorter amyloid fibrils (Fig. 20). This is an expected consequence of elongation inhibition. In addition, we observed that presence of EVs resulted in the formation of thicker fibrils which we ascribe to and discuss in terms of co-aggregation of EVs-associated proteins and/or lipids with the amyloid fibrils.

In **paper I**, we show that EVs inhibit the elongation of Aβ(1-42) amyloid fibrils and induce the formation of short fibril fragments. This suggests that EVs can have both neuroprotective effects by delaying the progression of Aβ aggregation and putatively neurodamaging effects by inducing the formation of short fibrillar Aβ(1-42) species that are more reactive in a cellular context[185]. **Paper I** thus extends the current knowledge around the role of cells-derived EVs in Aβ pathology.

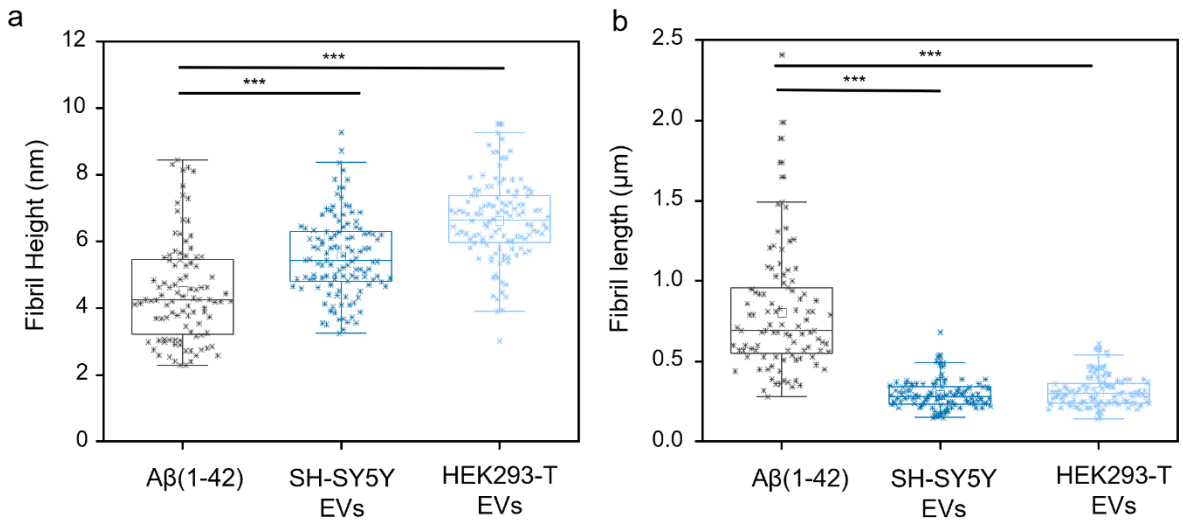

Figure 20. Morphological characterisation of Aβ(1-42) amyloid fibrils. a, Aβ(1-42) fibrils height formed in absence and presence of 7.2e9/mL EVs. b, Aβ(1-42) fibrils length formed in absence and presence of 7.2e9/mL EVs.

4.2 Lipid-induced inhibition and acceleration of Aβ amyloid aggregation

After the identification of the inhibitory effect of EVs on the aggregation of Aβ(1-42) in **paper I**, we were interested to understand the effect of AD pathogenesis-associated lipids on the Aβ(1-42) amyloid formation mechanism. Therefore, we made large unilamellar vesicles (LUVs) with DMPC as a base and with different proportions of GM1, cholesterol (Chol) and sphingomyelin (SM) lipids. We used DMPC as the base in our vesicles since it does not affect the aggregation of Aβ(1-42) as also shown by others[47]. We prepared a total of 20 different LUVs with different combinations of 10 or 20 mol% of GM1, SM or Chol. After characterization of the membrane fluidity of a subset of these LUVs using the Laurdan fluorescence assay (Fig. 21), we monitored the effect of these LUVs on the aggregation kinetics of monomeric Aβ(1-42) peptides (2 µM) into amyloid fibrils (Fig. 22).

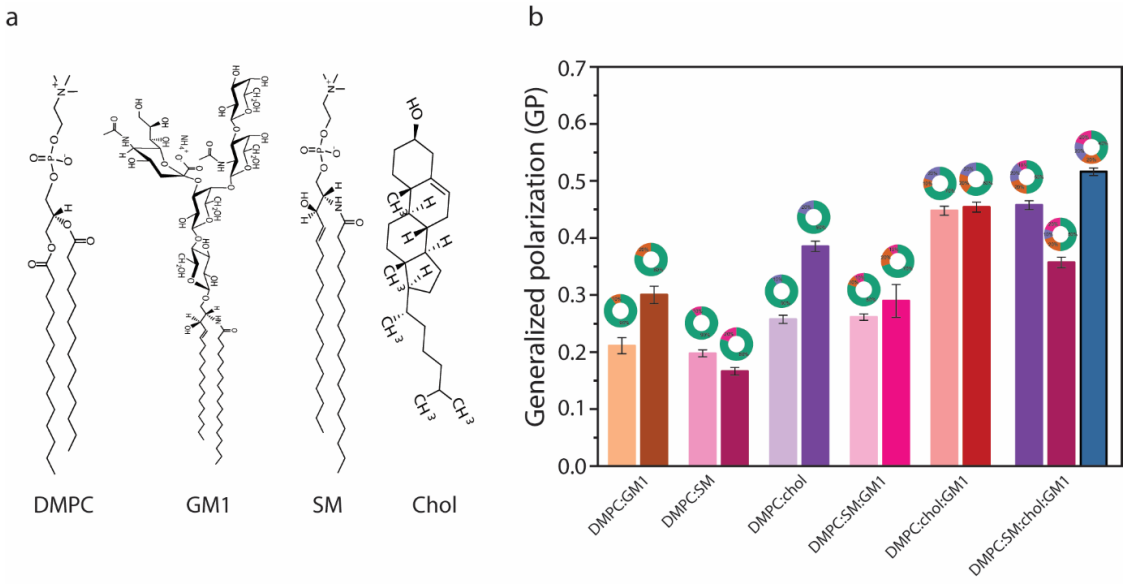

*Figure 21. Chemical structure of the different lipids used in this study. **b** Generalized fluorescence polarization (GP) of Laurdan recorded at 37°C.*

Our result show that LUVs composed of DMPC and 10-20 mol% GM1 inhibit Aβ(1-42) amyloid formation while presence of 10-20 mol% Chol or SM in DMPC-based LUVs accelerate the aggregation reaction (Fig. 22a-f). In addition to studying the individual effects of these lipids, we systematically explored their combinations into more complex lipid membranes. We observed that in the case of SM:GM1 mixtures, the SM lipid retained its acceleratory effect, dominating the aggregation rate of Aβ(1-42) and overruling the observed inhibitory effect of GM1 (Fig. 22i-j) whereas in LUVs with Chol:GM1, we observed competition between Chol-mediated acceleration and GM1-mediated inhibition that was dependent on total lipid concentration (Fig. 22g-j).

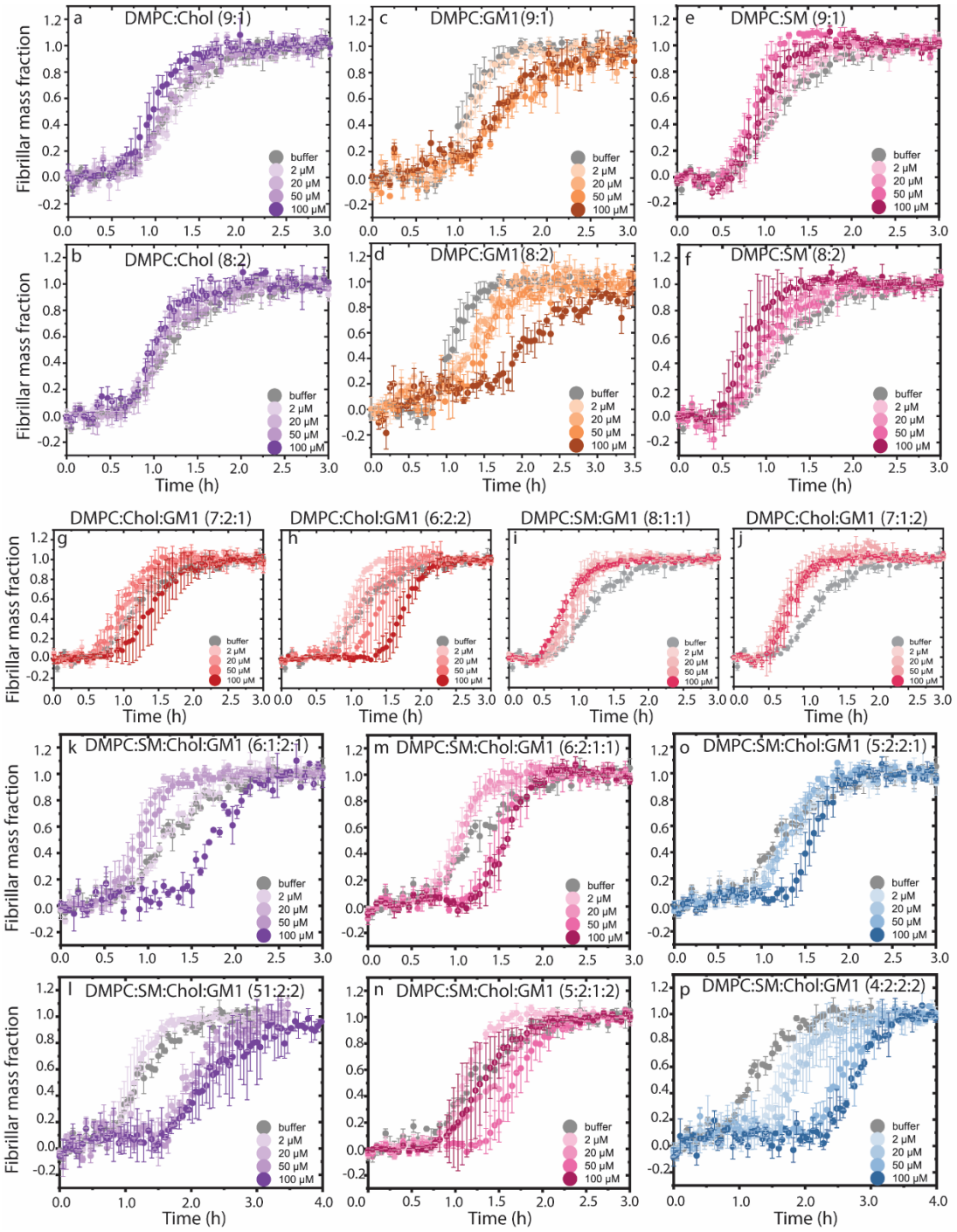

Figure 22. Aggregation kinetics of 2μM Aβ(1-42) in absence (buffer) or presence of 2-100 μM (lipid equivalents) of the different lipid vesicles as denoted in the headings. The numbers in parenthesis represents molar ratio of the different lipid constituents.

Thereafter, we parameterised the Aβ(1-42) aggregation kinetic curves to obtain reaction half-times, lag-times and growth-times (Fig. 23). The data in this figure show that there is a qualitative good correlation between the increase in reaction half-times and lag-times suggesting that the duration of the lag-phase is the dominating determinant of the reaction rate of Aβ(1-42). The trends were also clearly related to GM1 content. Based on this, seeded data and mathematical modelling of kinetic curves we could conclude that GM1 inhibits primary nucleation. In parallel, we observed that almost all LUVs induced a decrease of the growth-time of Aβ(1-42) aggregation, suggesting that a wide variety of membrane compositions may commonly lead to catalysis of secondary nucleation. This points out the complexity and intricate balance of different aggregation modulatory factors in biological membranes.

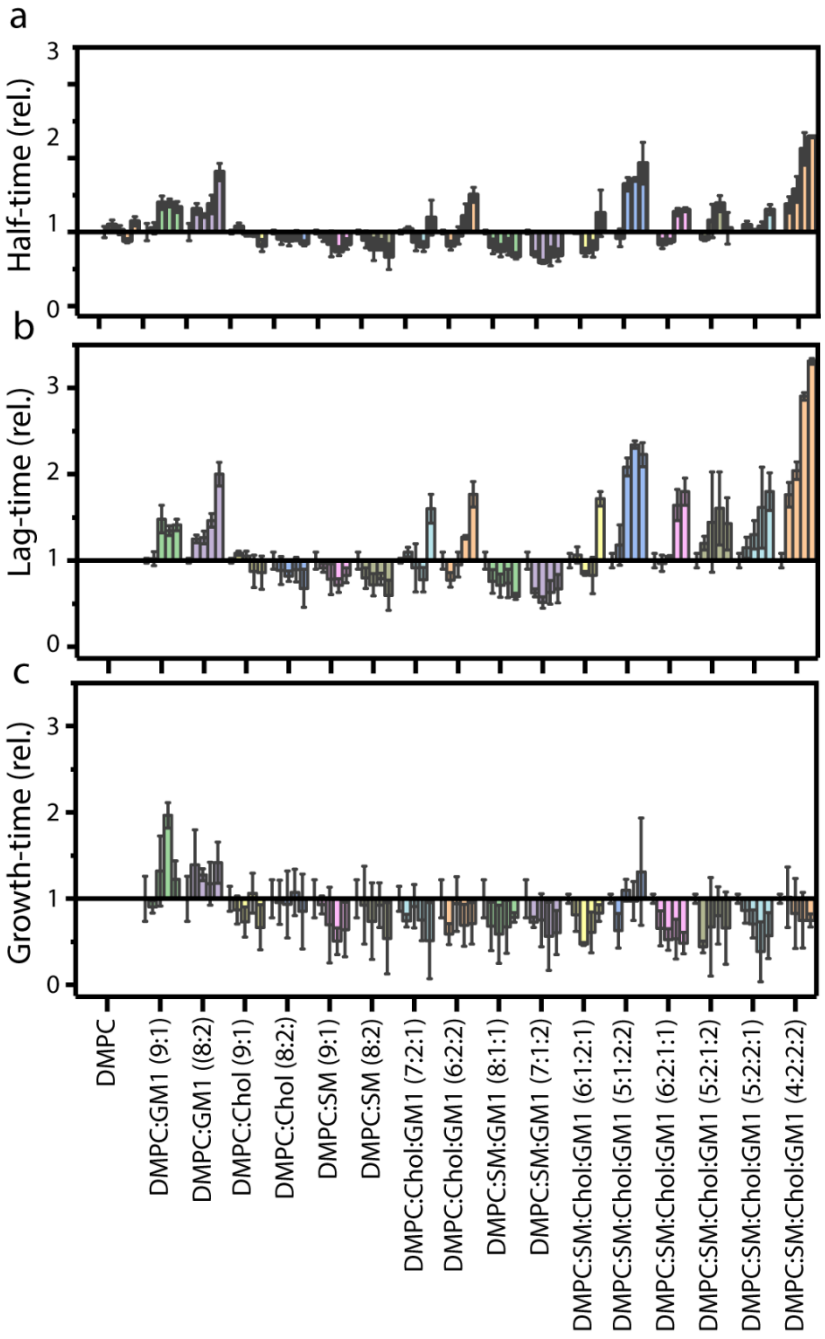

Figure 23. Normalized change in half-time, lag-time and growth-time of Aβ(1-42) aggregation taken from the kinetic curves in Fig. 22.

We further determined the exact mechanisms of respectively Chol-mediated and SM-mediated catalysis of Aβ(1-42) aggregation. Incorporation of Chol in DMPC membranes was found to induce primary nucleation, a conclusion that corroborates previous results by Habchi et al.[47]. We suggest that Chol increases head-group spacing and facilitates hydrophobic interactions at the membrane interface such that Aβ(1-42) monomers can oligomerize. SM, on the other hand, appears to mainly fluidize the lipid bilayer and, as such, enhances secondary nucleation.

After having determined the principle modulatory mechanisms of GM1, Chol and SM in isolation, we next investigated the balance between GM1-mediated primary nucleation inhibition and the catalytic effects of Chol or SM using ternary composition LUVs. As mentioned above, Chol and GM1 appears to compete in a lipid concentration-dependent manner. The catalytic effect of Chol dominates at low lipid concentrations where the peptide-to-lipid ratio is high, presumably because this facilitates oligomerization. GM1, on the other hand, dominates at high lipid concentrations which we propose is related to its ability to sequester Aβ(1-42). The competition between SM and GM1 is different since the SM-mediated acceleratory effect completely dominates already with 10% mol SM and since an increase in GM1 content does not alter the Aβ(1-42) aggregation rate (Fig. 22, 23).

Lastly, we studied the kinetics of Aβ(1-42) aggregation in presence of LUVs with quaternary lipid compositions, containing different ratios of DMPC, GM1, Chol and SM. These lipid vesicles had high Laurdan GP values (Fig. 21) indicating that their membranes are in mixed L_o/L_d phase, which is consistent with the propensity of such lipid mixtures to form lipid rafts. The quaternary LUVs showed diverse effects on the aggregation kinetic of Aβ(1-42) ranging from strongly inhibitory in LUVs with high GM1 and Chol content (Fig. 22, 23) to rather benign effects in LUVs with high levels of SM. Throughout, there was, however, a strong positive correlation between the extension of the lag-times and the reaction half-times (Fig. 23), emphasizing, the importance of the lipid membrane's ability to modulate primary nucleation. Notably SM retains some of its ability to accelerate Aβ(1-42) aggregation at high peptide-to-lipid ratios (low total lipid concentrations). However, in the complex mixture LUV systems, SM can no longer dominate the aggregation behavior of Aβ(1-42), presumably because it takes on a different role when it contributes to facilitating the formation of lipid rafts which have new biophysical properties that override the some of the lipids' individual effects. On the other hand, our data suggest that the GM1-mediated inhibition of the Aβ(1-42) aggregation kinetics is stronger in the quaternary LUV systems and thus facilitated by membrane segregation and the formation of lipid raft domains.

In conclusion, we have used kinetic analyses to reveal a specific, inhibitory effect of GM1 gangliosides in the aggregation of Aβ(1-42). GM1 binds soluble Aβ(1-42), retards primary nucleation, and delays the onset of aggregation. The inhibition is significantly aggravated by raft-enabling Chol and SM, although these lipids, individually, catalyse Aβ(1-42) aggregation by altering head-group spacing and hydrophobic core exposure of membranes. These results identify important trade-offs between the specific chemical properties of lipids and their general contributions to the physical state of membranes, thereby helping to rationalize the role of lipids in the molecular pathology of Alzheimer's disease.

5. Metal ions and Aβ pathogenesis

This Chapter describes the main results of **papers III** and **IV** and focuses on how metal ions may contribute to Aβ pathogenesis, both in the context of amyloid formation and the interactions of Aβ(1-42) with cells. In **paper III**, we investigated the effect of copper ions, in both redox form, on the *in vitro* aggregation of Aβ(1-42) peptides into amyloid fibrils. In **paper IV**, we focused on the effects of copper, and also zinc, ions on the uptake of Aβ(1-42) into human neuroblastoma cells and discovered a new co-uptake mechanism. Furthermore, we explored the cellular consequences of this co-uptake by analyzing transcriptomics profiles of the cells aiming to gain deeper understanding of the down-stream effects of the accumulation of metal ions and Aβ(1-42) peptides in endolysosomes.

5.1 Copper ions modulate Aβ amyloid fibril formation

The core of this subsection consists of results of **paper III**. Despite relatively extensive research on the interactions of copper ions with Aβ peptides[158] and the subsequent effects of such interactions on amyloid formation, the literature has been rather inconclusive and has not contained detailed information on the mechanistic effect of copper ions on the aggregation process, as discussed in detail in section 2.3. Therefore, in **paper III**, we revisited the question of how copper ions influence Aβ(1-42) aggregation into amyloid fibrils using detailed kinetic analyses of the type also used in **papers I** and **II**. First, we studied the kinetics of 2.6 μM Aβ(1-42) in presence of increasing concentrations of divalent copper ions (Cu^{2+}). The concentration range of Cu^{2+} was chosen to obtain a metal to protein ratio from 0.5 to 2 since the binding stoichiometry of Cu^{2+} to Aβ(1-42) is reported as 1:1[186], but in some cases also 2:1 albeit with much weaker binding affinity for the second ion[136]. Our results show that the Cu^{2+} slows down the aggregation of Aβ(1-42) into amyloid fibrils (Fig. 24). In addition, we observed that the endpoint ThT fluorescence emission decreased with increasing concentrations of Cu^{2+}. Therefore, we speculated that Cu^{2+} not only slows down the aggregation reaction, but also prevents amyloid formation.

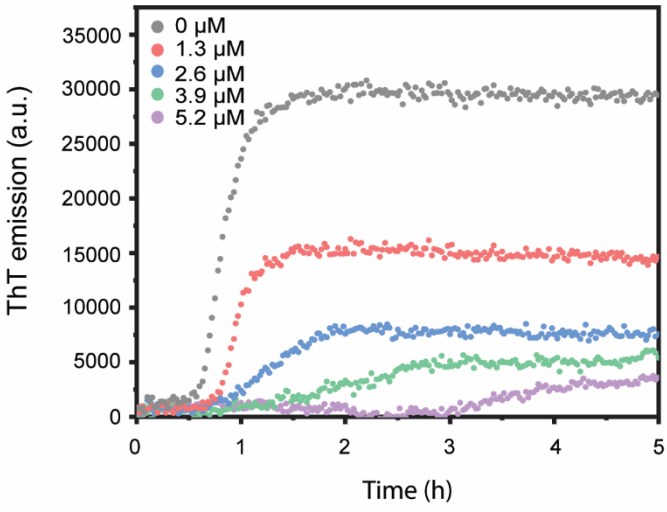

Figure 24. Amyloid formation kinetics of 2.6 μM Aβ(1-42) in absence and presence of increasing concentration of Cu^{2+}.

To prove our speculation, we performed a dot blot assay with the conformation-specific LOC antibody which recognizes amyloid fibrils[187]. The dot blot assay confirmed that Cu^{2+} reduces the amount of Aβ(1-

42) fibrils formed (Fig. 25). To understand the mechanism by which Cu^{2+} interferes with the aggregation process we performed seeded aggregation experiments and fitted the kinetic data.

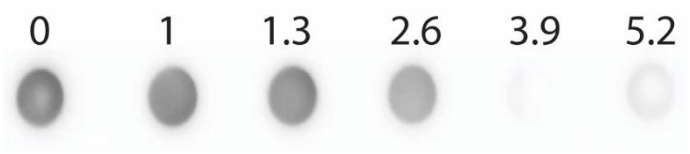

Figure 25. Dot blot assay showing LOC positive Aβ(1-42) fibrillar species formed in absence and presence of Cu^{2+} at the endpoint of the kinetic experiment shown in Fig 24.

We observed that the Cu^{2+}-mediated inhibition of Aβ(1-42) amyloid formation was retained under both low (5%) and highly (25%) seeded conditions (Fig. 26). As discussed for EVs in **paper I**, this is an indication of that Cu^{2+} slows down fibril elongation. This was further confirmed by mathematical fitting of the aggregation kinetic data, which showed that the best fit when the elongation rate constant (k_+) was probed as a fitting parameter and the primary nucleation (k_n) and secondary nucleation (k_2) rate constants were fitted as fixed global parameters (Fig. 26). The estimated elongation rate constant (k_+) overlapped very well with the elongation rate constant obtained from the slope of the fitted line to the initial growth phase upon aggregation of Aβ(1-42) in presence of 25% seeds (Fig. 26f). Altogether these observations support our conclusion that Cu^{2+} inhibits Aβ(1-42) aggregation by acting on the fibril elongation step.

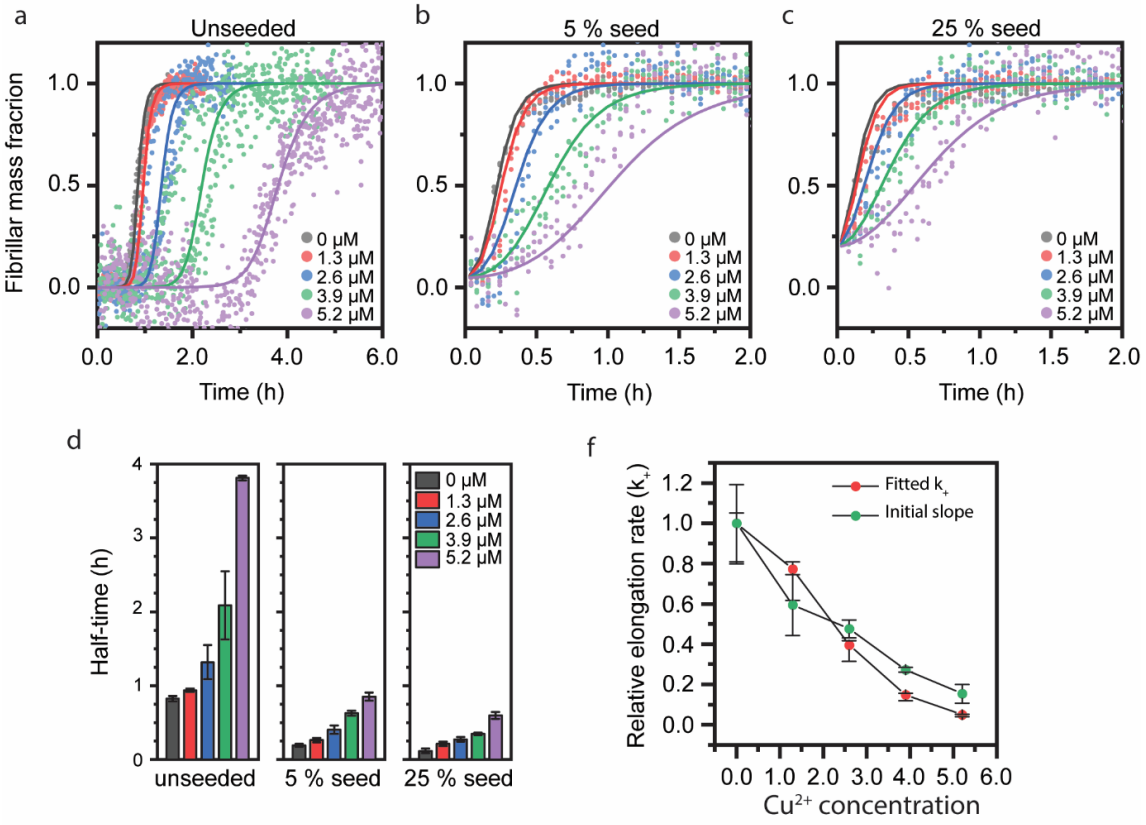

Figure 26. Effect of Cu^{2+} on seeded Aβ(1-42) amyloid formation. a-c, Normalized kinetic profiles of 2.6 μM Aβ(1-42) in absence and presence of Cu^{2+}. Solid lines are the global fits to data using a model for Cu^{2+}-dependent variation in the elongation rate constant (k_+). d, Half-times of Aβ(1-42) aggregation, extracted from the data in (a-c). f, Relative change in the elongation rate constant (k_+) determined from the fitting compared to the relative rate determined via the linear approximation of the initial slope at 25% seeds.

After having established the inhibitory mechanism of Cu^{2+}, we explored the pH-dependence of this effect, which is relevant in light of the acidification of the endolysosomes. The importance of addressing this question relates to the fact that early pathological aggregation and accumulation of Aβ(1-42) in AD occurs in the endolysosomes[80]. To be able to lower the pH down to 5.0 which is the lysosome-associated pH, we used 200 mM citrate phosphate buffer. We observed that at pH 7.0 and 6.0, Cu^{2+}-mediated inhibition became extra potent with extended lag-phases and increased halftimes (Fig. 27). We propose that the coordination mode and binding stoichiometry of Cu^{2+}-Aβ(1-42) which involves histidine residues and is thus pH dependent, causes this effect. However, upon lowering the pH to 5.0 where histidine residues become fully protonated resulted in a complete obviation of the interaction between Cu^{2+} and Aβ(1-42) and hence no effect on the peptide's aggregation rate. This suggests that Cu^{2+} is an extracellular inhibitor of Aβ self-assembly.

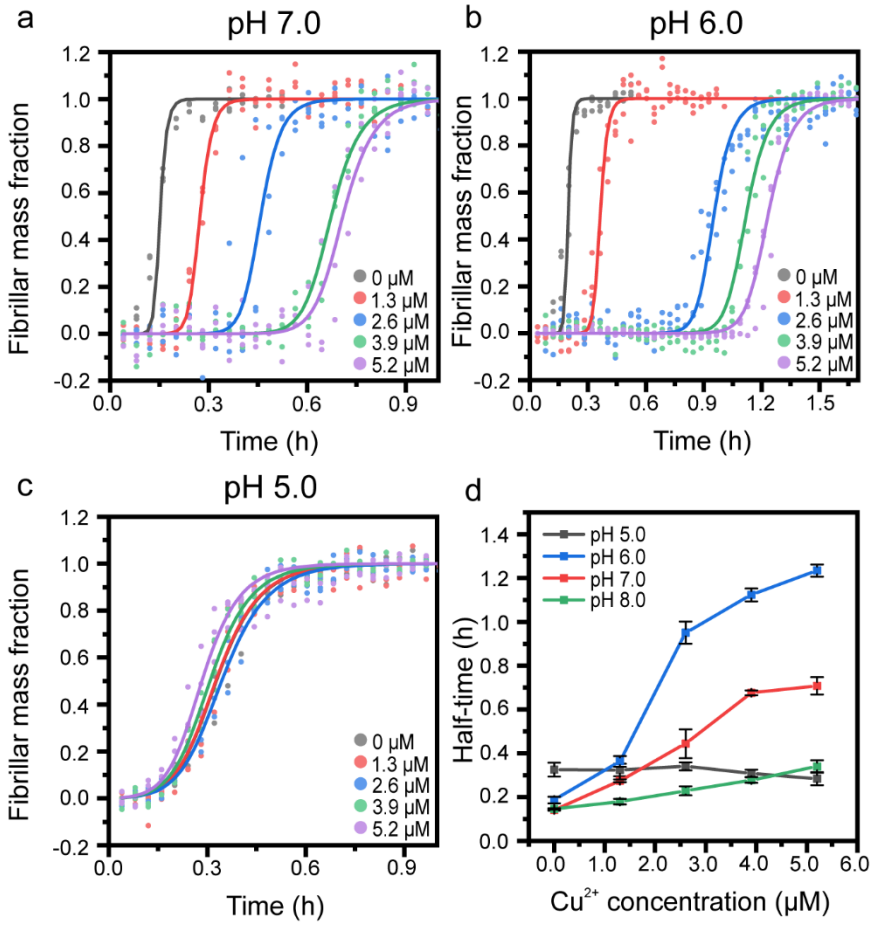

Figure 27. Cu^{2+} inhibition of Aβ(1-42) amyloid formation at different pHs. a, Normalized kinetic profiles of 2.6 μM Aβ(1-42) in a 200 mM sodium phosphate buffer, pH 7.0. b, Normalized kinetic profiles of 2.6 μM Aβ(1-42) in a 200 mM sodium phosphate buffer, pH 6.0. c, Normalized kinetic profiles of 2.6 μM Aβ(1-42) in a 200 mM sodium phosphate buffer, pH 6.5. d, Half-times of the aggregation of 2.6 μM Aβ(1-42) at various pHs in the presence of increasing concentrations of Cu^{2+}.

Copper can exist in two redox states (Cu^{2+} and Cu^{+}) outside and inside cells but previous studies on the interaction with Aβ(1-42) have mainly focused on the oxidized form (Cu^{2+}). In **Paper III**, we therefore explored the effect of Cu^{+} on the aggregation of Aβ(1-42), using dithiothreitol (DTT) as a reducing agent. Opposite to Cu^{2+}, Cu^{+} showed a modest acceleratory effect on the aggregation of Aβ(1-42) (Fig. 28). Seeded aggregation experiments in presence of Cu^{+} showed that the modulatory effect of Cu^{+}

disappeared in presence of the seeds (Fig. 28) and we could therefore conclude that Cu^{+} accelerates the primary nucleation rate, as was further confirmed by fitting of the aggregation data.

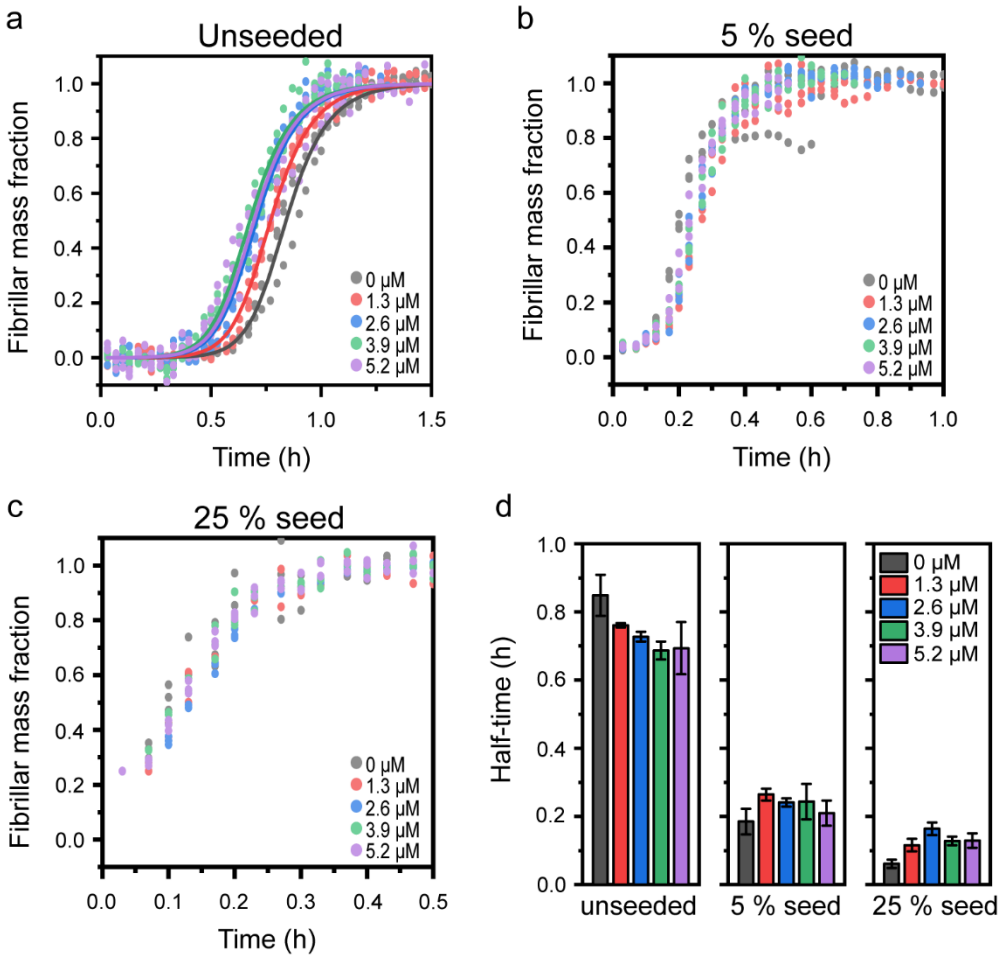

Figure 28. Effect of Cu^{+} on the seeded Aβ(1-42) amyloid formation. a-c, Normalized kinetic profiles of 2.6 μM Aβ(1-42) in the presence of indicated concentration of Cu^{+} and seeds. d, Half-times of Aβ(1-42) aggregation extracted from data shown in a-c.

In conclusion, **paper III** shows that Cu^{2+} impedes Aβ(1-42) aggregation by inhibiting fibril elongation at sub- and super-stoichiometry ratios. The inhibition of fibril formation can implicate neuroprotective roles of extracellular Cu^{2+} and inspire possible therapeutic strategies to tackle AD based on metal ion homeostasis. However, the inhibition of an elongation process leads to formation of smaller fibrils which may also enhance Aβ toxicity. Moreover, we showed that the inhibitory effect of Cu^{2+} on Aβ(1-42) aggregation is obviated under pH conditions that resemble that in lysosomes (pH=5.0), suggesting that Cu^{2+} has no effect on the Aβ aggregation events that may be the earliest in AD. Our study also extends the current knowledge around the interaction of Cu^{+} and Aβ and shows that the role of copper ions in Aβ pathology is dependent on the reducing potential of the surrounding environment.

5.2 Metal ions enhance the cellular uptake of Aβ peptides

The biophysical study in **paper III** showed that Cu^{2+} ions are potent inhibitors of the primary nucleation of Aβ(1-42), hence keeping the peptide monomeric. Moreover, we found that the Cu-mediated inhibitory effect was eliminated at acidic pH resembling that in endolysosomes; an effect that we ascribed to the titration of histidine residues involved in the metal ion coordination. Since previous work in the group has shown that Aβ peptides are effectively internalized into cells via endocytosis and in monomeric form[92], we were interested in the possible effect of metal ions (Cu^{2+} and Zn^{2+}) on the uptake of Aβ(1-42). In **Paper IV**, we therefore explored the uptake of Aβ(1-42) into human neuroblastoma cells (SH-SY5Y) using fluorescently labelled synthetic Aβ(1-42) which were tagged with the HF488 dye at the N-terminus.

We first analysed the effect of Cu^{2+} alone, or together with Aβ(1-42), on the metabolic activity of the cells using the Alamar blue assay, which measures the chemical reduction potential of cells[188]. This showed that Aβ(1-42) does not alter the metabolic activity of cells, whereas co-incubation of Aβ(1-42) with Cu^{2+} decreased the metabolic activity by 10-20% (Fig. 29). Treatment with Cu^{2+} alone resulted in a reduction in metabolic activity at low Cu^{2+} concentration albeit at higher Cu^{2+} concentration the metabolic activity increased.

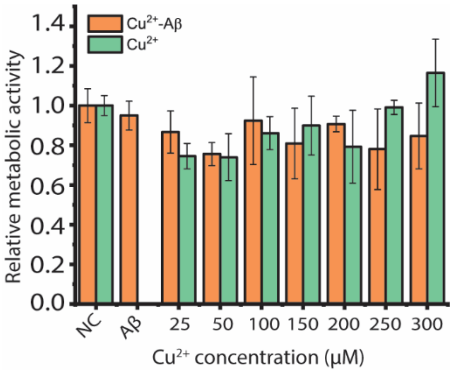

Figure 29. Alamar Blue assay of SH-SY5Y cells treated with indicated concentrations of Cu^{2+} in absence and presence of 1 μM Aβ(1-42) for 4 h.

Thereafter, we studied the effect of Cu^{2+} on Aβ(1-42) uptake by treating the SH-SY5Y cells with solutions containing a fixed concentration of HF488-Aβ(1-42) and increasing concentrations of Cu^{2+} for 4 hours. The uptake was analysed by flow cytometry and quantitative confocal microscopy (Fig. 30), which revealed an up to 2-fold increase in the intracellular accumulation of HF488-Aβ(1-42) in presence of Cu^{2+} (at 150 μM concentration). However, at higher concentrations of Cu^{2+} (> 150 μM), the uptake of Aβ(1-42) peptides started to decrease. Confocal imaging showed that the Aβ(1-42) peptides (green) were localized within the cell body and accumulated into discrete puncta (Fig. 30), which is consistent with uptake through an endocytosis process as previously reported[92,100]. In addition, the confocal images show a lack of surface associated Aβ(1-42) peptides. The increase in uptake was not caused by any general Cu^{2+}-mediated effects on cellular endocytic rate, as shown by the very limited effect of Cu^{2+} on the cellular uptake of the generic fluid-phase endocytosis marker dextran (Fig. 30a). Additional experiments where cells were pre-treated with Cu^{2+} prior to addition of Aβ(1-42) (in a medium without Cu^{2+}) furthermore suggests that the uptake-promoting effect of Cu^{2+} is related to the formation of an Cu^{2+}-Aβ(1-42) complex.

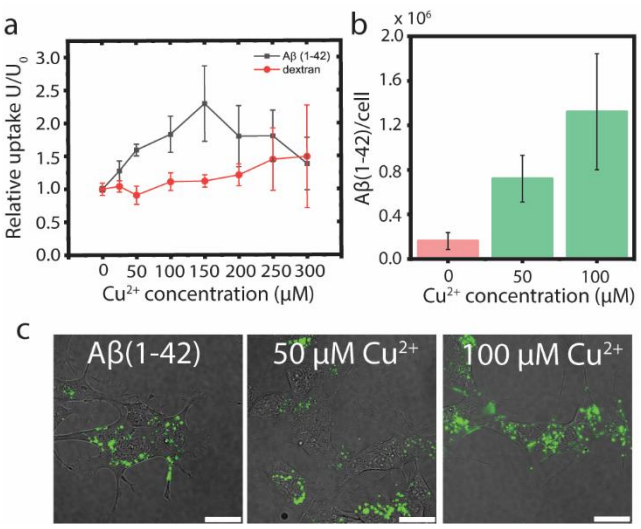

Figure 30. Effect of Cu^{2+} on the cellular uptake of Aβ(1-42). a, Mean cellular uptake of HF488-labelled Aβ(1-42) and AF488-labelled 125 μg/mL 10 kDa. b, Quantification of the amount of intracellular HF488-labelled Aβ(1-42) following incubation with 1 μM of the peptide for 4 h. c, Representative confocal images of live SH-SY5Y cells exposed to HF488-labelled Aβ(1-42) for 4 h in absence or presence of indicated concentrations of Cu^{2+}. The scale bars are 20 μm.

To assess how many Cu^{2+} ions that may co-internalize with Aβ(1-42), I setup a quantitative confocal imaging assay[92] to estimate the number of internalized Aβ(1-42) peptides per cell (Fig. 30b). This indicated an accumulation of ~160,000 Aβ(1-42) peptides per cell in absence of Cu^{2+} and ~1,300,000 Aβ(1-42) in presence of 100 μM Cu^{2+}. Assuming a total lysosomal load of 10 μm^3 per cell, this corresponds to lysosomal Aβ(1-42) concentrations of 24 μM and 195 μM respectively. If we assume that Cu^{2+} and Aβ(1-42) are taken up as a 1:1 complex, this data suggest that Aβ(1-42) can increase lysosomal concentration of metal ions substantially.

Following this new finding that Cu^{2+} enhances the uptake of Aβ(1-42), I decided to test if this would also happen for Zn^{2+}, another metal with strong coordination to the Aβ(1-42) N-terminus and a primary nucleation inhibitory effect on its aggregation[45]. Zn^{2+} ions alone or in presence of Aβ(1-42) were considerably more toxic than Cu^{2+} (Fig. 31a), but they nevertheless promoted the uptake of Aβ(1-42) into SH-SY5Y cells (Fig. 31b), again via an endocytic pathway (Fig. 31d). The maximal uptake-promoting effect occurred at a lower metal ions concentration (50 μM) and started to decrease in the concentration range where Zn^{2+} became highly toxic. The quantification of the number of internalized Aβ(1-42) peptides by confocal microscopy shows that the intravesicular concentration of Aβ(1-42) reaches to 60 μM and 105 μM in presence of 50 μM and 100 μM Zn^{2+} respectively upon incubation of cells with 1 μM Aβ(1-42) for 4 h (Fig. 31c).

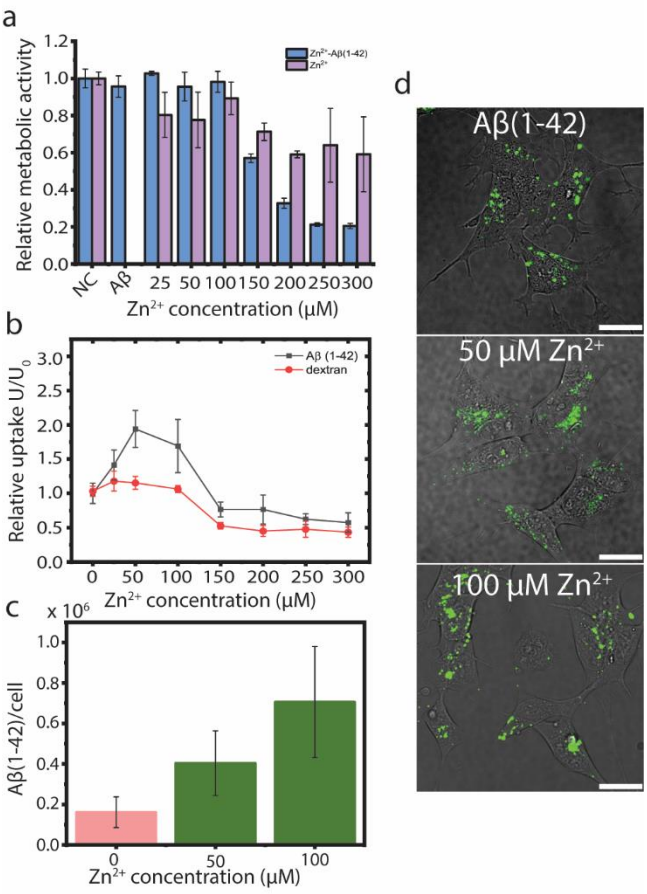

Figure 31. Effect of Zn^{2+} on the uptake of Aβ(1-42). a, metabolic activity of SH-SY5Y cells incubated with different concentration of Zn^{2+} in absence and presence of 1 μM Aβ(1-42) for 4 h measured by Alamar Blue assay. b, cellular uptake of 1 μM of HF488 labelled Aβ(1-42) and AF488 labelled 125 μg/mL dextran 10 kDa after 4 h incubation in presence of increasing concentration of Zn^{2+}. Mean cellular AF488 and HF488 ± SD (N=3, n=3) is reported as proportional value to mean cellular intensity in absence of Zn^{2+}. c, Confocal imaging based quantification of cellular Aβ(1-42) following incubation with 1 μM of Aβ(1-42) for 4 h. The data is presented as mean ± SD from the analysis of 16 images. Each image shown on average 30 cells. d, Representative confocal images of live SH-SY5Y cells exposed to HF488-labelled Aβ(1-42) for 4 h in absence or presence of indicated concentrations of Zn^{2+}. The scale bars are 20 μm.

5.3 Metal ions and Aβ(1-42) changes the transcriptomic profile of SH-SY5Y cells

We performed mRNA sequencing and transcriptomic analysis to better understand the cellular effects of the metal-ion mediated uptake of Aβ(1-42) and to explore putative uptake-promoting mechanisms and pathways. PCA analysis showed that cells that were co-treated with metal ions and Aβ(1-42) had distinctive transcriptomics profiles (Fig. 32a) that were different from Aβ(1-42) or metal ions alone. To elucidate this difference, we used unsupervised k-means clustering[189] to divide the top 2,000 ranked genes into different clusters based on the expression profiles of genes among all the different samples (Fig. 32b). We thereafter did an enrichment analysis to functionally annotate the regulated genes based on Gene Ontology (GO) for biological process. Three clusters had meaningful annotations that allowed us to identify key biological traits that are affected by Aβ(1-42) and/or the metal ion treatments, including up-regulation of biological processes related to synaptic vesicle function, and an expected significant upregulation of cellular detoxification and stress responses to metal ions (Fig. 32b). Many of the dysregulated genes in the synaptic vesicle related cluster were specifically up-regulated in the cells that had been co-treated with Aβ(1-42) and metal ions, but not in cells treated with Aβ(1-42) alone,

nor in the cells treated with only metals. This suggests that metal ions may be important mediators to the Aβ-induced impairment of neuronal synapses that is observed in AD[190,191].

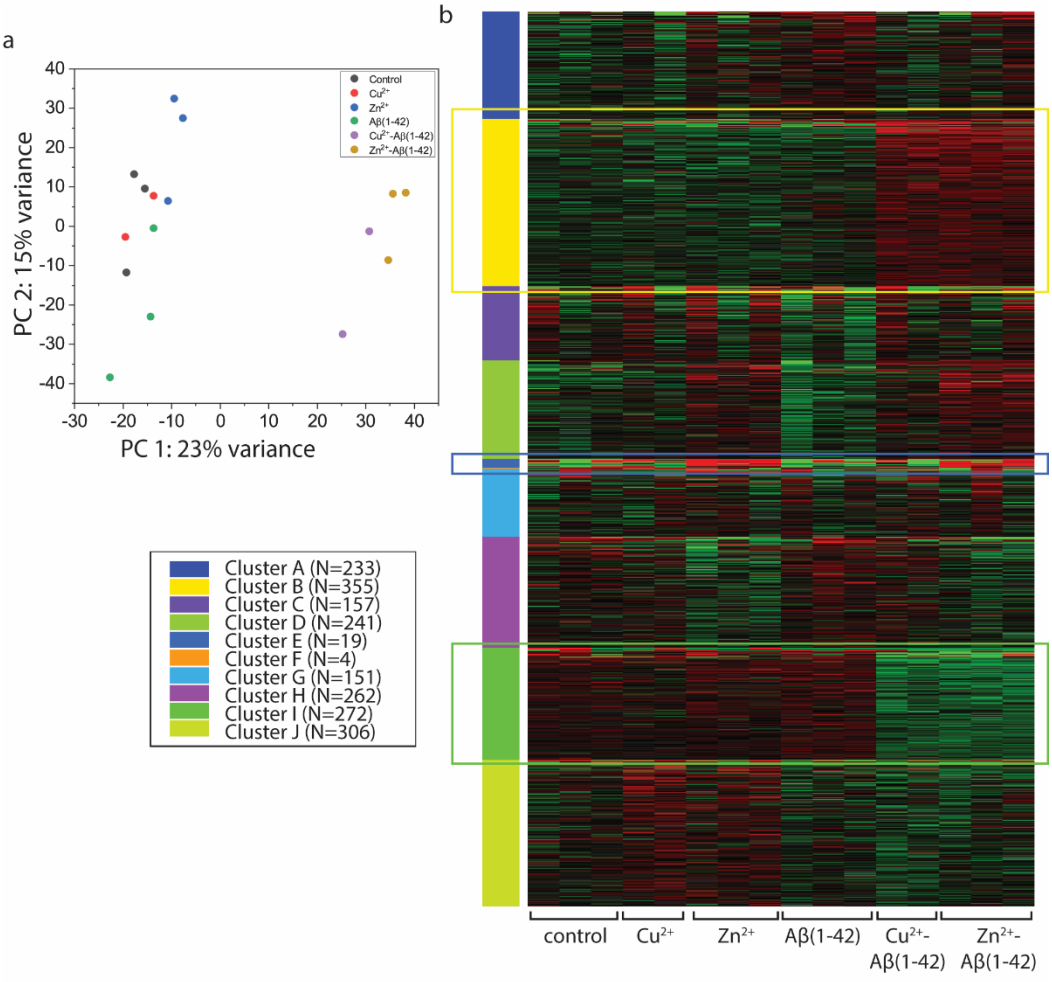

Figure 32. Gene expressions and transcriptomics profiles of SH-SY5Y cells exposed to Aβ(1-42) and metal ions. a, Principal component analysis (PCA) plot is showing that the samples were treated with Cu^{2+}-Aβ(1-42) and Zn^{2+}-Aβ(1-42) clusters together and separated from the rest of samples including cells were treated with metal ions or Aβ(1-42) alone. b, Heatmap showing the unsupervised k-means clustering of the top 2,000 differentially expressed genes in the SH-SY5Y cells into 10 clusters.

To understand in more detail the transcriptome level effect of the different metal ions and Aβ(1-42) treatments, we performed gene set enrichment analysis (GSEA)[192] using the fast gene set enrichment algorithm (*fgsea*)[192] on GO Biological process (Fig. 33a) and KEGG (Kyoto Encyclopaedia of Genes and Genomes) pathways (Fig. 33b). The most marked cellular effects were, expectedly, related to upregulation of metal detoxification responses, and the effects appeared overall similar for Cu^{2+} and Zn^{2+}, as well as in both absence and presence of Aβ(1-42). These responses are therefore likely to be related to the free pool of metal ions in the extracellular medium (due to the excess of added metal ions in relation to Aβ(1-42)).

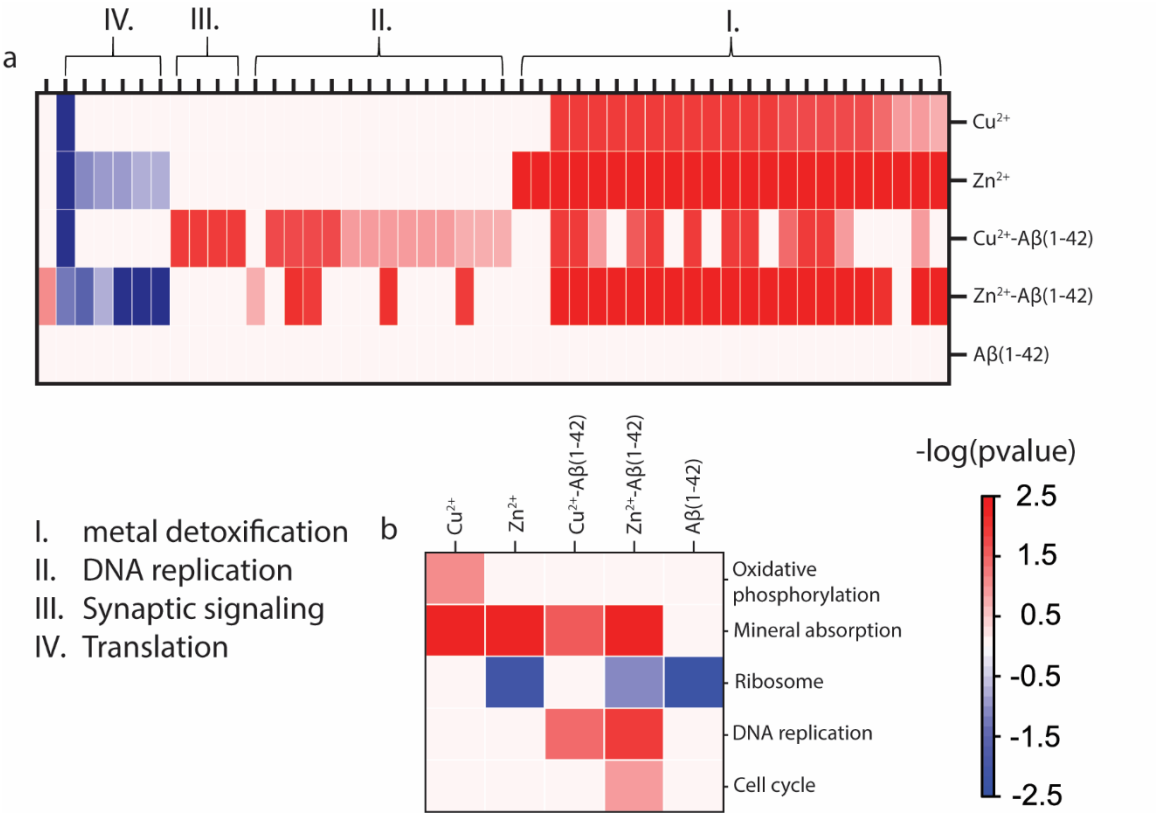

Figure 33. Gene set enrichment analysis (GSEA) using a, GO Biological Process data base and b, KEGG data base.

6. Characterization of physical properties of amyloid fibrils

This chapter describes the development of a method for visualization and characterisation of single amyloid fibrils in solution using a nanofluidic device and summarizes the results of **paper V**.

6.1 Method development

Due the nanometer size of amyloid fibrils and the diffraction limit of light, it is not easy to visualize single amyloid fibrils with conventional light microscopes or even confocal microscopes. Advanced electron microscopy[193,194], AFM[195,196] and in some reports, total internal reflection (TIRF) microscopy[197] have conventionally been used to study individual amyloid fibrils, but the drawback with these methods is that the fibrils are typically immobilized and/or dried on a surface. In **paper V**, we used nanofluidic devices of the type depicted in Fig. 34a to confine and align amyloid fibrils, whilst keeping them in solution. This enabled their fluorescence-assisted visualization under a normal epi-fluorescence microscope without any need for surface attachment to keep the fibrils in focus. Since nanochannels are restricted in the direction perpendicular to the imaging plane the devices increased the contrast and suppressed the out-of-focus fluorescence that is typical in epi-fluorescence. The nanofluidic devices consisted of parallel nanochannels fabricated between two microchannels (nanoslits) that are connected to the reservoirs (Fig. 34a). Due to positively charged side chains and hydrophobicity of amyloid fibrils, they tend to stick to negatively charged materials such as SiO_2 which is the material of nanofluidic devices. This issue is exacerbated in nanochannels due to high surface-to-volume ratio. To overcome this problem, we used supported lipid bilayer (SLB) as a passivation layer in the devices[198]. This allowed us to establish a platform to study single amyloid fibrils in solution (Fig. 34b-c).

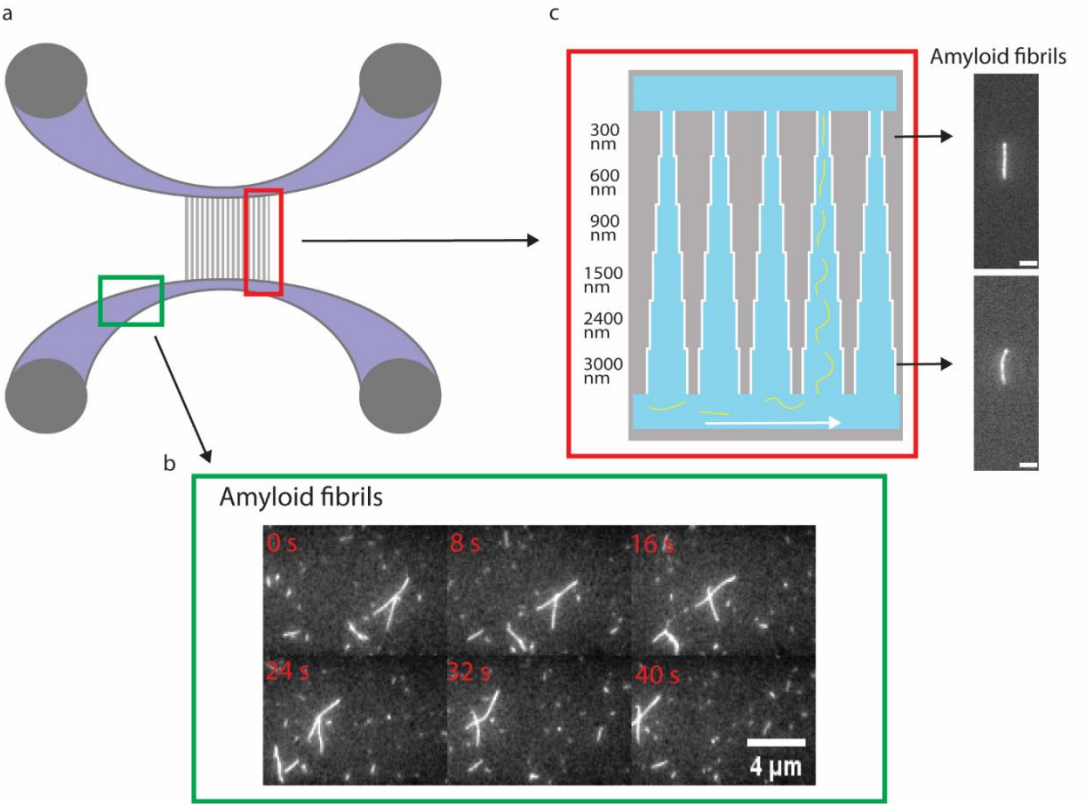

Figure 34. Nanofluidic device for studying amyloid fibrils. a, schematic illustration of a nanofluidic device. b, The recorded snap shots of Aβ(1-42) amyloid fibrils in the micro channel. c, The snap shot of a Aβ(1-42) amyloid fibril in the narrow and wide end of a nanochannel.

6.2 Persistence length of amyloid fibrils

In **paper V**, we used a nanofluidic device with tapered nanochannels as shown in Fig. 34c. The width of the nanochannels was varied between 300 nm to 3000 nm whereas the height was constant (300 nm). The change of the width of channels changes the degree of confinement of the amyloid fibrils, which in turn affects their physical extensions. Since amyloid fibrils are stiff, the extension of the amyloid filaments in different nanochannel geometries follow the scaling proposed by Odijk for biopolymers in a confined environment

$$x = L \times \left(1 - B \times \left[\left(\frac{D1}{P}\right)^{\frac{2}{3}} + \left(\frac{D2}{P}\right)^{\frac{2}{3}}\right]\right) \qquad (7)$$

where *x* is the measured extension of the biopolymer, L is the contour length, P is the persistence length, B is a constant which has been numerically estimated to 0.085[199] and D_1 and D_2 are the channel dimensions. In our device D_1 is 300 nm and D_2 varies from 300 nm to 1500 nm.

By fitting Equation 7 to the extension of each individual amyloid fibril in the different channel geometries we were able to determine their persistence lengths and contour lengths (Fig. 35). We prepared Aβ(1-42) amyloid fibrils and α-syn amyloid fibrils using peptides that were tagged with fluorescent dye at a 10% ratios (to unlabeled wt peptides). In addition to persistence and contour length, we recorded the per pixel emission intensity for each filament.

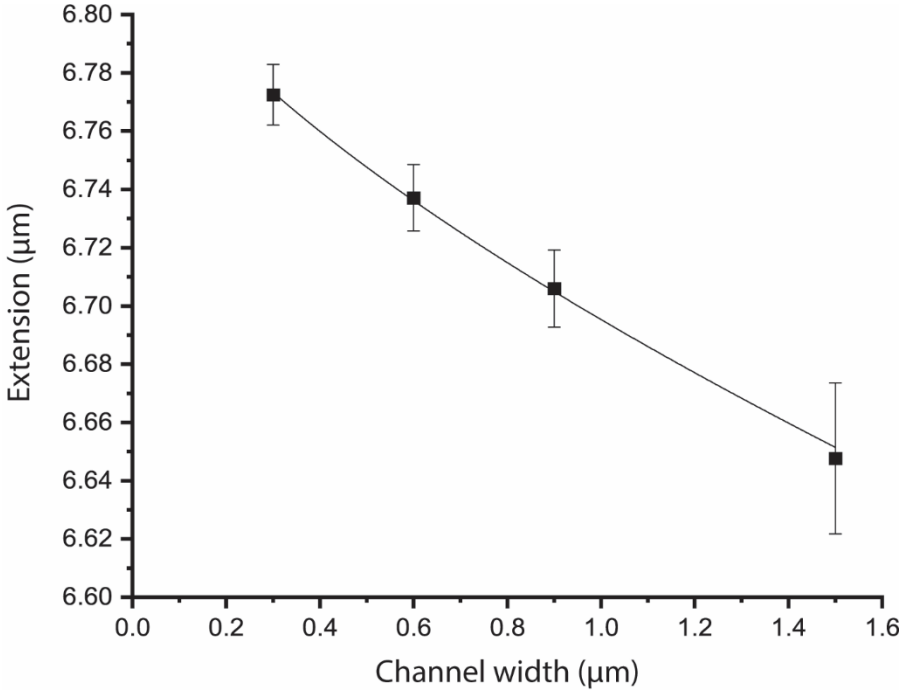

Figure 35. Measurement of different extension of a amyloid fibril and calculation of persistence length. The change in extension with channel width for Aβ(1-42) amyloid fibril. The solid line is the fit to Equation 7.

Using Odijk's theory, we determined the persistence and contour length of 82 individual Aβ(1-42) amyloid fibrils (Fig. 36). We observed that the measured persistence lengths varied from 1.6 µm to 16.4 µm composing to main populations with 3.0 ± 0.3 µm and 7.3 ± 0.8 µm averages. The overall average

of the persistence length of all 82 amyloid fibrils was 5.9 ± 4.5 µm. In addition to persistence length, the measured contour length of Aβ(1-42) amyloid fibrils varied from 6.9 µm to 17.6 µm with an average of 11.8 ± 2.6 µm (Fig. 36a). The observation of at least two major populations of amyloid fibrils with regards to their persistence length suggests that there are at least two polymorphs present in the Aβ(1-42) amyloid fibrils sample which corroborates previous reports on the heterogeneity of Aβ(1-42) amyloid fibrils formation[29].

The method presented in **paper V** had the capacity to detect and quantify fibril polymorphism at the level of mesoscopic morphological characteristics of the fibrils (here persistence length). To explore the polymorphism concept further, we analyzed the correlation between persistence length and contour length of Aβ(1-42) amyloid fibrils (Fig. 36a). The lack of correlation suggests that different polymorphic variants do not elongate at substantially different rates. We also investigated the relation between fluorescence emission intensity per unit length of the amyloid fibrils and the persistence length of Aβ(1-42) amyloid fibrils (Fig. 36b). The fluorescence emission intensity per unit length should be proportional to the fibril mass per unit length and hence the number of protofilament in the fibril. We found no correlation in this case either, which was more surprising. If we assume that variations in fluorescence intensity would relate to the number of protofilaments in each fibril [28,200], and vary less with different packing geometries of monomers in the fibril core, this suggests that persistence length variations takes root in differences in the dimerization mode of two Aβ(1-42) filaments rather than in the occurrence of fibrils with a difference in the number of protofilaments.

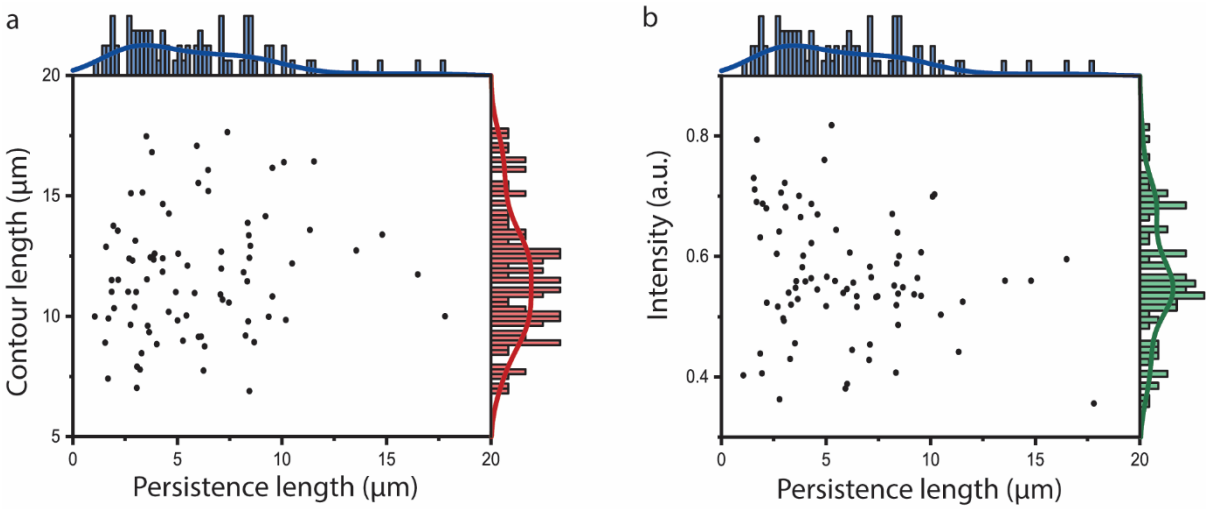

Figure 36. Persistence length, contour length and intensity of amyloid fibrils measured in nano device. a, Scatter plot of persistence length versus contour length measured for 82 Aβ(1-42) amyloid fibrils. b, Scatter plot of persistence length versus intensity measured for 82 Aβ(1-42) amyloid fibrils.

In **paper V**, we also compared the persistence lengths of Aβ(1-42) and α-syn amyloid fibrils. The α-syn fibrils were considerably shorter (7.3 ± 0.7 µm) (Fig. 37a). The average of measured persistence lengths for 46 individual α-syn amyloid fibrils was 3.0 ± 1.6 µm, which was considerably lower than the average persistence length of Aβ(1-42) amyloid fibrils. Although the distribution of α-syn fibrils' persistence length is bimodal (showing presence of polymorphism) just as observed for Aβ(1-42) fibrils, the distribution is much narrower, suggesting lesser heterogeneity (Fig. 37a). Just as for Aβ(1-42) fibrils we could not identify correlations between the persistence length of α-syn fibrils and their contour lengths (Fig. 37a).

Comparing the persistence length versus fluorescence intensity (Fig. 37b), we observe an extremely low variation in the distribution of fluorescence intensity, indicating a single population of amyloid fibrils. This would be consistent with cryoEM structures of α-syn fibrils which identified polymorphs with different monomer packing but the same number of protofilaments[32]. The lack of correlation between fluorescence intensity and persistence length strengthens our hypothesis that fibril stiffness is foremost related to monomer packing within protofilaments and to a lesser extent, if at all, related to the number of filaments in the mature fibril.

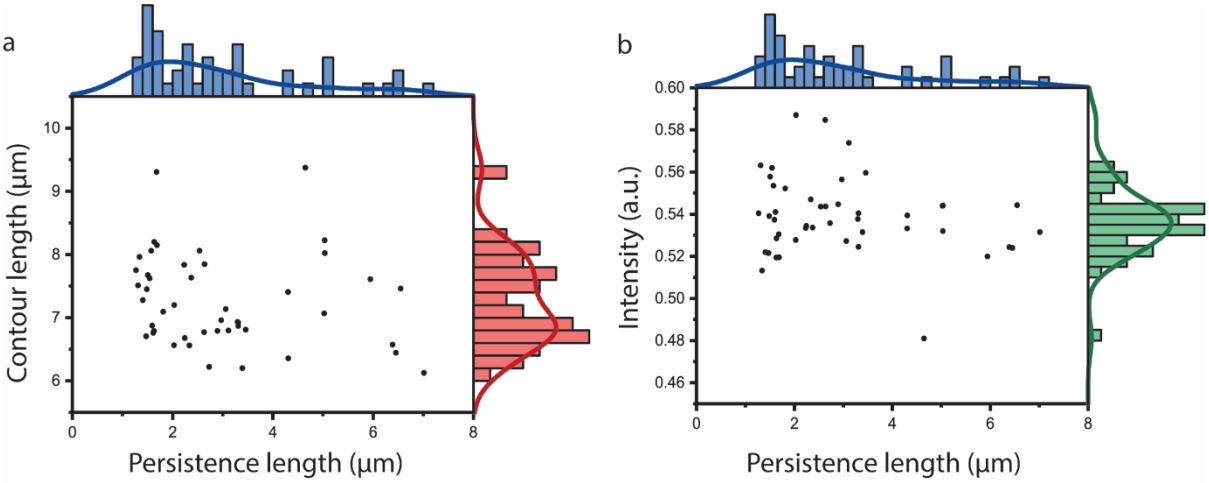

Figure 37. Persistence length, contour length and intensity of amyloid fibrils measured in nano device. a, Scatter plot of persistence length versus contour length measured for 46 α-synuclein amyloid fibrils. b, Scatter plot of persistence length versus intensity measured for 46 α-synuclein amyloid fibrils.

To conclude, we have developed a method for studying single amyloid fibrils in solution and applied it to define physical characteristics i.e, persistence length and contour length of amyloid fibrils. We observed variations in persistence length that indicate the co-existence of several fibril polymorphs and note that the subtle packing and structure of the amyloid fold may have measurable effects on the fibril physical properties and thus that polymorphism exists on the mesoscale.

7. Therapeutic potential of graphene-based nanoparticles for Parkinson's disease

Preventing the aggregation of amyloidogenic proteins is considered a key strategy to combat neurodegenerative diseases[201]. In this context, many studies have been done on developing nanomaterials such as gold nanoparticles, graphene oxide materials, graphene quantum dots and carbon nanotubes which are able to suppress amyloid formation of proteins such as Aβ, insulin and islet amyloidogenic polypeptide (IAPP)[202-206]. Graphene-based nanoparticles such as graphene oxide sheets (GO) and graphene quantum dots (GQD) have been proposed as effective inhibitors of *in vitro* aggregation of amyloidogenic proteins such as Aβ[204,207-209], IAPP[210,211] and α-syn[212,213]. In this project, we explored in more depth the effect of GO sheets and GQD nanoparticles on the kinetics of α-syn aggregation into amyloid fibrils and the mechanism by which they can affect the aggregation process.

First, we studied the aggregation kinetics of 50 μM monomeric α-syn into amyloid fibrils in the absence and presence of GO and GQD with the help of ThT fluorescence. We observed that both GO and GQD inhibit α-syn aggregation in a dose-dependent manner (Fig. 38).

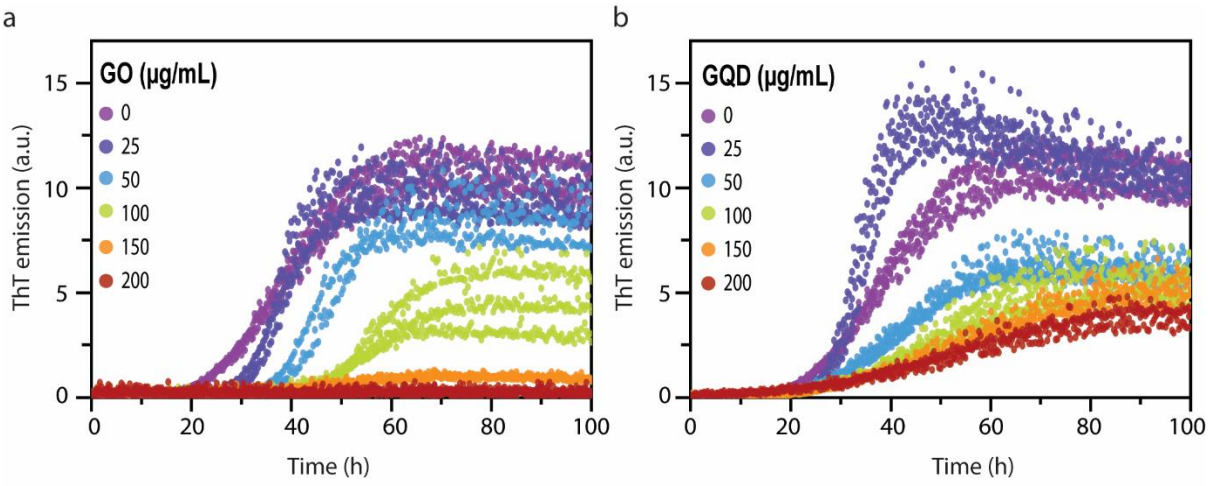

Figure 38. Aggregation kinetic of α-syn. a, Aggregation kinetic of 50 μM α-syn in presence of in GO nanoparticles. b, Aggregation kinetic of 50 μM α-syn in presence of GQD nanoparticles.

To understand the mechanism by which GO and GQD inhibit α-syn amyloid formation, we derived the lag-time and maximum slope of the kinetic curves, in addition to half-times (Fig. 39). These values reveal that GO extends the lag-time of α-syn aggregation more prominently and have more significant effect on the maximum slope than GQD even if the increase in the aggregation reaction half-times of aggregation were relatively similar. This suggests that GO and GQD inhibit α-syn amyloid formation through different mechanisms. As discussed before, lag-time is dominated by primary nucleation and maximum slope, and growth-time is associated with elongation process and/or secondary nucleation process.

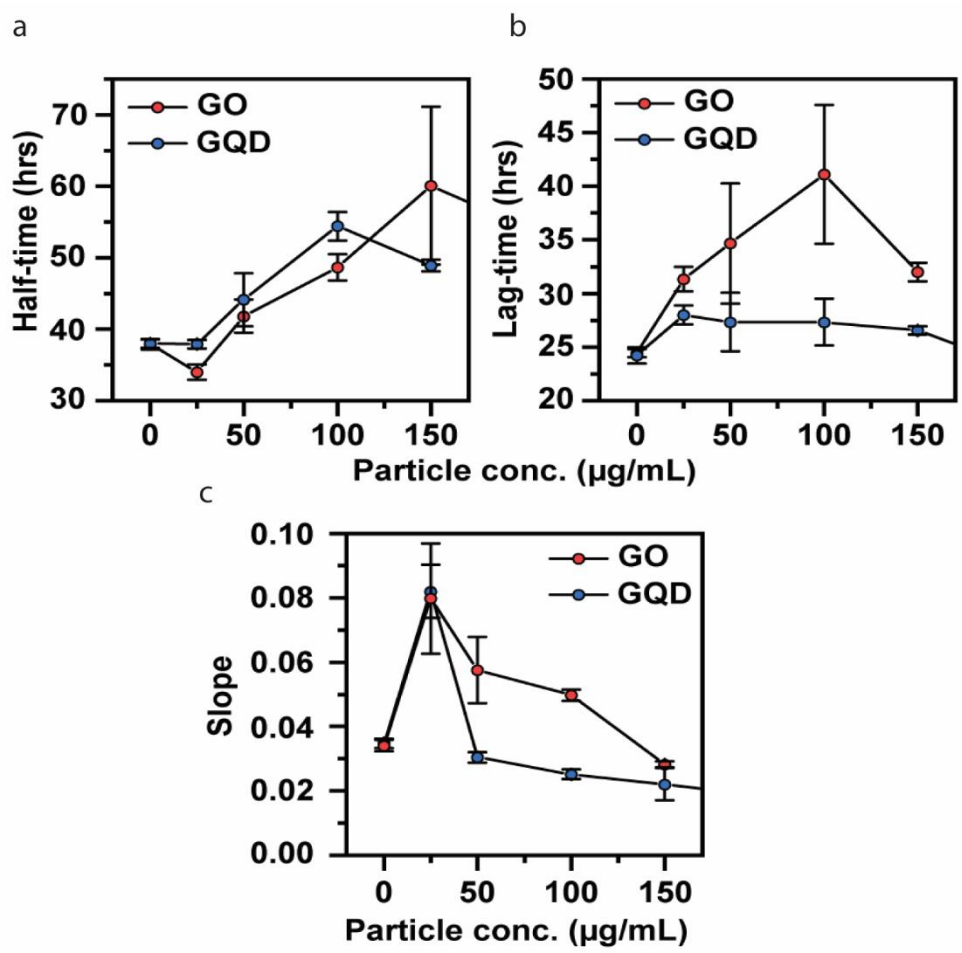

Figure 39. Calculated kinetic parameters describing the aggregation kinetic of 50 µM α-syn in presence of GO and GQD shown in Fig. 38. a, Half-time. b, Lag-time. c, Maximum slope.

To better understand the molecular basis of the inhibitory effect, we also measured the binding of monomeric and fibrillar α-syn to GO and GQD. This analysis was facilitated by that GO and GQD quench the intrinsic fluorescence of α-syn emanating from its four tyrosine residues[214]. The degree of quenching which is shown as F_0/F (F_0 is the fluorescent emission of α-syn alone and F is the fluorescent emission of α-syn in presence of different concentration of nanoparticles) versus nanoparticle concentration suggests that monomeric α-syn interacts with both GO and GQD with the same affinity while α-syn amyloid fibrils interact with GO nanoparticles more strongly than GQD nanoparticles (Fig. 40).

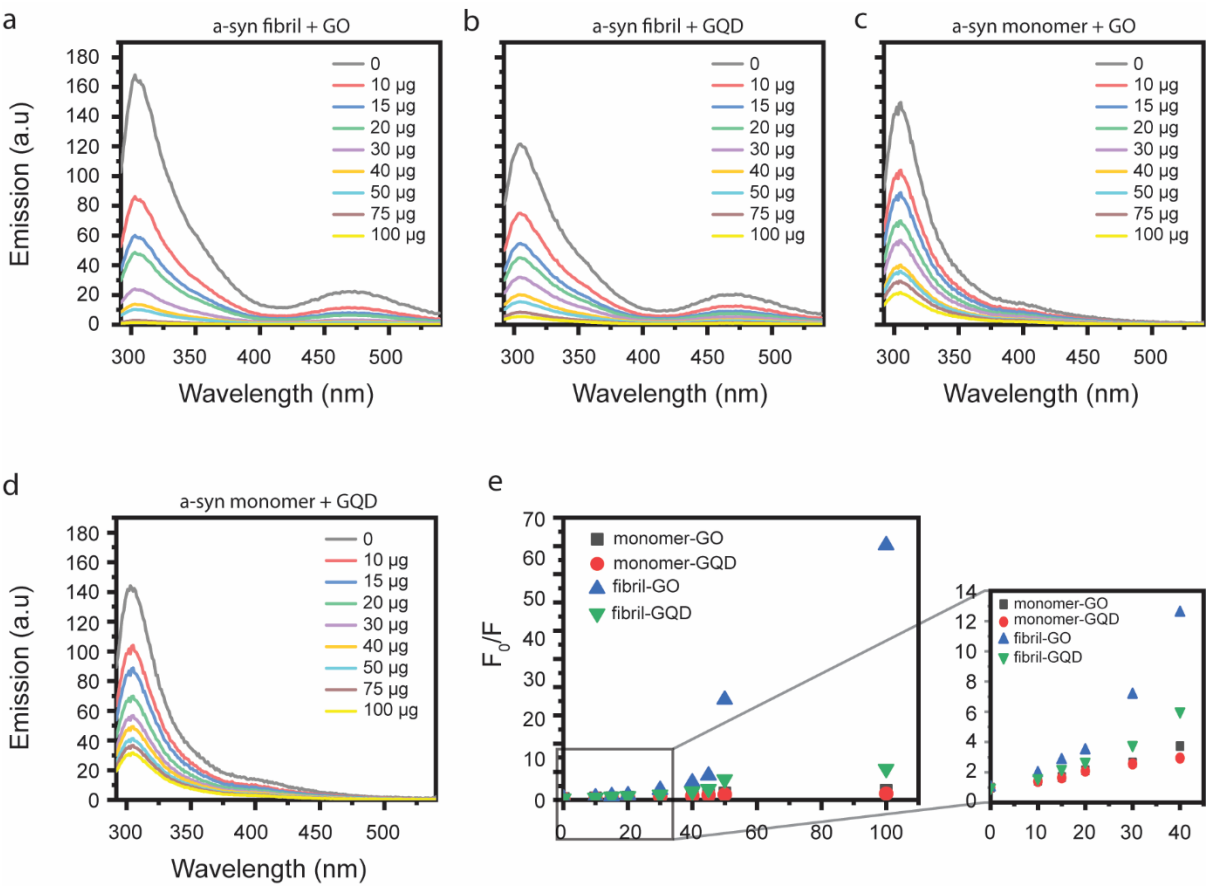

Figure 40. Interaction of GO and GQD with monomeric and fibrilla α-syn. a, Tyrosine fluorescence quenching of 50 µM fibrillar α-syn in presence GO. b, Tyrosine fluorescence quenching of 50 µM fibrillar α-syn in presence GQD. c, Tyrosine fluorescence quenching of 50 µM monomeric α-syn in presence GO. d, Tyrosine fluorescence quenching of 50 µM monomeric α-syn in presence GQD. e, Stern-Volmer plot of quenching efficiency of GO and GQD nanoparticles on tyrosine amino acids in monomeric and fibrillar α-syn.

Thereafter, we explored the effect of GO and GQD nanoparticles on the structure and morphology of the resulting amyloid fibrils. Analysis of their secondary structure using CD spectroscopy showed that the amyloid fibrils that formed in presence of both GO or GQD were similar in terms of β-sheet content to those formed in the absence of nanoparticles (Fig. 41).

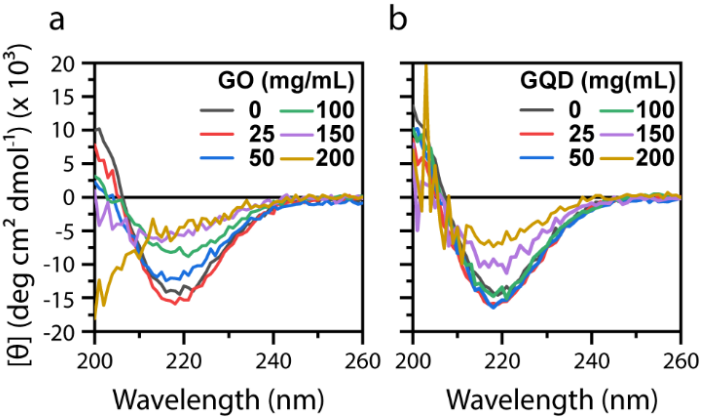

Figure 41. Circular dichroism spectra of 50 µM α-syn in presence of a, GO and b, GQD.

Finally, we examined the morphology of the amyloid fibrils with AFM (Fig. 42). The result shows that the height (thickness) of amyloid fibrils is decreased when they form in presence of both GO and GQD. This suggests the formation of different polymorphs of α-syn filaments compared to ones formed in the absence of nanoparticles[32]. The lengths of amyloid fibrils are decreased upon incubation with GO and GQD, although the decrease is more drastic in the case of GO compared to GQD. We attribute the length reduction to the increased shear force due to presence of nanoparticles.

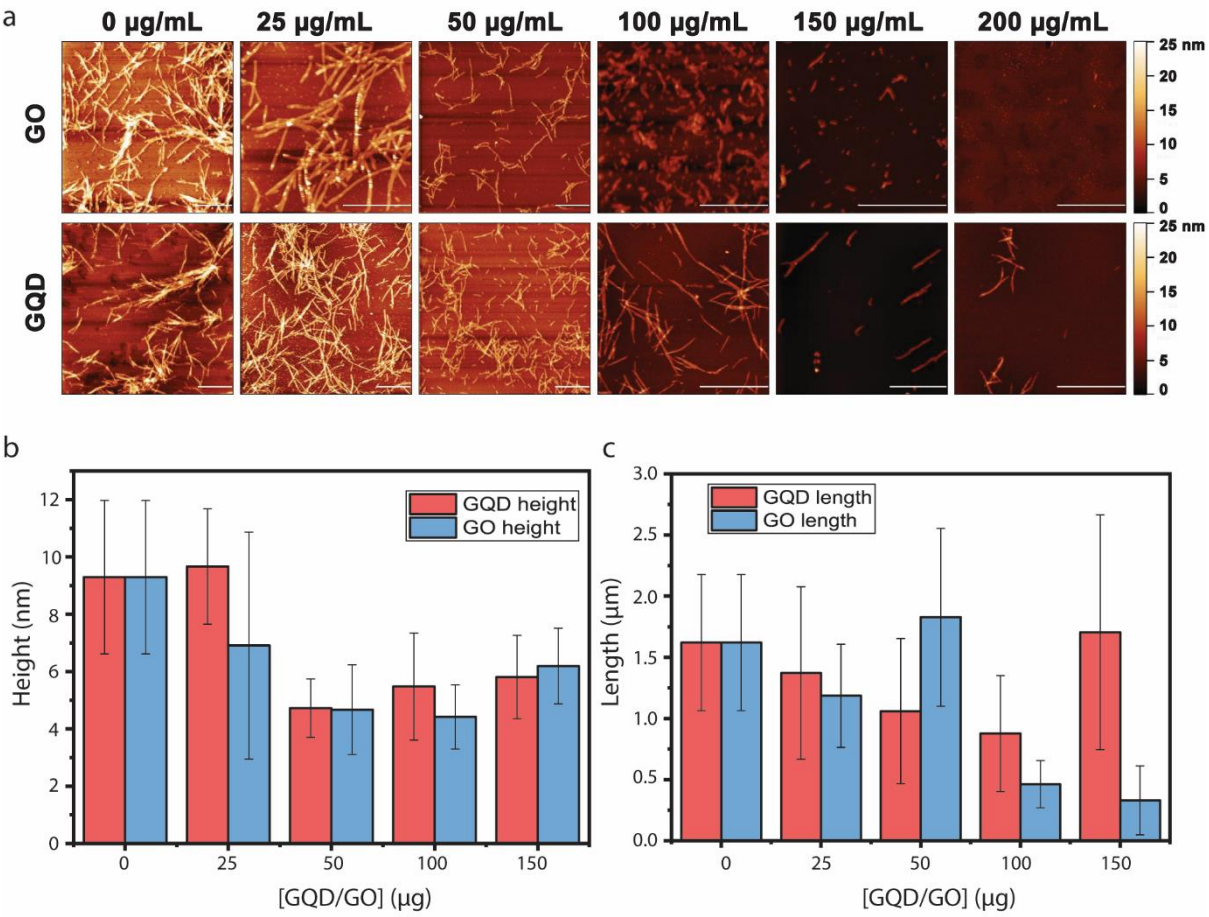

Figure 42. Morphology analysis of α-syn formed fibrils by AFM. a, Representative AFM images of 50 μM α-syn in absence and presence of different concentrations of GO and GQD. b, Height analysis of α-syn amyloid fibrils. c, Length analysis of α-syn amyloid fibrils.

8. Concluding remarks

Hardy and Higgins early postulated the amyloid cascade hypothesis which, in its earliest form, linked Aβ amyloid fibril plaque deposition to Alzheimer's disease (AD)[215] but since, there has been extensive studies that show that senile plaque load is not correlating well with the severity of cognitive impairment[216]. Therefore, the research focus has shifted more towards the identification of neurotoxic, often oligomeric, species whose presence in the brain were found to correlate better with disease severity[217]. The failure of clinical trials of drugs targeting amyloid plaques has even made some parts of the research community reject the amyloid cascade hypothesis[218,219]. However, in 2022 and just prior to the completion of this thesis, there has been positive news on the success of monoclonal antibodies including Aducanumab and Lecanemab[220] which was developed by Lannfelt and coworkers[221] in decreasing the amyloid load and improving cognitive impairment of patients in early stages of AD[220,222]. In addition to being incredibly positive news to patients with substantial unmet medical needs, it shows the importance of the role of amyloid fibrils in AD pathology. Therefore, it emphasizes again the relevance of, and need, to thoroughly understand the amyloid formation mechanisms of Aβ and the role of different intrinsic and extrinsic modifiers in this phenomenon.

The main aim of my thesis is to shed light on the effect of various extrinsic modifiers on the aggregation of specifically Aβ(1-42). I have focused on lipids and metal ions, due to the reported significance of dyshomeostasis of these chemicals in AD pathology, and on their effects on the molecular mechanisms and toxicity of Aβ amyloid formation.

The role of lipids in the aggregation of Aβ(1-42) was investigated in **Papers I** and **II**. We studied both complex biological vesicles (cell-derived EVs) and synthetic lipid vesicles where the lipid composition could be exactly controlled and systematically varied. In **Paper I**, we found that EVs, purified from two different cell lines, slowed down Aβ(1-42) amyloid formation substantially by interfering with the fibril elongation step. This led to the formation of short fibrils, with different morphological characteristics. Although the EV-mediated retardation of amyloid formation could be considered as neuroprotective, it should be noted that the formation of shorter fibrils can increase the efficiency of uptake of amyloid fibrils by cells[185]. Moreover, retardation of the elongation process can increase amyloid toxicity by maintaining a high oligomer generation rate through monomer-dependent secondary nucleation process for a longer time frame[223]. Therefore, the possible role of EVs in the pathology of Aβ is more complex than the simple inhibition of amyloid formation and more studies are needed to gain deeper understanding. For example, exploring the toxicity effect of amyloid fibrils formed in presence of EVs on neurons is a necessary next step.

Since EVs are highly complex and consist of both lipids and proteins, we also used a bottom-up approach to explore the aggregation modulatory effect of different brain-relevant lipids that have been suggested to play a role in AD pathology (**Paper II**). In this paper, we systematically explored the individual as well as combinatorial contribution of lipids to Aβ(1-42) amyloid formation, demonstrating that biological lipid membranes contain both enhancers and inhibitors and that these can act on different microscopic mechanisms in the Aβ(1-42) amyloid formation process. For example, we showed that GM1 inhibits Aβ(1-42) aggregation by retarding primary nucleation while cholesterol (Chol) and sphingomyelin (SM) accelerate Aβ(1-42) amyloid formation by boosting the primary nucleation and secondary nucleation respectively. In **Paper II**, we discuss these results in terms of a model where lipids can have specific effects due to their interaction with Aβ(1-42) (relevant for GM1) or more generic effects due to their influence on membrane behavior. Chol and SM can, in this respect, increase head-group spacing and therefore increase Aβ(1-42) accessibility to the hydrophobic core, facilitating respectively oligomerization and fibril binding. A conceptually important aspect of **Paper II** was the

investigation of the combinatory effects of GM1, Chol and SM lipids. This allowed for better understanding of how biologically relevant lipid membranes interplay with Aβ(1-42) and modulate its aggregation, but it is also, to my knowledge, the first study to highlight and systematically explore competitive effects in an amyloid system. For example, we found a total lipid concentration-dependent competition between Chol and GM1, whereas SM mostly seemed to outcompete GM1, probably because of its potent fluidizing effect on the lipid bilayer. One important outcome of **Paper II** is that it can explain ambiguous results in previous reports regarding the role of GM1 in Aβ aggregation and pathology. Furthermore, the study highlights the importance of considering lipid segregation and not just simply the concentration of each lipid component, as LUVs composed of SM, Chol and GM1 in combinations that have high propensity to form lipid rafts, as confirmed with the Laurdan assay, have particularly strong inhibitory effects on the Aβ(1-42) aggregation. Altogether, **paper II**, in addition to providing detailed information on the effect of different lipids on Aβ(1-42) amyloid formation, shows that the incorporation and ratio of various lipids, each of which contribute specifically and combinatorically to the surface chemistry as well as biophysical characteristics of the lipid membranes, play a pivotal role in the influence of lipid bilayers on the aggregation of Aβ(1-42).

In **paper III** and **IV**, I investigated the role of metal ions in Aβ pathogenesis using *in vitro* biophysical analyses (**paper III**) and *in vivo* cell experiments (**paper IV**). In **paper III**, we showed that the divalent copper ion (Cu^{2+}) inhibits Aβ(1-42) amyloid formation by attenuating the elongation process as had previously been reported for Zn^{2+} in Aβ(1-40) aggregation[45]. Although the impeding of the elongation process by Cu^{2+} could act to decrease the extracellular amyloid load, it should be noted that the formation of more toxic smaller Aβ aggregate such as protofilaments and oligomers[217] can be boosted under elongation inhibitory conditions. Opposite to Cu^{2+}, we have also shown that Cu^{+} has promoting effects on the Aβ(1-42) aggregation and induces primary nucleation. The importance of studying Cu^{+} is that redox cycling of Cu ions bound to Aβ could potentiate amyloid formation and potentially overrule the inhibitory effect of Cu^{2+} under certain redox conditions. Moreover, we reported the complete loss of effect of Cu^{2+} at lower pH (pH=5) associated with lysosomes. This indicates that presence of Cu^{2+} at lysosomes together with Aβ has no inhibitory effect on the amyloidogenesis of Aβ possibly due to protonation of histidine residues. Altogether, **paper III** enhanced our understanding of redox and pH dependent effects of Cu ions on the Aβ(1-42) aggregation *in vitro*.

As both divalent Cu (**paper III**) and Zn[45] ions have been shown to play an active role in retarding the aggregation of Aβ and keep Aβ in monomeric states, we also set out to explore if the metal ion - Aβ(1-42) interaction influenced the uptake of the peptide into human neuroblastoma cells (**paper IV)**. We found that co-incubation of both Cu^{2+} and Zn^{2+} with Aβ(1-42) monomers enhanced endocytic uptake and lead to the accumulation of high concentrations of both Aβ(1-42) peptides and metal ions in endolysosomes. This result suggests that in order to correctly interpret and understand the full effect of an extrinsic aggregation modifier (metal ions here), more aspects than their direct effect on aggregation need to be considered. With the help of RNAseq analysis, we showed that accumulation of metal ions together with Aβ(1-42) in endolysosomal compartments upregulated genes that are related to the pre-synaptic vesicle cycle and that were, conspicuously, downregulated upon the internalization and accumulation of Aβ(1-42) alone. To further deepen our understanding around the role of metal ions in AD pathogenesis, it would be informative to investigate the effect of metal ions in the intracellular aggregation of Aβ with the help of microscopic[100] and other biochemical techniques[224].

In **paper V**, we developed a new method based on nanofluidics and fluorescence microscopy to investigate amyloid fibrils at the single fibril level. Since the design of nanochannels is tailorable[225], there is ample opportunity to further develop this method for studying for example interactions of amyloid fibrils with other proteins such as chaperones[226] by using nanofluidic designs that allows

following the dynamic interaction of extended and confined individual amyloid fibrils with other molecules[227]. We, however, used a design that let us to follow the extension of an individual amyloid fibril in different confinements across a single nanochannel. Using this design, we could estimate the persistence lengths and contour lengths of amyloid fibrils. This allowed us to identify polymorphs of amyloid fibrils that differed in their persistence length. Although less detailed than cryoEM, this method enables a fast and simple, low sample volume, method to probe for variations in amyloid fibril properties within a single sample. For example, the effect of co-aggregation of Aβ with EV lipids and proteins that we propose in **paper I**, would be exciting to investigate further using the nanofluidic method.

As I discussed in the beginning of this chapter, one of the therapeutic strategies to deal with neurodegenerative diseases is impeding amyloid formation of relevant amyloidogenic proteins to reduce the amyloid load in patients. In **paper VI**, we developed graphene-based nanoparticles (GO and GQD) capable of retardation of α-syn aggregation proteins into amyloid fibrils, a reaction that is associated with Parkinson's disease. We showed that both nanoparticles inhibited α-syn aggregation, but we could also see enhancing effects at low nanoparticle-to-protein ratios. This serves as another example of the amyloid modulation, and it's associated biological outcomes, are sensitive and context-independent and that the balance between different modulating effects need to be taken into account when designing therapeutic strategies. In addition to the aggregation modulatory role of graphene nanoparticles, we observed that they alter the morphology of formed fibrils. GO in particular induced the formation of shorter fibrils. Thus, also here the neurotoxicity of α-syn amyloid fibrils formed in presence of GO would need to be further addressed, as we know that the shorter fibrils are more potently taken up by cells and show more toxicity[185]. Moreover, we observed that both GO and GQD incubation with α-syn leads to formation of thinner amyloid fibrils showing formation of different polymorph of α-syn amyloid fibrils. The method we developed in **paper V** could be used to determine the persistence length of these thin amyloid fibrils, although cryo-EM and/or ssNMR should be used to obtain information on molecular structure of these amyloids to find their similarity and differences to other polymorphs of α-syn.

Acknowledgment

I especially want to thank the following people for their help, support, and encouragement.

First, I would like to thank my supervisor **Elin Esbjörner Winters**, for being so kind and welcoming since the first time I set foot in her office with a blush on my face. Thanks for believing in me and thanks for your continuous support and your patience during the ups and downs. You are an inspiring scientist and compassionate group leader. I could not have asked for a better supervisor, and I wish I could grow as a scientist like you. In addition to being my supervisor, you have been always a great mentor and friend.

I would also like to thank my co-supervisor **Fredrik Westerlund** who has been a great support all these years. I have learned a great deal from you since I was a master student and took a course with you which was apparently one of the most difficult ones in the program, but you had made it understandable for everyone. You are an excellent teacher, and that is perhaps not news to you. I appreciate all your support in the nanofluidic project.

I was lucky to have a second co-supervisor. I would like to thank **Fredrik Höök**, for being so generous, supportive, inspiring and welcoming. Never in my scientific career have I seen such a humble, and great scientist, and I probably will never see again. I enjoyed and learned a lot from your invaluable input on LUVs project.

I would like to thank my examiner **Pernilla Wittung Stafshede**. I am very proud to have you as my examiner. I will always tell everyone, the person who chooses Nobel Laureates has approved my thesis. I could not wish for a more supportive examiner. Thanks for always being available and responsive. I would not have been able to finish the copper project and this thesis without your support and inputs.

I would like to thank **Sandra Rocha**. Sandra, despite what I learned from you; you mean a lot to me. I could not have continued and finished my Ph.D. without your support. Your support and friendship are invaluable, and I am grateful to have you as my colleague and friend.

To **David**, **Emelie** and **Audrey**, you were great colleagues and friends. I have learned everything in the lab from you guys. You were generous in sharing your extensive knowledge and very patient and supportive. Without you by my side, I would not be standing where I am now.

To **Shadi**, I am very thankful for all your help and support in metal ions-Aβ uptake project. You patiently and generously taught me how to do transcriptomic analysis which is very invaluable.

To **Vesa**, you are a great friend and colleague, and more importantly a dedicated scientist. I enjoyed a lot working with you. Special thanks for proofreading the thesis.

I would also thank all my colleagues in Elin's group including, **Marziyeh**, **Karin**, **Andrea**, **Fritjof** and **Dory** who made pleasant working environment. We had also many collaborations together which were fun.

To **Istvan**, Thanks for answering all my questions with patience and for your inputs in the copper project.

To all previous and current colleagues in ChemBio division, thank you.

I want to thank my dear friends who are like family to me **Mohammad**, **Nastaran**, **Saeed**, **Shima**, **Roujin**, **Amir** and many others which I cannot list here. You made all these years very enjoyable for me. I have made many nice memories with you all.

Finally, I want to thank my parents, **Farideh** and **Nersi**. Without your patience and 24/7 support, I would not have been able to finish my Ph.D.

References

1 Alzheimer, A., Stelzmann, R. A., Schnitzlein, H. N. & Murtagh, F. R. An English translation of Alzheimer's 1907 paper," Uber eine eigenartige Erkankung der Hirnrinde". *Clinical anatomy (New York, NY)* **8**, 429-431 (1995).

2 Bondi, M. W., Edmonds, E. C. & Salmon, D. P. Alzheimer's disease: past, present, and future. *Journal of the International Neuropsychological Society* **23**, 818-831 (2017).

3 Collaborators, G. M. D. Global, regional, and national burden of 12 mental disorders in 204 countries and territories, 1990–2019: a systematic analysis for the Global Burden of Disease Study 2019. *The Lancet Psychiatry* **9**, 137-150 (2022).

4 攀苏. Stereochemistry of polypeptide chain configurations.". *J. mol. Biol* **7**, 95-99 (1963).

5 Anfinsen, C. B. Principles that govern the folding of protein chains. *Science* **181**, 223-230 (1973).

6 Dill, K. A. & MacCallum, J. L. The protein-folding problem, 50 years on. *science* **338**, 1042-1046 (2012).

7 Dill, K. A. Dominant forces in protein folding. *Biochemistry* **29**, 7133-7155 (1990).

8 Levinthal, C. Are there pathways for protein folding? *Journal de chimie physique* **65**, 44-45 (1968).

9 Aronsson, G., Brorsson, A.-C., Sahlman, L. & Jonsson, B.-H. Remarkably slow folding of a small protein. *FEBS letters* **411**, 359-364 (1997).

10 Thompson, P. A. *et al.* The helix-coil kinetics of a heteropeptide. *The Journal of Physical Chemistry B* **104**, 378-389 (2000).

11 Baldwin, R. L. Matching speed and stability. *Nature* **369**, 183-184 (1994).

12 Bryngelson, J. D., Onuchic, J. N., Socci, N. D. & Wolynes, P. G. Funnels, pathways, and the energy landscape of protein folding: a synthesis. *Proteins: Structure, Function, and Bioinformatics* **21**, 167-195 (1995).

13 Alberts, B. *et al.* Molecular biology of the cell. *Scandinavian Journal of Rheumatology* **32**, 125-125 (2003).

14 Gething, M.-J. & Sambrook, J. Protein folding in the cell. *Nature* **355**, 33-45 (1992).

15 Chiti, F. & Dobson, C. M. Protein misfolding, functional amyloid, and human disease. *Annual review of biochemistry* **75**, 333-366 (2006).

16 Shirahama, T. & Cohen, A. S. High-resolution electron microscopic analysis of the amyloid fibril. *The Journal of cell biology* **33**, 679-708 (1967).

17 Gazit, E. The "correctly folded" state of proteins: is it a metastable state? *Angewandte Chemie International Edition* **41**, 257-259 (2002).

18 Jahn, T. R. & Radford, S. E. The Yin and Yang of protein folding. *The FEBS journal* **272**, 5962-5970 (2005).

19 Vendruscolo, M. & Dobson, C. M. Towards complete descriptions of the free–energy landscapes of proteins. *Philosophical Transactions of the Royal Society A: Mathematical, Physical and Engineering Sciences* **363**, 433-452 (2005).

20 Uversky, V. N. & Fink, A. L. Conformational constraints for amyloid fibrillation: the importance of being unfolded. *Biochimica et Biophysica Acta (BBA)-Proteins and Proteomics* **1698**, 131-153 (2004).

21 Uversky, V. N., Oldfield, C. J. & Dunker, A. K. Intrinsically disordered proteins in human diseases: introducing the D2 concept. *Annual review of biophysics* **37**, 215-246 (2008).

22 Sunde, M. & Blake, C. The structure of amyloid fibrils by electron microscopy and X-ray diffraction. *Advances in protein chemistry* **50**, 123-159 (1997).

23 Bonar, L., Cohen, A. S. & Skinner, M. M. Characterization of the amyloid fibril as a cross-β protein. *Proceedings of the Society for Experimental Biology and Medicine* **131**, 1373-1375 (1969).

24 Eanes, E. & Glenner, G. X-ray diffraction studies on amyloid filaments. *Journal of Histochemistry & Cytochemistry* **16**, 673-677 (1968).

25 Sunde, M. *et al.* Common core structure of amyloid fibrils by synchrotron X-ray diffraction. *Journal of molecular biology* **273**, 729-739 (1997).
26 Jimenez, J. L. *et al.* The protofilament structure of insulin amyloid fibrils. *Proceedings of the National Academy of Sciences* **99**, 9196-9201 (2002).
27 Makin, O. S. & Serpell, L. C. Structures for amyloid fibrils. *The FEBS journal* **272**, 5950-5961 (2005).
28 Colvin, M. T. *et al.* Atomic resolution structure of monomorphic Aβ42 amyloid fibrils. *Journal of the American Chemical Society* **138**, 9663-9674 (2016).
29 Fändrich, M. *et al.* Amyloid fibril polymorphism: a challenge for molecular imaging and therapy. *Journal of Internal Medicine* **283**, 218-237 (2018).
30 Gallardo, R., Ranson, N. A. & Radford, S. E. Amyloid structures: much more than just a cross-β fold. *Current opinion in structural biology* **60**, 7-16 (2020).
31 Gremer, L. *et al.* Fibril structure of amyloid-β (1–42) by cryo–electron microscopy. *Science* **358**, 116-119 (2017).
32 Li, B. *et al.* Cryo-EM of full-length α-synuclein reveals fibril polymorphs with a common structural kernel. *Nature communications* **9**, 1-10 (2018).
33 Schmidt, M. *et al.* Peptide dimer structure in an Aβ (1–42) fibril visualized with cryo-EM. *Proceedings of the National Academy of Sciences* **112**, 11858-11863 (2015).
34 Spillantini, M. G. *et al.* α-Synuclein in Lewy bodies. *Nature* **388**, 839-840 (1997).
35 Tuttle, M. D. *et al.* Solid-state NMR structure of a pathogenic fibril of full-length human α-synuclein. *Nature structural & molecular biology* **23**, 409-415 (2016).
36 Wälti, M. A. *et al.* Atomic-resolution structure of a disease-relevant Aβ (1–42) amyloid fibril. *Proceedings of the National Academy of Sciences* **113**, E4976-E4984 (2016).
37 Bouter, Y. *et al.* N-truncated amyloid β (Aβ) 4-42 forms stable aggregates and induces acute and long-lasting behavioral deficits. *Acta neuropathologica* **126**, 189-205 (2013).
38 Kumar, S. *et al.* Extracellular phosphorylation of the amyloid β-peptide promotes formation of toxic aggregates during the pathogenesis of Alzheimer's disease. *The EMBO journal* **30**, 2255-2265 (2011).
39 Kummer, M. P. *et al.* Nitration of tyrosine 10 critically enhances amyloid β aggregation and plaque formation. *Neuron* **71**, 833-844 (2011).
40 Zhang, Y.-Q. & Sarge, K. D. Sumoylation of amyloid precursor protein negatively regulates Aβ aggregate levels. *Biochemical and biophysical research communications* **374**, 673-678 (2008).
41 Meisl, G., Yang, X., Frohm, B., Knowles, T. P. & Linse, S. Quantitative analysis of intrinsic and extrinsic factors in the aggregation mechanism of Alzheimer-associated Aβ-peptide. *Scientific reports* **6**, 1-12 (2016).
42 Yang, X. *et al.* On the role of sidechain size and charge in the aggregation of A β 42 with familial mutations. *Proceedings of the National Academy of Sciences* **115**, E5849-E5858 (2018).
43 Cohen, S. I. *et al.* Distinct thermodynamic signatures of oligomer generation in the aggregation of the amyloid-β peptide. *Nature chemistry* **10**, 523-531 (2018).
44 Kusumoto, Y., Lomakin, A., Teplow, D. B. & Benedek, G. B. Temperature dependence of amyloid β-protein fibrillization. *Proceedings of the National Academy of Sciences* **95**, 12277-12282 (1998).
45 Abelein, A., Gräslund, A. & Danielsson, J. Zinc as chaperone-mimicking agent for retardation of amyloid β peptide fibril formation. *Proceedings of the National Academy of Sciences* **112**, 5407-5412 (2015).
46 Baumann, K. N. *et al.* A Kinetic Map of the Influence of Biomimetic Lipid Membrane Models on Aβ42 Aggregation. *bioRxiv* (2022).
47 Habchi, J. *et al.* Cholesterol catalyses Aβ42 aggregation through a heterogeneous nucleation pathway in the presence of lipid membranes. *Nature chemistry* **10**, 673-683 (2018).

48 Knowles, T. P. *et al.* An analytical solution to the kinetics of breakable filament assembly. *Science* **326**, 1533-1537 (2009).
49 De Yoreo, J. J. & Vekilov, P. G. Principles of crystal nucleation and growth. *Reviews in mineralogy and geochemistry* **54**, 57-93 (2003).
50 Sasahara, K., Yagi, H., Sakai, M., Naiki, H. & Goto, Y. Amyloid nucleation triggered by agitation of β2-microglobulin under acidic and neutral pH conditions. *Biochemistry* **47**, 2650-2660 (2008).
51 Tanaka, M., Collins, S. R., Toyama, B. H. & Weissman, J. S. The physical basis of how prion conformations determine strain phenotypes. *Nature* **442**, 585-589 (2006).
52 Cohen, S. I. *et al.* Proliferation of amyloid-β42 aggregates occurs through a secondary nucleation mechanism. *Proceedings of the National Academy of Sciences* **110**, 9758-9763 (2013).
53 Collins, S. R., Douglass, A., Vale, R. D. & Weissman, J. S. Mechanism of prion propagation: amyloid growth occurs by monomer addition. *PLoS biology* **2**, e321 (2004).
54 Ruschak, A. M. & Miranker, A. D. Fiber-dependent amyloid formation as catalysis of an existing reaction pathway. *Proceedings of the National Academy of Sciences* **104**, 12341-12346 (2007).
55 Arosio, P., Knowles, T. P. & Linse, S. On the lag phase in amyloid fibril formation. *Physical Chemistry Chemical Physics* **17**, 7606-7618 (2015).
56 Bemporad, F. & Chiti, F. Protein misfolded oligomers: experimental approaches, mechanism of formation, and structure-toxicity relationships. *Chemistry & biology* **19**, 315-327 (2012).
57 Linse, S. Toward the equilibrium and kinetics of amyloid peptide self-assembly. *Current Opinion in Structural Biology* **70**, 87-98 (2021).
58 Hellstrand, E., Boland, B., Walsh, D. M. & Linse, S. Amyloid β-protein aggregation produces highly reproducible kinetic data and occurs by a two-phase process. *ACS chemical neuroscience* **1**, 13-18 (2010).
59 Cohen, S. I., Vendruscolo, M., Dobson, C. M. & Knowles, T. P. Nucleated polymerization with secondary pathways. II. Determination of self-consistent solutions to growth processes described by non-linear master equations. *The Journal of chemical physics* **135**, 08B611 (2011).
60 Cohen, S. I., Vendruscolo, M., Dobson, C. M. & Knowles, T. P. From macroscopic measurements to microscopic mechanisms of protein aggregation. *Journal of molecular biology* **421**, 160-171 (2012).
61 Meisl, G. *et al.* Differences in nucleation behavior underlie the contrasting aggregation kinetics of the Aβ40 and Aβ42 peptides. *Proceedings of the National Academy of Sciences* **111**, 9384-9389 (2014).
62 Meisl, G. *et al.* Molecular mechanisms of protein aggregation from global fitting of kinetic models. *Nature protocols* **11**, 252-272 (2016).
63 Mathews, V. H., van Holde, K. & Kevin, G. (Person Education Inc, 2000).
64 Zetterberg, H., Blennow, K. & de Leon, M. Alzheimer's disease. *Lancet* **368**, 387 (2006).
65 Association, A. s. 2015 Alzheimer's disease facts and figures. *Alzheimer's & Dementia* **11**, 332-384 (2015).
66 Winblad, B. *et al.* Defeating Alzheimer's disease and other dementias: a priority for European science and society. *The Lancet Neurology* **15**, 455-532 (2016).
67 Hebert, L. E., Weuve, J., Scherr, P. A. & Evans, D. A. Alzheimer disease in the United States (2010–2050) estimated using the 2010 census. *Neurology* **80**, 1778-1783 (2013).
68 Prince, M. *et al.* The global prevalence of dementia: a systematic review and metaanalysis. *Alzheimer's & dementia* **9**, 63-75. e62 (2013).
69 Selkoe, D. J. & Hardy, J. The amyloid hypothesis of Alzheimer's disease at 25 years. *EMBO molecular medicine* **8**, 595-608 (2016).

70 Pimplikar, S. W. Reassessing the amyloid cascade hypothesis of Alzheimer's disease. *The international journal of biochemistry & cell biology* **41**, 1261-1268 (2009).
71 Goate, A. *et al.* Segregation of a missense mutation in the amyloid precursor protein gene with familial Alzheimer's disease. *Nature* **349**, 704-706 (1991).
72 Levy-Lahad, E. *et al.* Candidate gene for the chromosome 1 familial Alzheimer's disease locus. *Science* **269**, 973-977 (1995).
73 Sherrington, R. *et al.* Cloning of a gene bearing missense mutations in early-onset familial Alzheimer's disease. *Nature* **375**, 754-760 (1995).
74 Raber, J., Huang, Y. & Ashford, J. W. ApoE genotype accounts for the vast majority of AD risk and AD pathology. *Neurobiology of aging* **25**, 641-650 (2004).
75 Mayeux, R. & Stern, Y. Epidemiology of Alzheimer disease. *Cold Spring Harbor perspectives in medicine* **2**, a006239 (2012).
76 Corder, E. H. *et al.* Gene dose of apolipoprotein E type 4 allele and the risk of Alzheimer's disease in late onset families. *Science* **261**, 921-923 (1993).
77 Grundke-Iqbal, I. *et al.* Abnormal phosphorylation of the microtubule-associated protein tau (tau) in Alzheimer cytoskeletal pathology. *Proceedings of the National Academy of Sciences* **83**, 4913-4917 (1986).
78 Masters, C. L. *et al.* Amyloid plaque core protein in Alzheimer disease and Down syndrome. *Proceedings of the National Academy of Sciences* **82**, 4245-4249 (1985).
79 Kang, J. *et al.* The precursor of Alzheimer's disease amyloid A4 protein resembles a cell-surface receptor. *Nature* **325**, 733-736 (1987).
80 LaFerla, F. M., Green, K. N. & Oddo, S. Intracellular amyloid-β in Alzheimer's disease. *Nature Reviews Neuroscience* **8**, 499-509 (2007).
81 Soba, P. *et al.* Homo-and heterodimerization of APP family members promotes intercellular adhesion. *The EMBO journal* **24**, 3624-3634 (2005).
82 Cupers, P., Orlans, I., Craessaerts, K., Annaert, W. & De Strooper, B. The amyloid precursor protein (APP)-cytoplasmic fragment generated by γ-secretase is rapidly degraded but distributes partially in a nuclear fraction of neurones in culture. *Journal of neurochemistry* **78**, 1168-1178 (2001).
83 Selkoe, D. J. Cell biology of the amyloid beta-protein precursor and the mechanism of Alzheimer's disease. *Annual review of cell biology* **10**, 373-403 (1994).
84 Wolfe, M. S. *et al.* Two transmembrane aspartates in presenilin-1 required for presenilin endoproteolysis and γ-secretase activity. *Nature* **398**, 513-517 (1999).
85 Murphy, M. P. & LeVine III, H. Alzheimer's disease and the amyloid-β peptide. *Journal of Alzheimer's disease* **19**, 311-323 (2010).
86 Younkin, S. G. The role of Aβ42 in Alzheimer's disease. *Journal of Physiology-Paris* **92**, 289-292 (1998).
87 Hardy, J. A. & Higgins, G. A. Alzheimer's disease: the amyloid cascade hypothesis. *Science* **256**, 184-185 (1992).
88 Terry, R. D. *et al.* Physical basis of cognitive alterations in Alzheimer's disease: synapse loss is the major correlate of cognitive impairment. *Annals of Neurology: Official Journal of the American Neurological Association and the Child Neurology Society* **30**, 572-580 (1991).
89 Takahashi, R. H., Nagao, T. & Gouras, G. K. Plaque formation and the intraneuronal accumulation of β-amyloid in Alzheimer's disease. *Pathology international* **67**, 185-193 (2017).
90 Kinoshita, A. *et al.* Demonstration by FRET of BACE interaction with the amyloid precursor protein at the cell surface and in early endosomes. *Journal of cell science* **116**, 3339-3346 (2003).
91 Koo, E. H. & Squazzo, S. L. Evidence that production and release of amyloid beta-protein involves the endocytic pathway. *Journal of Biological Chemistry* **269**, 17386-17389 (1994).

92 Wesén, E., Jeffries, G. D., Matson Dzebo, M. & Esbjörner, E. K. Endocytic uptake of monomeric amyloid-β peptides is clathrin-and dynamin-independent and results in selective accumulation of Aβ (1–42) compared to Aβ (1–40). *Scientific reports* **7**, 1-14 (2017).
93 Wesén, E., Lundmark, R. & Esbjörner, E. K. Role of Membrane Tension Sensitive Endocytosis and Rho GTPases in the Uptake of the Alzheimer's Disease Peptide Aβ (1-42). *ACS chemical neuroscience* **11**, 1925-1936 (2020).
94 Gouras, G. K. *et al.* Intraneuronal Aβ42 accumulation in human brain. *The American journal of pathology* **156**, 15-20 (2000).
95 Näslund, J. *et al.* Correlation between elevated levels of amyloid β-peptide in the brain and cognitive decline. *Jama* **283**, 1571-1577 (2000).
96 Reddy, P. H. *et al.* Differential loss of synaptic proteins in Alzheimer's disease: implications for synaptic dysfunction. *Journal of Alzheimer's Disease* **7**, 103-117 (2005).
97 Manczak, M. *et al.* Mitochondria are a direct site of Aβ accumulation in Alzheimer's disease neurons: implications for free radical generation and oxidative damage in disease progression. *Human molecular genetics* **15**, 1437-1449 (2006).
98 Hartmann, T. *et al.* Distinct sites of intracellular production for Alzheimer's disease Aβ40/42 amyloid peptides. *Nature medicine* **3**, 1016-1020 (1997).
99 Skovronsky, D. M., Doms, R. W. & Lee, V. M.-Y. Detection of a novel intraneuronal pool of insoluble amyloid β protein that accumulates with time in culture. *The Journal of cell biology* **141**, 1031-1039 (1998).
100 Esbjörner, E. K. *et al.* Direct observations of amyloid β self-assembly in live cells provide insights into differences in the kinetics of Aβ (1–40) and Aβ (1–42) aggregation. *Chemistry & biology* **21**, 732-742 (2014).
101 Friedrich, R. P. *et al.* Mechanism of amyloid plaque formation suggests an intracellular basis of Aβ pathogenicity. *Proceedings of the National Academy of Sciences* **107**, 1942-1947 (2010).
102 Cataldo, A. M. *et al.* Endocytic pathway abnormalities precede amyloid β deposition in sporadic Alzheimer's disease and Down syndrome: differential effects of APOE genotype and presenilin mutations. *The American journal of pathology* **157**, 277-286 (2000).
103 Nixon, R. A. Endosome function and dysfunction in Alzheimer's disease and other neurodegenerative diseases. *Neurobiology of aging* **26**, 373-382 (2005).
104 Grimm, M. O. *et al.* Regulation of cholesterol and sphingomyelin metabolism by amyloid-β and presenilin. *Nature cell biology* **7**, 1118-1123 (2005).
105 He, X., Huang, Y., Li, B., Gong, C.-X. & Schuchman, E. H. Deregulation of sphingolipid metabolism in Alzheimer's disease. *Neurobiology of aging* **31**, 398-408 (2010).
106 Li, S. *et al.* Soluble oligomers of amyloid β protein facilitate hippocampal long-term depression by disrupting neuronal glutamate uptake. *Neuron* **62**, 788-801 (2009).
107 Durell, S. R., Guy, H. R., Arispe, N., Rojas, E. & Pollard, H. B. Theoretical models of the ion channel structure of amyloid beta-protein. *Biophysical journal* **67**, 2137-2145 (1994).
108 Lashuel, H., Hartley, D., Petre, B., Walz, T. & Lansbury Jr, P. Neurodegenerative disease: amyloid pores from pathogenic mutations, Nature418, 291. *Google Scholar There is no corresponding record for this reference* (2002).
109 Kremer, J. J., Pallitto, M. M., Sklansky, D. J. & Murphy, R. M. Correlation of β-amyloid aggregate size and hydrophobicity with decreased bilayer fluidity of model membranes. *Biochemistry* **39**, 10309-10318 (2000).
110 Rudajev, V. & Novotny, J. The Role of Lipid Environment in Ganglioside GM1-Induced Amyloid β Aggregation. *Membranes* **10**, 226 (2020).
111 Gellermann, G. P. *et al.* Raft lipids as common components of human extracellular amyloid fibrils. *Proceedings of the National Academy of Sciences* **102**, 6297-6302 (2005).

112 Kaya, I. *et al.* Delineating amyloid plaque associated neuronal sphingolipids in transgenic Alzheimer's disease mice (tgArcSwe) using MALDI imaging mass spectrometry. *ACS chemical neuroscience* **8**, 347-355 (2017).
113 Liao, C. R. *et al.* Synchrotron FTIR reveals lipid around and within amyloid plaques in transgenic mice and Alzheimer's disease brain. *Analyst* **138**, 3991-3997 (2013).
114 Bertram, L. & Tanzi, R. E. Thirty years of Alzheimer's disease genetics: the implications of systematic meta-analyses. *Nature Reviews Neuroscience* **9**, 768-778 (2008).
115 Bu, G. Apolipoprotein E and its receptors in Alzheimer's disease: pathways, pathogenesis and therapy. *Nature Reviews Neuroscience* **10**, 333-344 (2009).
116 Bush, A. I. The metallobiology of Alzheimer's disease. *Trends in neurosciences* **26**, 207-214 (2003).
117 Li, F. *et al.* Increased plaque burden in brains of APP mutant MnSOD heterozygous knockout mice. *Journal of neurochemistry* **89**, 1308-1312 (2004).
118 Smith, D. G., Cappai, R. & Barnham, K. J. The redox chemistry of the Alzheimer's disease amyloid β peptide. *Biochimica et Biophysica Acta (BBA)-Biomembranes* **1768**, 1976-1990 (2007).
119 Beauchemin, D. & Kisilevsky, R. A method based on ICP-MS for the analysis of Alzheimer's amyloid plaques. *Analytical chemistry* **70**, 1026-1029 (1998).
120 Dong, J. *et al.* Metal binding and oxidation of amyloid-β within isolated senile plaque cores: Raman microscopic evidence. *Biochemistry* **42**, 2768-2773 (2003).
121 Miller, L. M. *et al.* Synchrotron-based infrared and X-ray imaging shows focalized accumulation of Cu and Zn co-localized with β-amyloid deposits in Alzheimer's disease. *Journal of structural biology* **155**, 30-37 (2006).
122 Curtain, C. C. *et al.* Alzheimer's disease amyloid-β binds copper and zinc to generate an allosterically ordered membrane-penetrating structure containing superoxide dismutase-like subunits. *Journal of Biological Chemistry* **276**, 20466-20473 (2001).
123 Guilloreau, L., Combalbert, S., Sournia-Saquet, A., Mazarguil, H. & Faller, P. Redox chemistry of copper–amyloid-β: The generation of hydroxyl radical in the presence of ascorbate is linked to redox-potentials and aggregation state. *ChemBioChem* **8**, 1317-1325 (2007).
124 Huang, X. *et al.* Cu (II) potentiation of Alzheimer Aβ neurotoxicity: correlation with cell-free hydrogen peroxide production and metal reduction. *Journal of Biological Chemistry* **274**, 37111-37116 (1999).
125 Opazo, C. *et al.* Metalloenzyme-like activity of Alzheimer's disease β-amyloid: Cu-dependent catalytic conversion of dopamine, cholesterol, and biological reducing agents to neurotoxic H2O2. *Journal of Biological Chemistry* **277**, 40302-40308 (2002).
126 Reybier, K. *et al.* Free superoxide is an intermediate in the production of H2O2 by copper (I)-Aβ peptide and O2. *Angewandte Chemie* **128**, 1097-1101 (2016).
127 Mathys, Z. K. & White, A. R. Copper and Alzheimer's disease. *Neurotoxicity of Metals*, 199-216 (2017).
128 Squitti, R. *et al.* Copper dyshomeostasis in Wilson disease and Alzheimer's disease as shown by serum and urine copper indicators. *Journal of Trace Elements in Medicine and Biology* **45**, 181-188 (2018).
129 Deibel, M., Ehmann, W. & Markesbery, W. Copper, iron, and zinc imbalances in severely degenerated brain regions in Alzheimer's disease: possible relation to oxidative stress. *Journal of the neurological sciences* **143**, 137-142 (1996).
130 Danscher, G. *et al.* Increased amount of zinc in the hippocampus and amygdala of Alzheimer's diseased brains: a proton-induced X-ray emission spectroscopic analysis of cryostat sections from autopsy material. *Journal of neuroscience methods* **76**, 53-59 (1997).
131 Corrigan, F. M., Reynolds, G. P. & Ward, N. I. Hippocampal tin, aluminum and zinc in Alzheimer's disease. *Biometals* **6**, 149-154 (1993).

132 Panayi, A., Spyrou, N., Iversen, B., White, M. & Part, P. Determination of cadmium and zinc in Alzheimer's brain tissue using inductively coupled plasma mass spectrometry. *Journal of the neurological sciences* **195**, 1-10 (2002).
133 Samudralwar, D., Diprete, C., Ni, B., Ehmann, W. & Markesbery, W. Elemental imbalances in the olfactory pathway in Alzheimer's disease. *Journal of the neurological sciences* **130**, 139-145 (1995).
134 Thompson, C., Markesbery, W., Ehmann, W., Mao, Y. & Vance, D. Regional brain trace-element studies in Alzheimer's disease. *Neurotoxicology* **9**, 1-7 (1988).
135 Religa, D. *et al.* Elevated cortical zinc in Alzheimer disease. *Neurology* **67**, 69-75 (2006).
136 Guilloreau, L. *et al.* Structural and thermodynamical properties of CuII amyloid-β16/28 complexes associated with Alzheimer's disease. *JBIC Journal of Biological Inorganic Chemistry* **11**, 1024-1038 (2006).
137 Karr, J. W. & Szalai, V. A. Cu (II) binding to monomeric, oligomeric, and fibrillar forms of the Alzheimer's disease amyloid-β peptide. *Biochemistry* **47**, 5006-5016 (2008).
138 Sarell, C. J., Syme, C. D., Rigby, S. E. & Viles, J. H. Copper (II) binding to amyloid-β fibrils of Alzheimer's disease reveals a picomolar affinity: stoichiometry and coordination geometry are independent of Aβ oligomeric form. *Biochemistry* **48**, 4388-4402 (2009).
139 Syme, C. D., Nadal, R. C., Rigby, S. E. & Viles, J. H. Copper binding to the amyloid-β (Aβ) peptide associated with Alzheimer's disease: folding, coordination geometry, pH dependence, stoichiometry, and affinity of Aβ-(1–28): insights from a range of complementary spectroscopic techniques. *Journal of Biological Chemistry* **279**, 18169-18177 (2004).
140 Faller, P. & Hureau, C. Bioinorganic chemistry of copper and zinc ions coordinated to amyloid-β peptide. *Dalton transactions*, 1080-1094 (2009).
141 Bin, Y., Chen, S. & Xiang, J. pH-dependent kinetics of copper ions binding to amyloid-β peptide. *Journal of inorganic biochemistry* **119**, 21-27 (2013).
142 Atwood, C. S. *et al.* Characterization of Copper Interactions with Alzheimer Amyloid β Peptides: Identification of an Attomolar-Affinity Copper Binding Site on Amyloid β1-42. *Journal of neurochemistry* **75**, 1219-1233 (2000).
143 Yako, N. *et al.* Copper binding and redox chemistry of the Aβ16 peptide and its variants: insights into determinants of copper-dependent reactivity. *Metallomics* **9**, 278-291 (2017).
144 Shearer, J. & Szalai, V. A. The amyloid-β peptide of Alzheimer's disease binds CuI in a linear bis-his coordination environment: Insight into a possible neuroprotective mechanism for the amyloid-β peptide. *Journal of the American Chemical Society* **130**, 17826-17835 (2008).
145 Furlan, S., Hureau, C., Faller, P. & La Penna, G. Modeling the Cu+ Binding in the 1− 16 Region of the Amyloid-β Peptide Involved in Alzheimer's Disease. *The journal of physical chemistry B* **114**, 15119-15133 (2010).
146 Minicozzi, V. *et al.* Identifying the minimal copper-and zinc-binding site sequence in amyloid-β peptides. *Journal of Biological Chemistry* **283**, 10784-10792 (2008).
147 Abelein, A. *et al.* The hairpin conformation of the amyloid β peptide is an important structural motif along the aggregation pathway. *JBIC Journal of Biological Inorganic Chemistry* **19**, 623-634 (2014).
148 Wärmländer, S. *et al.* Biophysical Studies of the Amyloid β-Peptide: Interactions with Metal Ions and Small Molecules. *ChemBioChem* **14**, 1692-1704 (2013).
149 Danielsson, J., Pierattelli, R., Banci, L. & Gräslund, A. High-resolution NMR studies of the zinc-binding site of the Alzheimer's amyloid β-peptide. *The FEBS journal* **274**, 46-59 (2007).
150 Tickler, A. K. *et al.* Methylation of the imidazole side chains of the Alzheimer disease amyloid-β peptide results in abolition of superoxide dismutase-like structures and inhibition of neurotoxicity. *Journal of Biological Chemistry* **280**, 13355-13363 (2005).

151 Bolognin, S. *et al.* Aluminum, copper, iron and zinc differentially alter amyloid-Aβ1–42 aggregation and toxicity. *The international journal of biochemistry & cell biology* **43**, 877-885 (2011).
152 Brzyska, M., Trzesniewska, K., Wieckowska, A., Szczepankiewicz, A. & Elbaum, D. Electrochemical and Conformational Consequences of Copper (CuI and CuII) Binding to β-Amyloid (1–40). *ChemBioChem* **10**, 1045-1055 (2009).
153 Dai, X., Sun, Y., Gao, Z. & Jiang, Z. Copper enhances amyloid-β peptide neurotoxicity and non β-aggregation: a series of experiments conducted upon copper-bound and copper-free amyloid-β peptide. *Journal of molecular neuroscience* **41**, 66-73 (2010).
154 Gu, M., Bode, D. C. & Viles, J. H. Copper redox cycling inhibits Aβ fibre formation and promotes fibre fragmentation, while generating a dityrosine Aβ dimer. *Scientific reports* **8**, 1-14 (2018).
155 Mold, M., Ouro-Gnao, L., Wieckowski, B. M. & Exley, C. Copper prevents amyloid-β1–42 from forming amyloid fibrils under near-physiological conditions in vitro. *Scientific reports* **3**, 1-6 (2013).
156 Sarell, C. J., Wilkinson, S. R. & Viles, J. H. Substoichiometric levels of Cu2+ ions accelerate the kinetics of fiber formation and promote cell toxicity of amyloid-β from Alzheimer disease. *Journal of biological chemistry* **285**, 41533-41540 (2010).
157 Smith, D. P. *et al.* Concentration dependent Cu2+ induced aggregation and dityrosine formation of the Alzheimer's disease amyloid-β peptide. *Biochemistry* **46**, 2881-2891 (2007).
158 Tõugu, V., Tiiman, A. & Palumaa, P. Interactions of Zn (II) and Cu (II) ions with Alzheimer's amyloid-beta peptide. Metal ion binding, contribution to fibrillization and toxicity. *Metallomics* **3**, 250-261 (2011).
159 Zou, J., Kajita, K. & Sugimoto, N. Cu2+ Inhibits the Aggregation of Amyloid β-Peptide (1–42) in vitro. *Angewandte Chemie International Edition* **40**, 2274-2277 (2001).
160 Tamano, H. *et al.* In vivo synaptic activity-independent co-uptakes of amyloid β1–42 and Zn2+ into dentate granule cells in the normal brain. *Scientific Reports* **9**, 1-8 (2019).
161 Grundke-Iqbal, I. *et al.* Amyloid protein and neurofibrillary tangles coexist in the same neuron in Alzheimer disease. *Proceedings of the National Academy of Sciences* **86**, 2853-2857 (1989).
162 Iwatsubo, T. *et al.* Visualization of Aβ42 (43) and Aβ40 in senile plaques with end-specific Aβ monoclonals: evidence that an initially deposited species is Aβ42 (43). *Neuron* **13**, 45-53 (1994).
163 Turner, R. S., Suzuki, N., Chyung, A. S., Younkin, S. G. & Lee, V. M.-Y. Amyloids and Are Generated Intracellularly in Cultured Human Neurons and Their Secretion Increases with Maturation (∗). *Journal of Biological Chemistry* **271**, 8966-8970 (1996).
164 Doherty, G. J. & McMahon, H. T. Mechanisms of endocytosis. *Annual review of biochemistry* **78**, 857-902 (2009).
165 Sorkin, A. & Von Zastrow, M. Endocytosis and signalling: intertwining molecular networks. *Nature reviews Molecular cell biology* **10**, 609-622 (2009).
166 Thottacherry, J. J. *et al.* Mechanochemical feedback control of dynamin independent endocytosis modulates membrane tension in adherent cells. *Nature communications* **9**, 1-14 (2018).
167 Omtri, R. S., Davidson, M. W., Arumugam, B., Poduslo, J. F. & Kandimalla, K. K. Differences in the cellular uptake and intracellular itineraries of amyloid beta proteins 40 and 42: ramifications for the Alzheimer's drug discovery. *Molecular pharmaceutics* **9**, 1887-1897 (2012).
168 Bi, X., Gall, C., Zhou, J. & Lynch, G. Uptake and pathogenic effects of amyloid beta peptide 1–42 are enhanced by integrin antagonists and blocked by NMDA receptor antagonists. *Neuroscience* **112**, 827-840 (2002).

169 Nagele, R., D'andrea, M., Anderson, W. & Wang, H.-Y. Intracellular accumulation of β-amyloid1–42 in neurons is facilitated by the α7 nicotinic acetylcholine receptor in Alzheimer's disease. *Neuroscience* **110**, 199-211 (2002).
170 Fuentealba, R. A. *et al.* Low-density lipoprotein receptor-related protein 1 (LRP1) mediates neuronal Aβ42 uptake and lysosomal trafficking. *PLoS One* **5**, e11884 (2010).
171 Meireles, J. & Massano, J. Cognitive impairment and dementia in Parkinson's disease: clinical features, diagnosis, and management. *Frontiers in neurology* **3**, 88 (2012).
172 Del Rey, N. L.-G. *et al.* Advances in Parkinson's disease: 200 years later. *Frontiers in neuroanatomy* **12**, 113 (2018).
173 Fahn, S. & Sulzer, D. Neurodegeneration and neuroprotection in Parkinson disease. *NeuroRx* **1**, 139-154 (2004).
174 Parkinson, J. An essay on the shaking palsy. *The Journal of neuropsychiatry and clinical neurosciences* **14**, 223-236 (2002).
175 Papapetropoulos, S., Adi, N., Ellul, J., Argyriou, A. A. & Chroni, E. A prospective study of familial versus sporadic Parkinson's disease. *Neurodegenerative diseases* **4**, 424-427 (2007).
176 Lashuel, H. A., Overk, C. R., Oueslati, A. & Masliah, E. The many faces of α-synuclein: from structure and toxicity to therapeutic target. *Nature Reviews Neuroscience* **14**, 38-48 (2013).
177 Braun, A. R., Lacy, M. M., Ducas, V. C., Rhoades, E. & Sachs, J. N. α-Synuclein's uniquely long amphipathic helix enhances its membrane binding and remodeling capacity. *The Journal of membrane biology* **250**, 183-193 (2017).
178 Meade, R. M., Fairlie, D. P. & Mason, J. M. Alpha-synuclein structure and Parkinson's disease–lessons and emerging principles. *Molecular neurodegeneration* **14**, 1-14 (2019).
179 Campbell, I. D. & Dwek, R. A. *Biological spectroscopy*. (Benjamin/Cummings Pub. Co., 1984).
180 Lamour, G., Kirkegaard, J. B., Li, H., Knowles, T. P. & Gsponer, J. Easyworm: an open-source software tool to determine the mechanical properties of worm-like chains. *Source code for biology and medicine* **9**, 1-6 (2014).
181 Abelein, A. *et al.* High-yield production of amyloid-β peptide enabled by a customized spider silk domain. *Scientific reports* **10**, 1-10 (2020).
182 El Andaloussi, S., Mäger, I., Breakefield, X. O. & Wood, M. J. Extracellular vesicles: biology and emerging therapeutic opportunities. *Nature reviews Drug discovery* **12**, 347-357 (2013).
183 Joshi, P., Benussi, L., Furlan, R., Ghidoni, R. & Verderio, C. Extracellular vesicles in Alzheimer's disease: friends or foes? Focus on aβ-vesicle interaction. *International journal of molecular sciences* **16**, 4800-4813 (2015).
184 Söllvander, S. *et al.* Accumulation of amyloid-β by astrocytes result in enlarged endosomes and microvesicle-induced apoptosis of neurons. *Molecular Neurodegeneration* **11**, 1-19 (2016).
185 Zhang, X. *et al.* Correlation between cellular uptake and cytotoxicity of fragmented α-synuclein amyloid fibrils suggests intracellular basis for toxicity. *ACS chemical neuroscience* **11**, 233-241 (2020).
186 Jiang, D. *et al.* Redox reactions of copper complexes formed with different β-amyloid peptides and their neuropathalogical relevance. *Biochemistry* **46**, 9270-9282 (2007).
187 Kayed, R. *et al.* Fibril specific, conformation dependent antibodies recognize a generic epitope common to amyloid fibrils and fibrillar oligomers that is absent in prefibrillar oligomers. *Molecular neurodegeneration* **2**, 1-11 (2007).
188 O'brien, J., Wilson, I., Orton, T. & Pognan, F. Investigation of the Alamar Blue (resazurin) fluorescent dye for the assessment of mammalian cell cytotoxicity. *European journal of biochemistry* **267**, 5421-5426 (2000).
189 Ge, S. X., Son, E. W. & Yao, R. iDEP: an integrated web application for differential expression and pathway analysis of RNA-Seq data. *BMC bioinformatics* **19**, 1-24 (2018).

190 Marsh, J. & Alifragis, P. Synaptic dysfunction in Alzheimer's disease: the effects of amyloid beta on synaptic vesicle dynamics as a novel target for therapeutic intervention. *Neural regeneration research* **13**, 616 (2018).
191 Shankar, G. M. *et al.* Amyloid-β protein dimers isolated directly from Alzheimer's brains impair synaptic plasticity and memory. *Nature medicine* **14**, 837-842 (2008).
192 Subramanian, A. *et al.* Gene set enrichment analysis: a knowledge-based approach for interpreting genome-wide expression profiles. *Proceedings of the National Academy of Sciences* **102**, 15545-15550 (2005).
193 Kollmer, M. *et al.* Cryo-EM structure and polymorphism of Aβ amyloid fibrils purified from Alzheimer's brain tissue. *Nature communications* **10**, 1-8 (2019).
194 Sagis, L. M., Veerman, C. & van der Linden, E. Mesoscopic properties of semiflexible amyloid fibrils. *Langmuir* **20**, 924-927 (2004).
195 Ruggeri, F. S. *et al.* Identification and nanomechanical characterization of the fundamental single-strand protofilaments of amyloid α-synuclein fibrils. *Proceedings of the National Academy of Sciences* **115**, 7230-7235 (2018).
196 vandenAkker, C. C., Engel, M. F., Velikov, K. P., Bonn, M. & Koenderink, G. H. Morphology and persistence length of amyloid fibrils are correlated to peptide molecular structure. *Journal of the American Chemical Society* **133**, 18030-18033 (2011).
197 Young, L. J., Schierle, G. S. K. & Kaminski, C. F. Imaging Aβ (1–42) fibril elongation reveals strongly polarised growth and growth incompetent states. *Physical Chemistry Chemical Physics* **19**, 27987-27996 (2017).
198 Persson, F. *et al.* Lipid-based passivation in nanofluidics. *Nano letters* **12**, 2260-2265 (2012).
199 Jo, K. *et al.* A single-molecule barcoding system using nanoslits for DNA analysis. *Proceedings of the National Academy of Sciences* **104**, 2673-2678 (2007).
200 Cukalevski, R. *et al.* The Aβ40 and Aβ42 peptides self-assemble into separate homomolecular fibrils in binary mixtures but cross-react during primary nucleation. *Chemical science* **6**, 4215-4233 (2015).
201 Dawson, V. L. & Dawson, T. M. Promising disease-modifying therapies for Parkinson's disease. *Science Translational Medicine* **11**, eaba1659 (2019).
202 Guo, J. *et al.* Exploring the influence of carbon nanoparticles on the formation of β-sheet-rich oligomers of IAPP22–28 peptide by molecular dynamics simulation. *PLoS One* **8**, e65579 (2013).
203 Li, C. & Mezzenga, R. The interplay between carbon nanomaterials and amyloid fibrils in bio-nanotechnology. *Nanoscale* **5**, 6207-6218 (2013).
204 Li, Q. *et al.* Modulating Aβ33–42 peptide assembly by graphene oxide. *Chemistry–A European Journal* **20**, 7236-7240 (2014).
205 Xie, L. *et al.* The molecular mechanism of fullerene-inhibited aggregation of Alzheimer's β-amyloid peptide fragment. *Nanoscale* **6**, 9752-9762 (2014).
206 Yousaf, M., Huang, H., Li, P., Wang, C. & Yang, Y. Fluorine functionalized graphene quantum dots as inhibitor against hIAPP amyloid aggregation. *ACS chemical neuroscience* **8**, 1368-1377 (2017).
207 Bag, S., Sett, A., DasGupta, S. & Dasgupta, S. Hydropathy: the controlling factor behind the inhibition of Aβ fibrillation by graphene oxide. *RSC advances* **6**, 103242-103252 (2016).
208 Liu, Y. *et al.* Graphene quantum dots for the inhibition of β amyloid aggregation. *Nanoscale* **7**, 19060-19065 (2015).
209 Yang, Z. *et al.* Destruction of amyloid fibrils by graphene through penetration and extraction of peptides. *Nanoscale* **7**, 18725-18737 (2015).
210 Nedumpully-Govindan, P. *et al.* Graphene oxide inhibits hIAPP amyloid fibrillation and toxicity in insulin-producing NIT-1 cells. *Physical Chemistry Chemical Physics* **18**, 94-100 (2016).

211 Wang, M. *et al.* Graphene quantum dots against human IAPP aggregation and toxicity in vivo. *Nanoscale* **10**, 19995-20006 (2018).
212 Kim, D. *et al.* Graphene quantum dots prevent α-synucleinopathy in Parkinson's disease. *Nature nanotechnology* **13**, 812-818 (2018).
213 Mohammad-Beigi, H. *et al.* Mechanistic understanding of the interactions between nano-objects with different surface properties and α-synuclein. *ACS nano* **13**, 3243-3256 (2019).
214 Li, S. *et al.* Graphene oxide as a quencher for fluorescent assay of amino acids, peptides, and proteins. *ACS applied materials & interfaces* **4**, 7069-7075 (2012).
215 Hardy, J. & Selkoe, D. J. The amyloid hypothesis of Alzheimer's disease: progress and problems on the road to therapeutics. *science* **297**, 353-356 (2002).
216 Nelson, P. T. *et al.* Correlation of Alzheimer disease neuropathologic changes with cognitive status: a review of the literature. *Journal of Neuropathology & Experimental Neurology* **71**, 362-381 (2012).
217 Walsh, D. M. *et al.* Naturally secreted oligomers of amyloid β protein potently inhibit hippocampal long-term potentiation in vivo. *Nature* **416**, 535-539 (2002).
218 Honig, L. S. *et al.* Trial of solanezumab for mild dementia due to Alzheimer's disease. *New England Journal of Medicine* **378**, 321-330 (2018).
219 Ostrowitzki, S. *et al.* A phase III randomized trial of gantenerumab in prodromal Alzheimer's disease. *Alzheimer's research & therapy* **9**, 1-15 (2017).
220 van Dyck, C. H. *et al.* Lecanemab in early Alzheimer's disease. *New England Journal of Medicine* (2022).
221 Tucker, S. *et al.* The murine version of BAN2401 (mAb158) selectively reduces amyloid-β protofibrils in brain and cerebrospinal fluid of tg-ArcSwe mice. *Journal of Alzheimer's Disease* **43**, 575-588 (2015).
222 Salloway, S. *et al.* Amyloid-related imaging abnormalities in 2 phase 3 studies evaluating aducanumab in patients with early Alzheimer disease. *JAMA neurology* **79**, 13-21 (2022).
223 Munke, A. *et al.* Phage display and kinetic selection of antibodies that specifically inhibit amyloid self-replication. *Proceedings of the National Academy of Sciences* **114**, 6444-6449 (2017).
224 Hu, X. *et al.* Amyloid seeds formed by cellular uptake, concentration, and aggregation of the amyloid-beta peptide. *Proceedings of the National Academy of Sciences* **106**, 20324-20329 (2009).
225 Frykholm, K., Müller, V., Sriram, K., Dorfman, K. D. & Westerlund, F. DNA in nanochannels: theory and applications. *Quarterly Reviews of Biophysics* **55**, e12 (2022).
226 Willander, H. *et al.* BRICHOS domains efficiently delay fibrillation of amyloid β-peptide. *Journal of Biological Chemistry* **287**, 31608-31617 (2012).
227 Öz, R., Sriram, K. & Westerlund, F. A nanofluidic device for real-time visualization of DNA–protein interactions on the single DNA molecule level. *Nanoscale* **11**, 2071-2078 (2019).